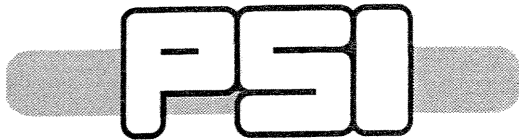
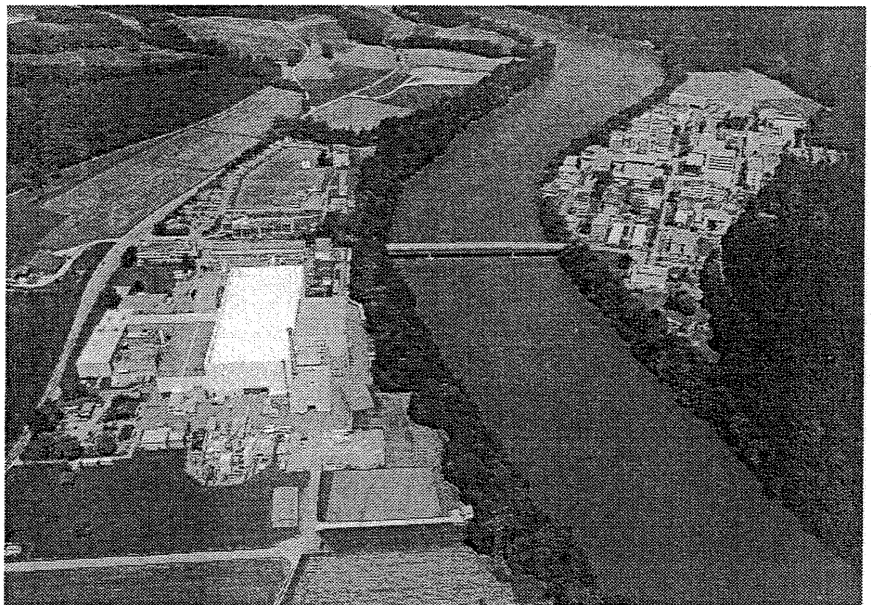


PAUL SCHERRER INSTITUT



ABSTRACTS



First International Symposium on Ultrasonic Doppler Methods for Fluid Mechanics and Fluid Engineering

Paul Scherrer Institute, Villigen, Switzerland
9. - 11. September, 1996

**First International Symposium
on Ultrasonic Doppler Methods
for Fluid Mechanics and Fluid Engineering
(1. ISUD)**

9. - 11. September, 1996

Paul Scherrer Institute

Villigen, Switzerland

Scientific Committee

Prof. M. Anliker (ETHZ, Fluid engineering/Medical)
Prof. M. Aritomi (Tokyo Inst. Technol., Fluid engineering/Nuclear)
Dr. M.P. Chauve (IRPHE, Univ. Marseille II, Physics)
Prof. F. Durst (LMST, Univ. Erlangen, Fluid engineering/Mechanics)
Dr. W.E. Fischer (PSI, Physics, Chairman)
Dr. Y. Takeda (PSI, Fluid engineering/Mechanics)
Prof. E. Windhab (ETHZ, Fluid engineering/Non-newtonian)

Organizing Committee

Dr. G. Bauer (PSI)
Dr. G. King (Univ. Warwick)
Dr. P. Le Gal (IRPHE, Univ. Marseille II)
Dr. Y. Takeda, (PSI, Chairman)
Dr. A. Tokuhiro (PNC)

1. International Symposium on Ultrasonic Doppler method in Fluid Mechanics and Fluid Engineering

Tentative Program

(* : Chairman)

9.9.1996

Time	Presentation
8:30 - 9:00	Registration
9:00 - 9:30	Welcome/Opening
9:30 - 10:30	Plenary lecture (1) * W. Fischer Dr. F. Busse, Uni. Bayreuth Sequences of Bifurcation in Fluid Flows and Coherent Structures in Turbulence
10:30 - 11:00	<i>Coffee break</i>
11:00 - 12:30	Session 1 : Rotating system * F. Durst
11:00 - 11:30	Schouveiler L., Le Gal, Chauve, Takeda, IRPHE Wave competition in the flow between rotating and a stationary disk
11:30 - 12:00	King, G., Lange, Takeda, U. Warwick Comparison of transition in concentric and eccentric Taylor-Couette flows
12:00 - 12:30	Takeda, Y., PSI Quasi-periodic state and transition to turbulence in a rotating Couette system
<i>12:30 - 14:00</i>	<i>Lunch break</i>
14:00 - 15:30	Session 2 : Flow Mapping * M.P. Chauve
14:00 - 14:30	Waechter, P., Durst, Hoefken, Steidl, LSTM Erlangen Application of the ultrasound velocity measuring technique to stirred vessel flows with multi element stirreres
14:30 - 15:00	Tokuhiro, A., Kobayashi, Ohki, Hayashida, Kamide, PNC An overview of experiments using the ultrasonic Doppler method at the PNC
15:00 - 15:30	Lemmin, U., Rolland, EPFL-LRH Acoustic Doppler Velocity Profilers : Application to turbulent flow in hydraulic open channel and lakes
<i>15:30 - 16:00</i>	<i>Photo/Coffee break</i>
16:00 - 17:30	Session 3 : Gas-Liquid system * E. Windhab
16:00 - 16:30	Nakamura, H., Kondo, Kukita, JAERI Simultaneous measurement of liquid velocity and interface profiles of horizontal duct wavy flow by ultrasonic velocity profile meter
16:30 - 17:00	Aritomi, M., Nakajima, Shou, Takeda, Mor, Yoshioka, TIT Measurement system of two-phase flow using ultrasonic velocity profile monitor
17:00 - 17:30	Zhou, S., Aritomi, Mizoguchi, Takeda, Mori, Yoshioka, TIT Multi-dimensional flow characteristics of countercurrent bubbly flow, (II) Effects of air and water flow rates

10.9.1996

Time	Presentation
8:30 - 10:30	Session 4 : Wake * M.Aritomi
8:30 - 9:00	Peschard, I., Le Gal, Takeda, IRPHE On the structure of the cylinder wake
9:00 - 9:30	Peschard, I., Ravoux, Le Gal, Takeda, Chauve, IRPHE Collective behavior of wakes shed by a row of cylinders
9:30 - 10:00	Inoue, Y., Yamashita, Kumada, Suzuka An experimental study on a wake of a torus using UVP monitor
10:00 - 10:30	Michaux-Leblond, N., Belorgey, Attiach, Uni. Havre Benard von Karman vortex street development behind a heated cylinder
10:30 - 11:00	<i>Coffee break</i>
11:00 - 12:00	Session 5 :Jet * Le Gal
11:00 - 11:30	Tokuhiro, A, PNC Investigation of free and forced flows of relevance to fast reactor thermohydraulics using the ultrasonic Doppler method
11:30 - 12:00	Sakakibara, J., Keio Vortex motion of free coaxial jet
12:00 - 13:30	<i>Lunch break</i>
14:00 - 16:00	Discussion Session :What can we do with the huge data set ? * G.King
14:10 - 15:00	Dr. T. Ertl, U. Erlangen Visualization Techniques for Fluid Flow Fields.
15:00 - 16:00	Discussion
16:30	Excursion
18:30	Dinner

11.9.1996

Time	Presentation
8:30 - 9:30	Plenary lecture (2) * E.Windhab Dr. Anliker, ETH Zurich TBD
9:30 - 10:30	Session 6 : Methodology & Rheological flow * G.King
9:30 - 10:00	Willemetz, J., SPSA Influence of fixed and moving interfaces in the measurement of the velocity profiles
10:00 - 10:30	B. Ouriev, Windhab, ETHZ TBA
10:30 - 11:00	<i>Coffee break</i>
11:00 - 12:30	Session 7 :Magnetic fluid * A.Tokuhiro
11:00 - 11:30	Sawada, T., Kikura, Tanahashi, Keio Univ. UVP measurement on magnetic fluid sloshing
11:30 - 12:00	Kikura, H., Takeda, Durst, LSTM Erlangen Taylor Vortex Flow of a magnetic fluid
12:00 - 12:30	Cardin, P., Nataf, Pascal, Attiach, ENS Velocity measurement in a vortex of liquid Gallium
12:30 - 14:00	<i>Lunch break</i>
14:00 - 15:00	Open Session * Y.Takeda
15:30	Closing

1. ISUD

1st International Symposium on Ultrasonic Doppler Methods
for Fluid Mechanics and Fluid Engineering
September 9-11, 1996
Paul Scherrer Institute, 5232 Villigen PSI, Switzerland

Sequences of Bifurcations in Fluid Flows and Coherent Structures in Trubulence

by F.H. Busse,
University of Bayreuth

Summary

Most systems of fluid flow find their simplest realisation in a geometrical configuration that is homogeneous in two spatial dimensions and in time. Fluid systems of this kind often exhibit sequences of bifurcations through which a stepwise evolution occurs from simple to complex structures of flow. While the basic primary state of flow reflects all symmetries of the system, the secondary state generically assumes the form of roll like motion. Only tertiary and higher states of motion exhibit characteristic properties of the system and of regions of the parameter space. Some of the characteristic structures persist as coherent structures far into the turbulent regime. Examples from the plane Couette flow system and from thermal convection are used to illustrate general aspects of the problem.

1. ISUD

1st International Symposium on Ultrasonic Doppler Methods
for Fluid Mechanics and Fluid Engineering

September 9-11, 1996

Paul Scherrer Institut, 5232 Villigen PSI, Switzerland

**WAVE COMPETITION IN THE FLOW
BETWEEN A ROTATING AND A STATIONARY DISK**

L. Schouveiler^①, Y. Takeda^②, P. Le Gal^① and M.P. Chauve^①

^①Institut de Recherche sur les Phénomènes Hors Equilibre
UM 138, CNRS - Universités d'Aix-Marseille I & II
12, Avenue Général Leclerc, 13003 Marseille, France

^②Laboratory for Spallation Neutron Source
Paul Scherrer Institut
CH-5232 Villigen PSI, Switzerland

ABSTRACT

This experimental work is devoted to the study of the dynamics of two systems of waves that appear in the flow between a rotating and a stationary parallel coaxial disk. Using visualization and Ultrasonic Doppler Anemometry, both a circular and a spiral system of waves are observed. Transition to turbulence seems to be driven by the non linear interactions between these two systems of waves.

1. Introduction

The study of the stability of flows between a rotating and a stationary disk is attractive because these flows produce various scenarios of transition to turbulence, when the angular velocity of the rotating disk is increased or when the aspect ratio h/R (where h is the axial distance between the disks and R their radius) is changed. This diversity was first recognized by Daily et al. [1] who distinguished mainly two types of transition which depend on the basic velocity profiles. When the disk boundary layers are merged at small aspect ratio, a first instability occurs and gives rise to different regular systems of waves extended over the whole depth of the gap (see San'kov et al. [2] and Sirivat [3]). Then, the next stages of the transition lead to the formation of turbulent spots and solitary waves (see [2]). For larger aspect ratios, the primary instability occurs on Batchelor type profiles where the two boundary layers are separated by an inviscid rotating core. The present study concerns this large aspect ratio instabilities, where the transition is quite different from before and involves non linear interactions of systems of waves.

2. Experimental details

2.1 Apparatus

The experimental apparatus (see Figure 1) consists of a horizontal rotating disk (radius $R = 140\text{mm}$) set in a water-filled cylindrical housing with a sliding fit. The angular velocity of the disk Ω can be continuously varied in the range $0 - 4\pi \text{ rad/s}$. The stationary disk is the top of the housing. The height of the rotating disk inside the housing is adjustable in such a way that the axial distance between the two disks h can be continuously varied up to 20mm . The control parameters of the flow are the aspect ratio h/R , the Ekman number $Ek^{-1} = \Omega \cdot h^2 / \nu$ (where ν is the kinematic viscosity of the working fluid) and the local Reynolds number $Re(r) = \Omega \cdot r^2 / \nu$ where r is the local radius.

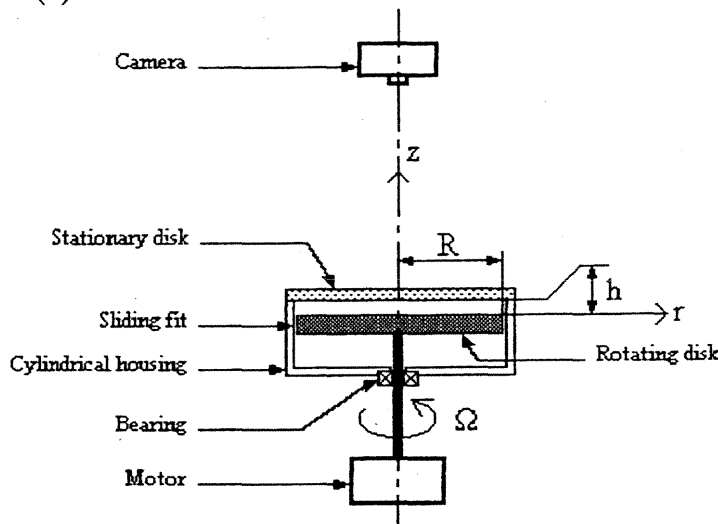


Figure 1: Experimental apparatus

2.2 Flow visualization and UDA techniques

A visualization technique is used to observe the different patterns of the flow. Visualization is performed with a small amount of anisotropic particles (flakes) added to the working fluid. These particles have a high reflective index and they tend to align themselves along stream surfaces, thus becoming visible under appropriate lighting conditions (for further details see Savas [4]). The images are captured with a CCD camera (see Fig. 1.) and recorded. Then, they are digitized and processed on a micro-computer through a standard library of image processing and graphics functions. In particular, a video line can be extracted at the video frequency (25 s^{-1}). Then, these lines are gathered in a space-time diagram representing the dynamics of the waves.

The velocity field is characterized using an Ultrasonic Doppler Anemometer [5]. UDA is a device for measuring a velocity component of a fluid flow at various points along the ultrasound beam axis. A single transducer emits ultrasonic bursts, of frequency f_e , and receives the echoes, of frequency f_r , reflected by the microparticles in suspension in the fluid flow. The velocity component V in the ultrasound beam direction is derived from the Doppler frequency $f_d = f_e - f_r$ with the relation $V = c \cdot f_d / 2 \cdot f_e$ (where c is the speed of ultrasound in the working fluid). The distance x from the particle to the transducer is obtained from the

time delay τ between the emission and the reception of the bursts with $x = c \cdot \tau / 2$. Measuring f_d at various times τ_i after the emission of one burst, instantaneous velocity profiles $V(x_i)$ are obtained.

3. Results and discussion

Figure 2 presents a mean velocity profile measured by the ultrasound anemometer, when the probe is set at a fixed angle of 20° versus the vertical axis. The local Reynolds number corresponding to this plot, is equal to 930 and the measured velocity is the time averaged projection of the velocity onto the beam direction. We recognize the fixed and the rotating boundary layers which are separated by the traditional inviscid core of the Batchelor's profile.

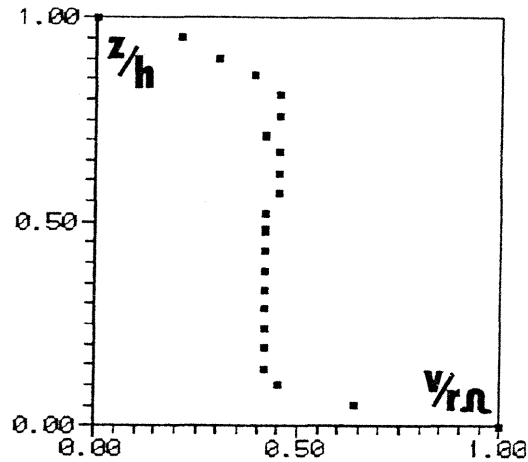


Figure 2: The Batchelor velocity profile of the rotating disk flow. $Ek^{-1}=48$, $Re=930$.

When increasing the rotating velocity to a certain threshold depending on the aspect ratio, a first instability arises and forms concentric circular waves which travel and grow from the border of the disk towards its center. At a slightly higher velocity, another system of spiral waves appears on the external half of the disk. Therefore, these two systems exist together and are located respectively at the center of the disk for the circular waves and at the periphery for the spirals. Figure 3 shows this complex wave pattern.

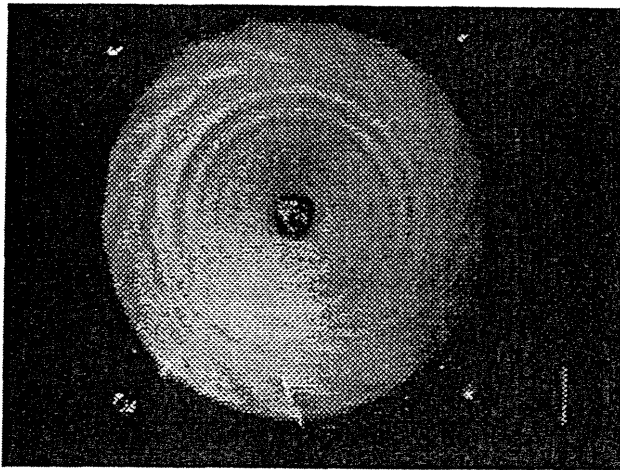


Figure 3: Visualization of the systems of waves. $Ek^{-1}=48$.

In order to study the spatio-temporal features of these waves, space time diagrams are built from the video image analysis presented before and from ultrasound anemometry. for this purpose, the ultrasound transducer is set in a groove machined in the sidewall in the radial direction. Thus the radial velocity profiles of the rotating flow is captured and analyzed. Figure 4 presents together a space time diagram built from (a) visualization and (b) anemometry.

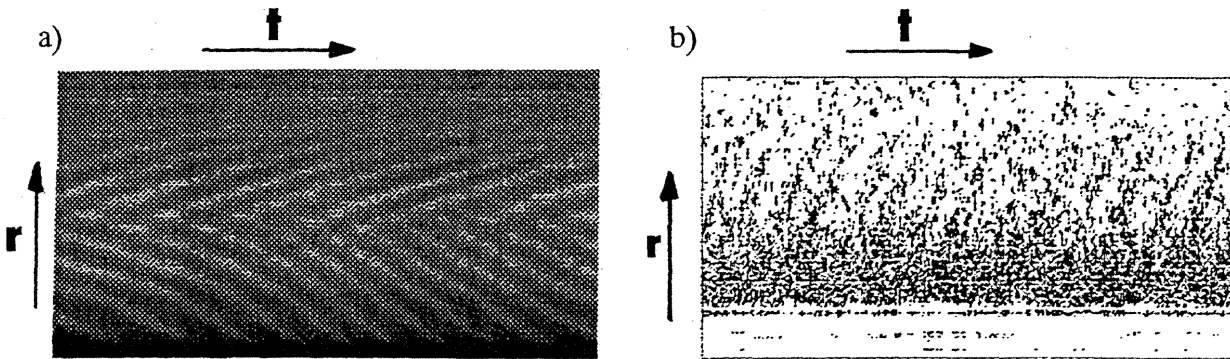


Figure 4: Space time diagrams built from a) visualization $Ek^{-1}=38$,
b) ultrasound anemometry $Ek^{-1}=53$.

Fourier analysis of these diagrams shows that in the interaction region, new frequencies corresponding to linear combinations of the circular and spiral wave frequencies, are generated. This is the signature of non linear interactions between the wave systems. When increasing the rotating velocity, more and more complex wave patterns such as figure 5 appear and lead to turbulence.

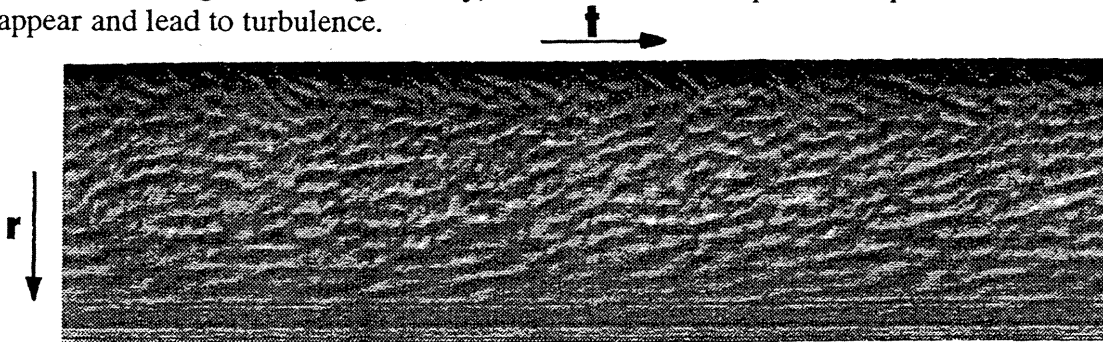


Figure 5: Space time diagrams built from visualization, $Ek^{-1}=63$.

4. References

- [1] Daily, J. W. and Nece, R. E., Chamber dimension effects on induced flow and frictional resistance of enclosed rotating disk, *J. Basic Eng.* **82** (1960) 217.
- [2] San'kov, P. L. and Smirnov, E. M., Bifurcation and transition to turbulence in the gap between rotating and stationary parallel disks, *Fluid Dyn.* **19** (5) (1985) 695.
- [3] Sirivat, A., Stability experiment of flow between a stationary and a rotating disk, *Phys. Fluids A* **3** (11) (1991) 2664.
- [4] Savas, Ö., On flow visualization using reflective flakes, *J. Fluid Mech.* **152** (1985) 235.
- [5] Takeda, Y., Fischer, W. E., Sakakibara, J. and Ohmura, K., Experimental observation of the quasiperiodic modes in a rotating Couette system, *Phys. Rev. E* **47** (1993) 4130.

1.ISUD
 1st International Symposium on Ultrasonic Doppler Methods
 for Fluid Mechanics and Fluid Engineering
 September 9–11, 1996
 Paul Scherrer Institut, 5232 Villigen PSI, Switzerland

Comparison of transition in concentric and eccentric Taylor-Couette flows

G. P. King*, M. Lange* and Y. Takeda†

*Departments of Engineering and Mathematics, University of Warwick, Coventry CV4 7AL, England.

†Paul Scherrer Institut, 5232 Villigen PSI, Switzerland

1 Introduction

Some years ago it was hoped that an understanding of the transition to turbulence could be achieved by analyzing the data from a single time series via the method of delays (c.f. [3]). This hope was driven by the then impracticality and/or high cost of multi-point measurements. Now that instruments are being developed that allow the measurement of flow quantities at several spatial positions as a function of time, the emphasis is on extracting information about the *spatial* character and time-evolution of spatially extended systems.

In this contribution we report on our current investigation of the effect of rotational symmetry on the transition to turbulence in the Taylor-Couette system. Velocity measurements are obtained using the Ultrasound Velocimeter Profiler (UVP) [1, 2]. The data are analyzed using Singular Systems Analysis [3, 4, 5, 6] which allows an investigation of the space-time evolution of spatial patterns and their quantification as a function of Reynolds number.

2 Experiment

The experiments were performed at the Paul Scherrer Institute and the data was obtained using the ultrasound velocimeter profiler (UVP) (see [1, 2]). The axial component of the velocity field in the flow between two rotating cylinders was measured at 128 equidistant positions in the centre part of the system. The spatial resolution was 0.74 mm, and the time between two succeeding profiles was 135.3 msec. The maximum velocity that could be detected was 90 mm/s, and the velocity resolution was 0.7 mm/s.

The dimensions of our Taylor-Couette apparatus are: inner cylinder radius $a = 95$ mm, outer cylinder radius $b = 110$ mm, and cylinder length $L = 202$ mm. Thus the system geometry is characterized by the radius ratio $\eta = a/b = 0.8636$, and the aspect ratio

$\Gamma = L/(b - a) = 13.47$. Removeable end plates allowed the change from the concentric to the eccentric geometry. The eccentricity is defined by $\epsilon = c/(b - a)$, where c is the distance between the axes of the two cylinders. Results are given here for $\epsilon = 0$ and 0.28.

The Reynolds number Re is defined by $Re = a\Omega(b - a)/\nu$ where Ω is the rotational speed of the inner cylinder (the outer cylinder is at rest) and ν is the kinematic viscosity of the fluid. The fluid is a mixture of glycerol and water. Reynolds numbers are expressed as $Re^* = Re/Re_c$ where Re_c is critical Reynolds number for the onset of Taylor-vortices.

For the concentric case axial velocity profiles were measured at only one angle, but for the eccentric case we measured the velocity profile at six angles spaced uniformly around the system. The angles reported here are given with respect to a coordinate system centred on the axis of the outer cylinder. The 0 degree position corresponds to the position of narrowest gap between the cylinders, and the angle increases in the direction of rotation of the inner cylinder. Measurements were carried out over the range $Re^* = (7.5, 30)$ for the concentric case and $Re^* = (8, 20)$ for the eccentric case.

3 Tools for Data Analysis

3.1 Singular Systems Analysis

The UVP technique enables us to measure the axial component of the velocity in the flow at 128 adjacent points in space during each sampling time. A time series of 1024 such velocity profiles are accumulated during each experimental run. The data is stored as a 1024×128 matrix V . Thus the j^{th} row of V is the velocity profile at time j , and the k^{th} column of V is the velocity time series at spatial position k . Most of the kinetic energy is contained in the motion of the fluid forming the Taylor-vortices. We are mainly interested in the fluctuation around this state. Therefore, we eliminate this dominating structure by subtracting the time averaged profile $\langle V \rangle_t$. That is, we subtract the mean value of each column from each entry of the column. In the following we will use the time-centred matrix X where $X = V - \langle V \rangle_t$.

We now carry out the singular system analysis of X [3, 4], which in the present case, since the columns label space, is the discretized version of the biorthogonal decomposition introduced by Aubry [5, 6]. The singular value decomposition of X is written

$$X = S\Sigma C^t \tag{1}$$

where $\Sigma = \text{diag}(\sigma_1, \sigma_2, \dots, \sigma_N)$ are the singular values. The columns of C are the *spatial* eigenvectors, and the columns of S are the *temporal* eigenvectors. We shall assume that the eigenfunctions have been ordered so that $\sigma_1 > \sigma_2 > \dots > \sigma_N$. (See [3] for a guide to the computational details.)

The idea is that for a given Re the state of the system can be described by the spatial and temporal eigenvectors combined in pairs $\{(c_k, s_k)\}$, and their corresponding eigenvalues $\{\sigma_k^2\}$, the squares of the singular values. (Note that s_k is the time evolution of the spatial mode c_k .)

3.2 Representational entropy

Aubry *et al.* [5, 6] suggested that the signal spectrum be quantified by its *representational entropy* and investigated as a function of Reynolds number. The representational entropy is introduced by first defining the probabilities (normalized energies)

$$p_k = \sigma_k^2/E, \quad E = \sum_k \sigma_k^2, \quad (2)$$

where E is the total energy of the signal. Then the entropy is given by

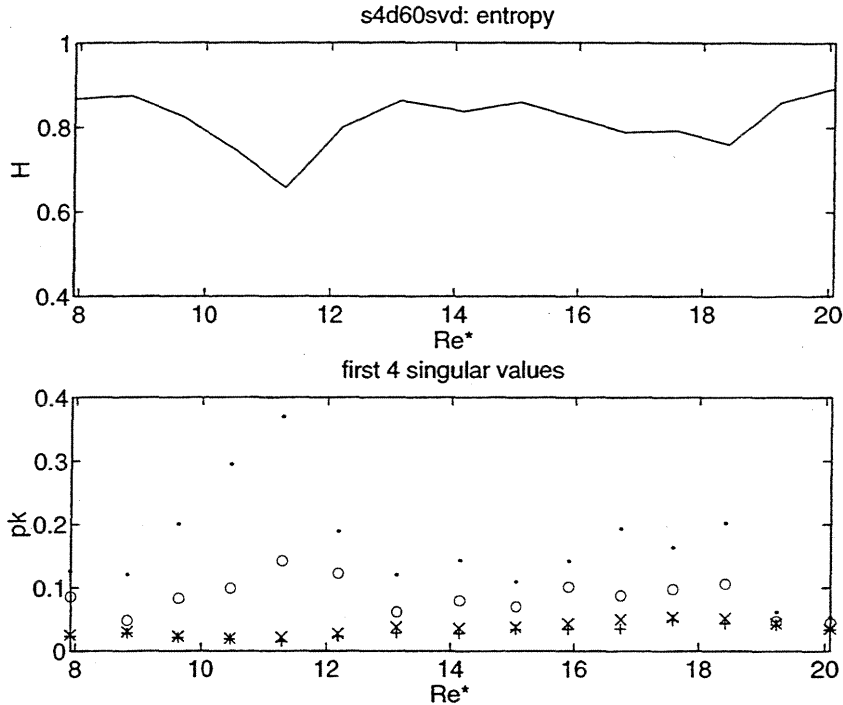
$$H(Re) = -\frac{1}{\log N} \sum_k p_k \log p_k \quad (3)$$

where N is the number of non-zero eigenvalues.

H is a measure of the complexity of the spectrum. If one single mode contains all the energy (i.e. $p_1 = 1$), it takes its minimum value $H = 0$. If the energy is uniformly distributed among all modes, then $p_k = 1/N$, and $H = 1$. During the transition to turbulence the entropy function is expected to increase as Re^* is increased since more and more modes are expected to participate in the complex motion of the fluid. By investigating H as a function of Re , one expects to observe features which mark qualitative changes in the flow structure (e.g., birth/death of a mode, mode competition, etc). (We note that we have also found that the number of eigenvectors containing 90% of the signal energy also provides a useful measure - especially in interpreting the onset of soft and/or hard turbulence.)

4 Results

A sample result of our investigation for $\epsilon = 0.28$ is shown in the figure where we plot the entropy (top), and the normalized energy p_k of the first four spatial-temporal eigenvectors as a function of Reynolds number. The velocities were measured at an angle of 60 degrees downstream from the position of narrowest gap. The dip in H at $Re^* \approx 11.5$ is suggestive of a change in the flow structure. We note however, that similar behaviour is seen at an angle of 120 degrees, but at $Re^* \approx 12.1$. All other angles indicate a rather complicated flow with no detectable change in structure over this range of Reynolds numbers. We hope to shed more light on these results soon.



References

- [1] Y.Takeda, em Nucl. Eng. Des. **126**, 277 (1990).
- [2] Y. Takeda, W.E. Fischer, J. Sakakibara, *Science* **263** 502 (1994).
- [3] D.S. Broomhead and G.P. King, Extracting qualitative dynamics from experimental data, *Physica* 20D, 217 (1986)
- [4] D.S. Broomhead and G.P. King, On the qualitatve analysis of experimental dynamical systems, *Nonlinear Phenomena and Chaos* Adam Hilger, Bristol 113-144 (1986)
- [5] N. Aubry, F. Carbone, R. Lima and S. Slimani, Wave propagation phenomena from a spatio-temporal viewpoint: resonances and bifurcations, *Journal of Statistical Physics* ?????
- [6] N. Aubry, R. Guyonnet and R. Lima, Spatio-temporal analysis of complex signals: theory and application, *Journal of Statistical Physics* 64, 683 (1991)

1. ISUD

1st International Symposium on Ultrasonic Doppler Methods
for Fluid Mechanics and Fluid Engineering
September 9-11, 1996
Paul Scherrer Institute, 5232 Villigen PSI, Switzerland

Quasi-periodic State and Transition to Turbulence in a Rotating Couette System

Y. Takeda

Paul Scherrer Institute, Villigen, Switzerland

ABSTRACT

Experimental study on flow transition in a rotating Couette system was made by investigating a spatio-temporal velocity field by ultrasonic Doppler method (UVP). Our Taylor-Couette system has a radius ratio $\eta = R_i/R_o = 0.904$ (R_i is the radius of the inner cylinder, 94.0 mm, and R_o that of the outer cylinder, 104.0 mm) and aspect ratio $\Gamma=L/d=20$ ($d=R_o-R_i$, L is the fluid height). Only the inner cylinder is rotated. The Reynolds number R is defined as $R = \Omega R_i d/\nu$ (Ω is the frequency of rotation of the inner cylinder, ν is the kinematic viscosity), and the reduced Reynolds number as $R^*=R/R_c$. In the present configuration, the critical Reynolds number R_c for the onset of TVF is 134.57. The liquid used in the experiments was a mixture of water and 30% Glycerol. The ultrasonic transducer was set outside of one of the stationary end walls, being perpendicular to it with its center on the outer cylinder wall position. The diameter of the ultrasonic beam was 5 mm. Thus the measuring volume of one point is a half disc shape of radius 2.5 mm and of thickness 0.75 mm. The measurement of the velocity profile was focused on the spatial range from 40 mm to 135 mm (i.e., from $Z=4d$ to $13.5d$) from the end wall in order to eliminate the end wall effect. This setup of the UVP required a measuring time of 130 msec for a velocity level of a few mm/sec. The 1024 successive profiles were recorded. We performed the measurement for R^* ranging from approximately 10 to >40 for most runs. This covers a flow regime of modulated wavy flow (MWV), for which the onset is at $R^*\approx 9$.

We performed one-dimensional Fourier analysis of the data: power spectrum [1] and energy spectral density (ESD) [2]. These spectra were computed by fast Fourier transformation (FFT) in the time and space domain independently, and obtained space-dependent power spectra and time-dependent energy spectral density for all the data sets. It was found that there are three intrinsic wave modes for the MWV regime and they can coexist. Furthermore, we also found that a significant change in the flow characteristics occurs at $R^*=21$, where the azimuthal wave mode (WVF mode) disappears: beyond it, the magnitude of power and energy of higher harmonic modes behaves very differently for $R^*>21$ than for $R^*<21$.

For investigating the nature of the quasi-periodic state quantitatively, a time domain Fourier analysis is not sufficient, since various spatial modes contribute to the same peak in the power spectrum. It is therefore necessary to decompose the velocity field with respect to space and time simultaneously. We

used a two-dimensional Fourier transformation in this study, since this flow configuration shows not only good temporal periodicity but also good spatial periodicity.

A two-dimensional FFT was computed on space and time coordinate as :

$$S(f,k) = \int_{-\infty}^{\infty} \int_{-\infty}^{\infty} V_z(z, t) \exp(-ikx) \exp(-ift) dx dt$$

where f is a frequency and k a wavenumber. For the present experimental setup of space and time resolution, we can obtain two-dimensional Fourier spectrum on the plane of $f=[0,7.57]$ (Hz) and $k=[0,1.33]$ (mm^{-1}) with resolutions of $[14.8\text{mHz}, 0.010\text{mm}^{-1}]$.

An example of the results is given by the surface plot in Fig.1. Reflecting the highly spatio-temporal nature of the flow field, the resulting Fourier spectrum has many isolated peaks. Each peak corresponds to each wave mode or their higher harmonics in a sense of two dimension. By filtering out peaks of higher harmonics and their linear combinations and then reconstructing the velocity field, we showed that the decomposition is successful and valid for investigating a flow field[3]. Using such decomposition analysis, we found that the so-called broad band component, which is attributed to chaos, corresponds to a flow motion which moves from roll to roll beyond a roll pair[3].

The same data sets have been analysed using an orthogonal decomposition technique. Among various techniques introduced so far, we adapted the singular system analysis (SSA). The eigenvalue spectrum shows a very sharp decrease for the initial few modes and thereafter it becomes very slow. This reflects the fact that only a few modes contribute to describe the velocity field.

The variation of the first 10 eigenvalues (Fig.2) shows a behavior which is quite similar to the one obtained by 2D-FFT. The first two modes have significant intensity and are approximately constant for $R^* < 21$ and then show a sharp decrease at $R^* \approx 21$. A broad peak is also seen for $R^* \approx 28$.

The total energy occupation (TEO) is defined as the number of modes which occupy 90% of total energy, designated here as N_{90} . It is an index to show the magnitude of the number of participating modes to the flow field.

$$\left\{ \sum_{i=0}^{N_{90}} E_i \right\} / E_{\text{total}} = 0.9$$

where $E_i = A_i^2$ (A_i is a Eigenvalue) and $E_{\text{total}} = \sum_{i=0}^N E_i$

Fig.3 shows the variation of TEO with respect to Reynolds number. The value of N_{90} increases slowly from 2 to 7 for $9 < R^* < 21$. Then at $R^* = 21$ there is a jump to $N_{90} = 35$, it shows a maximum at $R^* = 22$ and then slightly decreases. For R^* less than 21, the eigenfunctions of participating modes are more or less harmonic or at least highly periodic, while they are not for the larger R^* . It reaches a local maximum at $R^* \approx 22$ and a local minimum at $R^* \approx 28$. Since a dominant mode disappears at $R^* = 22$, the larger number of modes is needed to occupy total energy, whereas another mode (new mode) appears for $23 < R^* < 32$ which has a fairly large contribution to the total energy and thus N_{90} becomes smaller. Beyond this point, it shows a gradual increase up to 55 at $R^* \approx 100$. This large jump in N_{90} at $R^* = 21$ indicates the transition from quasi-periodic flow to turbulence, and at the same time, the transition itself is quite sharp. However, The value of N_{90} itself is still finite and not high, say in the order of 40 to 60.

A global entropy was introduced by Aubry et al.[4] in order to study the order of magnitude of participation of various modes. It shows maximal (equal to 1 when normalised) when energy is uniformly distributed among participating modes. When only a single mode is excited, the entropy is zero.

Fig.4 shows the variation of global entropy with respect to R^* . It is low, around 0.12, for Reynolds numbers less than 19. At around $R^* = 21$, it shows a fairly sharp peak which then decreases to 0.13 at

around $R^*=29$, and then increases again to about 0.4. This behavior corresponds to the transition scheme discussed earlier: while only two waves exist for MWV, it stays low. When the intensity of these two modes decreases sharply, the entropy increases sharply. When the third wave mode appears above $R^*\approx 23$, it again decreases, and it increases again when this mode disappears. Such variation reflects the idea of the global entropy that it increases when the number of participating modes increases, among which energy is distributed with equal share. In this context, the behavior is quite similar to TEO as shown in Fig.3. In the present case, a dip of the entropy at around $R^*\approx 23$ corresponds to the appearance of a new mode which occupies a considerable fraction of the total energy, and it is reflected also as the dip of the curve in N_{90} vs. R^* . It shows a considerable fluctuation beyond $R^*>40$, while N_{90} curve in Fig.3 is fairly smooth. The reason for this fluctuation is as yet unclear.

In the range $40 < R^* < 80$, the values of N_{90} and the global entropy stay fairly constant. However, N_{90} is around 40-60 being finite and the global entropy $H=0.6$. From these results, we consider the flow for this range is "soft turbulence"; there is no coherent structure which characterises the flow field, and the energy is shared among the considerable number of modes, but the number of participating modes is still small.

The "soft turbulence" was introduced by Heslot and Casting[20] from the convection experiment in Helium gas. They investigated a scaling law of Nusselt number to Reynolds number and showed a transition scheme from laminar to turbulence through various intermediate states as : convection - oscillation - chaos - transition - soft turbulence - hard turbulence. Our transition scheme is quite similar to this even though our flow configuration is quite different. The correspondence between the two cases is given in Table 1.

Table 1 Similarity in transition states and corresponding flow regime for convection and Taylor-Couette system

Rayleigh Benard	Taylor Couette system	Characteristics
Convection	TVF	Spatially periodic or symmetric
Oscillation	WVF	Temporally oscillating
Chaos	MWV	quasi periodic
Transition	Fast azimuthal wave mode	still coherent-structural
Soft turbulence	Soft turbulence	non-structural with soft spectrum
Hard turbulence	Hard turbulence	non-structural with hard spectrum

- [1] Takeda, Y., Fischer, W.E., Sakakibara, J. and Ohmura, K., Experimental observation of the quasiperiodic modes in a rotating Couette system, Phys. Rev. E, Vol.47 (1993), 4130.
- [2] Takeda, Y. Fischer, W.E. and Sakakibara, J., Measurement of energy spectral density of a flow in a rotating Couette system, Phys. Rev. Lett., Vol.70 (1993), p3569.
- [3] Takeda, Y., Fischer, W.E. and Sakakibara, J., Decomposition of the modulated waves in a rotating Couette system, Science, Vol.263 (1994), p502
- [4] Heslot, F., Casting, B. and Libchaber, A., Transition to turbulence in helium gas. Phys. Rev. A, 36 (1987) 5870;
Casting, B. et al., Scaling of hard thermal turbulence in Rayleigh-Benard convection, J. Fluid. Mech. 204 (1989) 1

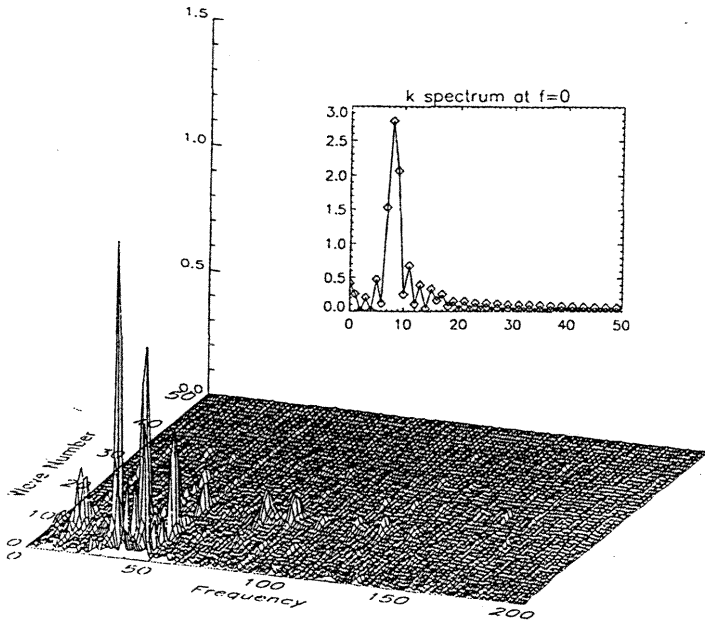


Fig.1 A surface plot of a part of two dimensional Fourier spectrum for the same data as for Fig.3. An insert is a k -spectrum at $f=0$ for clearer view.

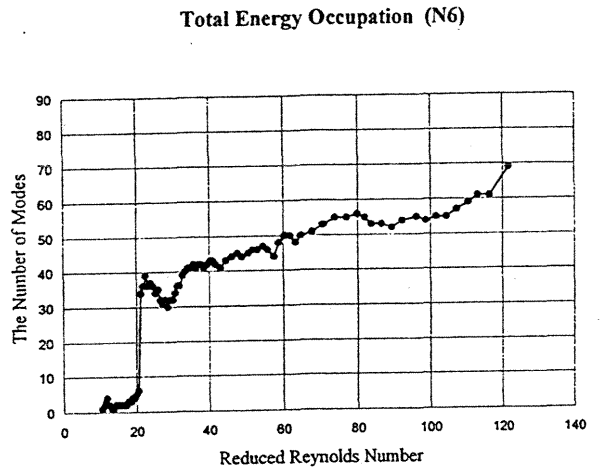


Fig.3 A variation of Total Energy Occupation (TEO) vs R^* .

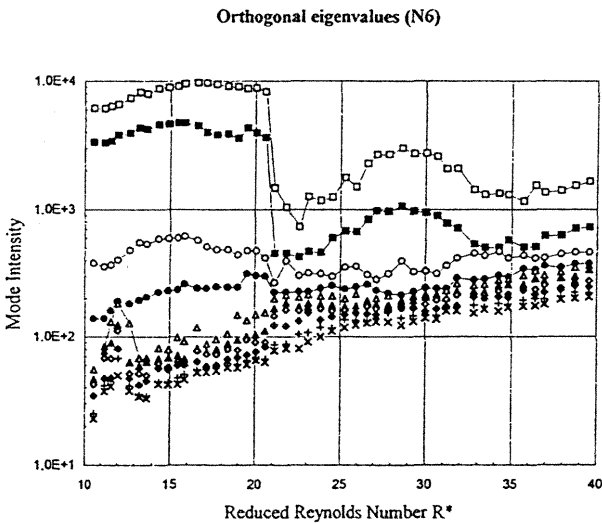


Fig.2 A variation of eigenvalues against R^* for the first 10 eigenmodes.

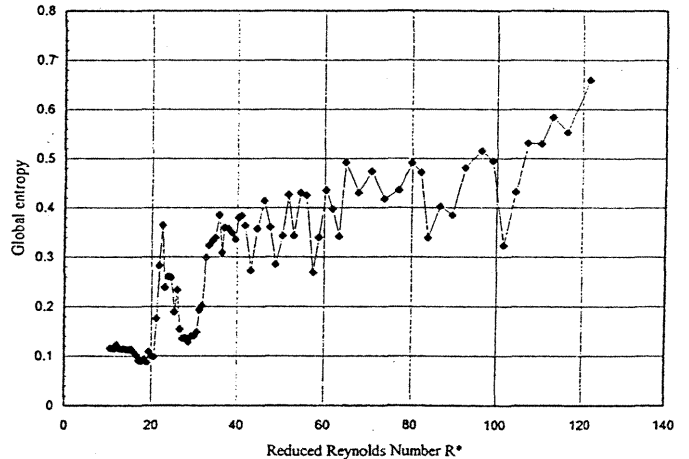


Fig.4 A variation of global entropy vs R^* .

1. ISUD
1st International Symposium on Ultrasonic Doppler Methods
for Fluid Mechanics and Fluid Engineering
September 9-11, 1996
Paul Scherer Institut, 5232 Villingen PSI, Switzerland

**Application of the Ultrasound Velocity Measuring Technique to
Stirred Vessel Flows with Multi Element Stirrers**

P. Wächter, W. Steidl, M. Höfken, F. Durst

Department of Fluid Mechanics, University of Erlangen-Nuremberg, Cauerstr. 4,
91058 Erlangen, Germany

ABSTRACT

1. Introduction

In many fields of the chemical industry, stirred vessel flows are of great importance. Flows of this kind are also of interest to people working in the field of sewage water treatment. Whereas the nature of stirred vessel flows is known and methods have been developed to upscale laboratory experiments, details of the flow are unknown but become of increased importance for detailed layouts of stirred reactors. Measuring techniques, such as laser Doppler anemometry (LDA) usually provide very accurate information but require optical access to the measuring point. This means the use of the LDA-technique in full scale reactors is normally complicated and requires extensive experience of the scientist. Furthermore, these measurements are usually time consuming and yield more detailed information than is needed in praxis. Because of this, an ultrasonic measuring technique (UVP-monitor) has been applied for flow field studies by the authors, providing velocity profile information along the penetration length of an ultrasound wave. Appropriate signal processing yields local velocity information of mean flow properties. This information provides an insight into the flow field of stirred reactor flows with multi element stirrers, studied in the present fluid mechanic research work.

2. Background

In waste water treatment plants biodegradation of pollutants takes place in stirred and aerated tanks. Flakes of sludge which consists out of different colonies of bacteria are responsible for the biological decomposition. These flows must be distributed homogeneously in the basins to use the whole volume. Furthermore deposits could disturb the process essentially. Therefore a minimum bottom velocity is required for waste water treatment plants by

German authorities. To guarantee the desired flow field for different tank geometries laboratory scale experiments are made. In the present work a hyperboloid stirrer which was developed at LSTM-Erlangen is employed. This agitator is distinguished by its special shape, which ensures an attached flow directly above the stirrer surface. Separations and related flow losses are thus minimised. The transport ribs on the stirrer surface cause the waste water to flow off in a radial direction and therefore enhance the circulation of the tank contents. Owing to its energy input near the bottom and the related high bottom velocities, the hyperboloid stirrer possesses good suspension qualities combined with low energy consumption. Increased movement of the water surface, and additional entry of oxygen during denitrification are avoided.

3. Test rig

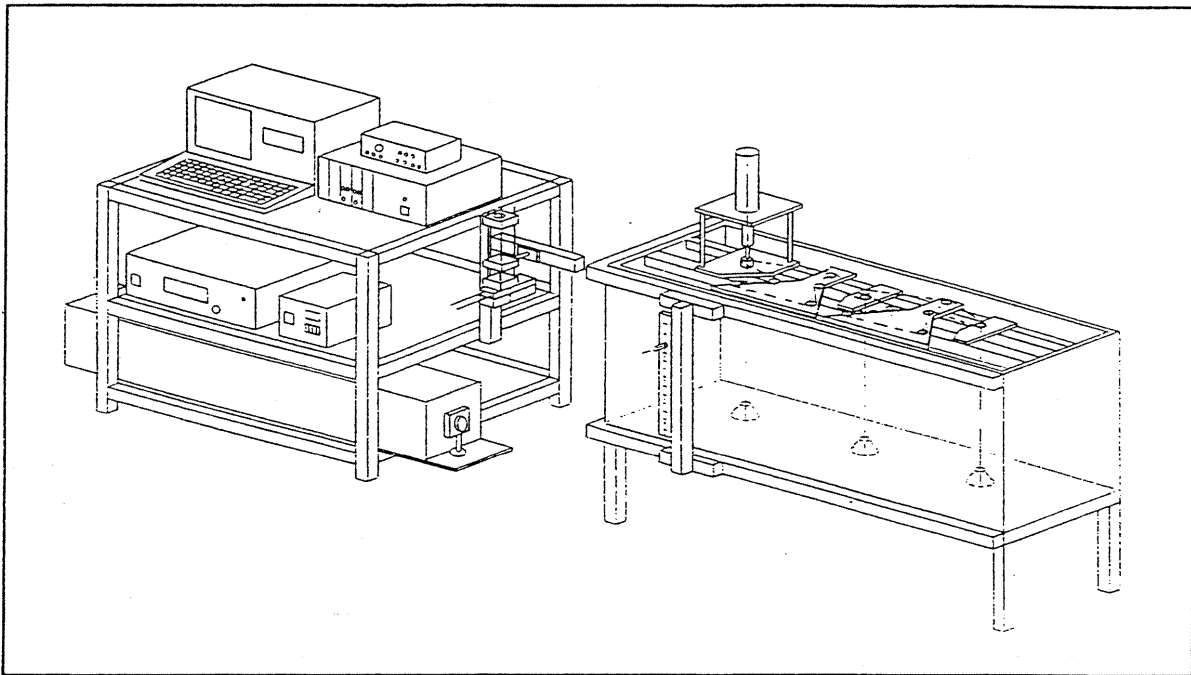


Fig. 1: Schematic drawing of the test rig

A test section was set up, as shown in figure 1 and 2 of the present abstract. The test rig was constructed to achieve geometrical similarity with the most rectangular basins which are used in practice. The volume of the tank can be reduced by a variable wall and so it is also possible to reach the shape of a square tank. Light sheet techniques were employed in order to characterize the flow field generated by one, two and three hyperboloid stirrers mounted in a test section. A UVP-monitor was used to map out the flow field. Prior to the main investigations, tests were made to select the most suitable scattering particles for measuring through a wall made of plexiglas.

The background of these experiments was to determine an installation specification for this kind of stirrer with an optimal relation of operational and investment costs. To reach this aim stir up tests were carried out with artificial sludge, whereby the velocity of the fluid was

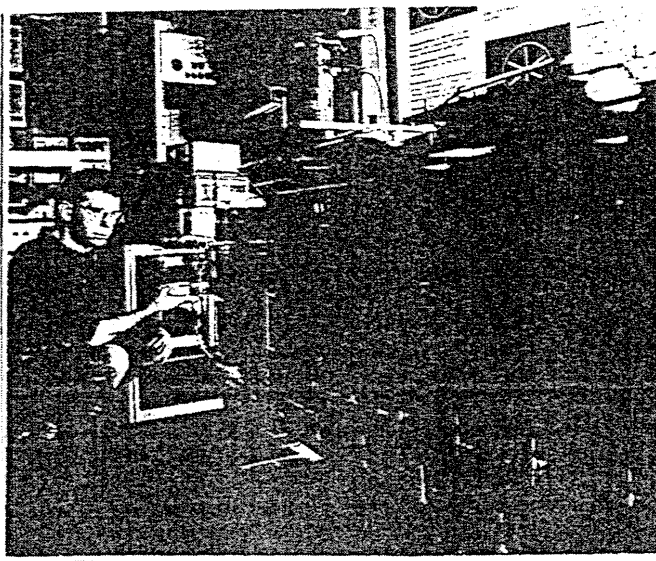


Fig. 2: Photo of the tank

measured at a representative point as a function of the rotational speed of the stirrer, the filling level and the relation of length to width of the tank. The measuring position was found on the basis of flow mapping. We determined that there is a region at the edge of the basin, where the axial component of the velocity is more than 99% of the resultant velocity. So we can characterize the effectiveness of the hyperboloid stirrer (the minimum rotational speed to ensure suspension of the artificial sludge) with just one measurement of one velocity component in the vessel. These results can be transferred to industrial plants.

The UVP-monitor was employed in order to map out the entire flow field inside of the water container. Local velocity information in horizontal planes is shown, for example, in figures 3 and 4. Information has also been acquired on turbulence properties and the local energy dissipation of the stirrer inside of the water container (see figures 5 and 6).

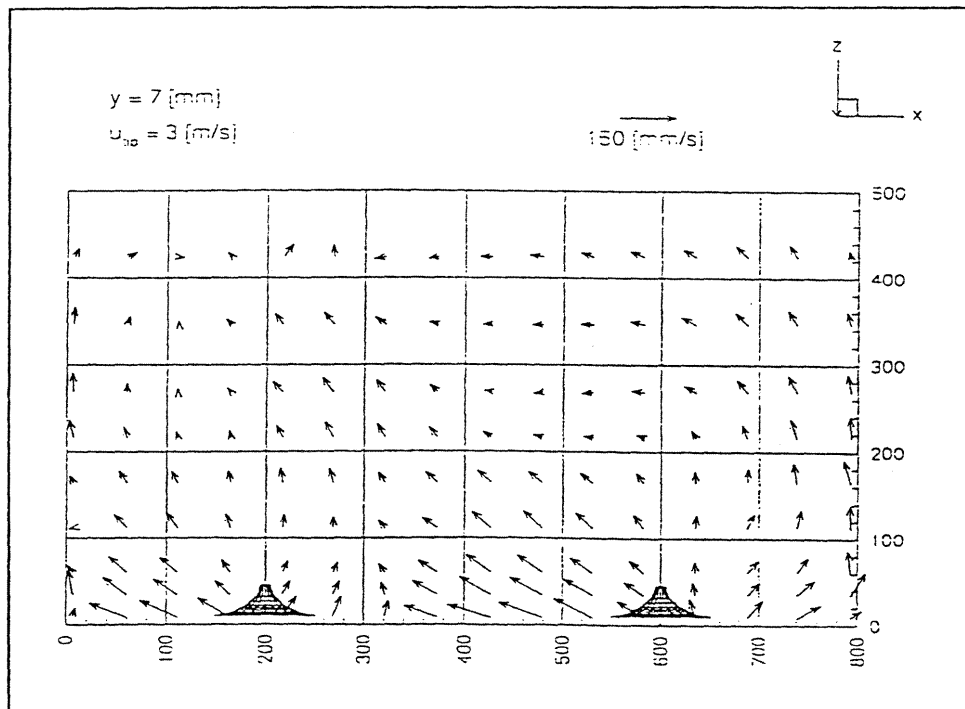


Fig. 3: Horizontal flow mapping of one plane

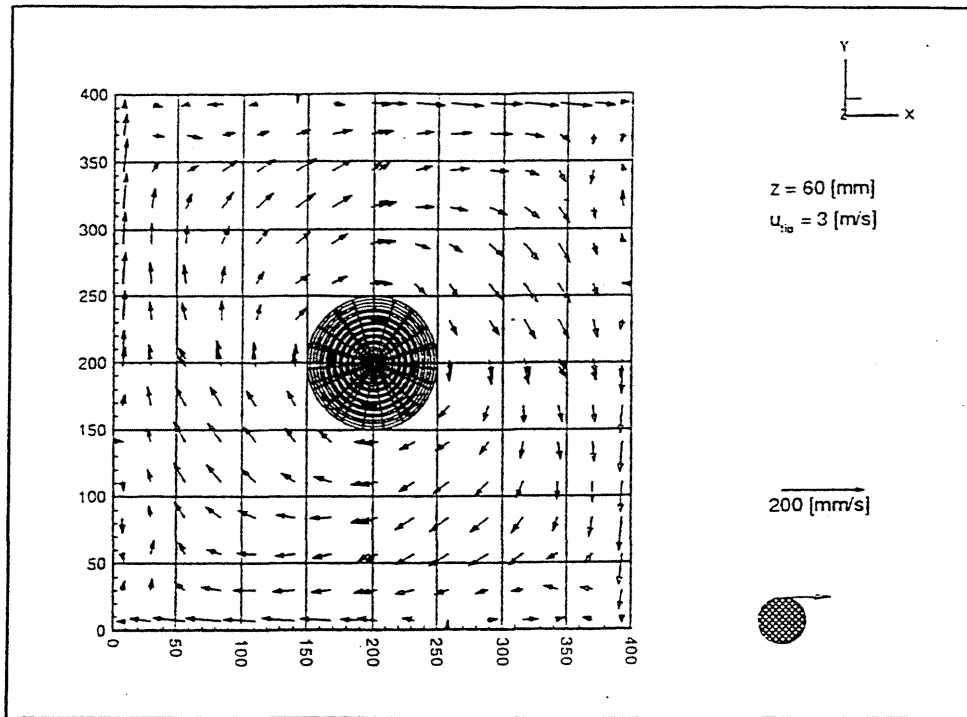


Fig. 4: Vertical flow mapping of one plane

The turbulent flowfield is composed of vortices with a different power density. These fluctuations of the local mean velocity contribute to an effective mixing in a stirred tank. The vortices decay step by step in smaller units and ultimately dissipate. To stir a mixture gently a homogeneous distribution of the dissipated energy is strived for in the whole tank.

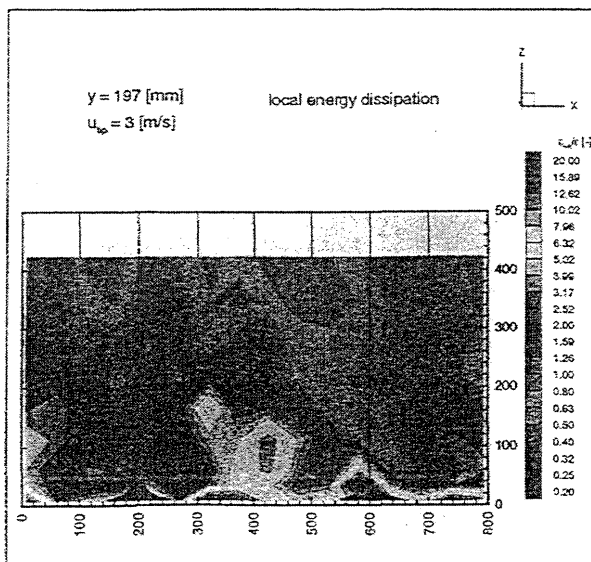


Fig. 5: Turbulence intensity of a horizontal plane

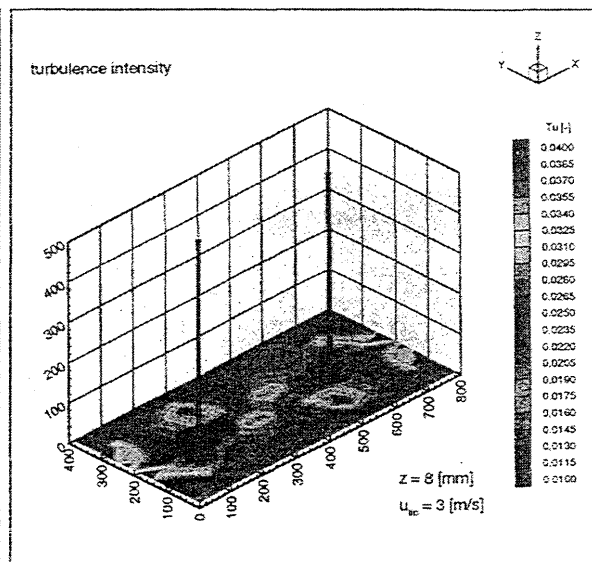


Fig. 6: Local energy dissipation in a vertical plane

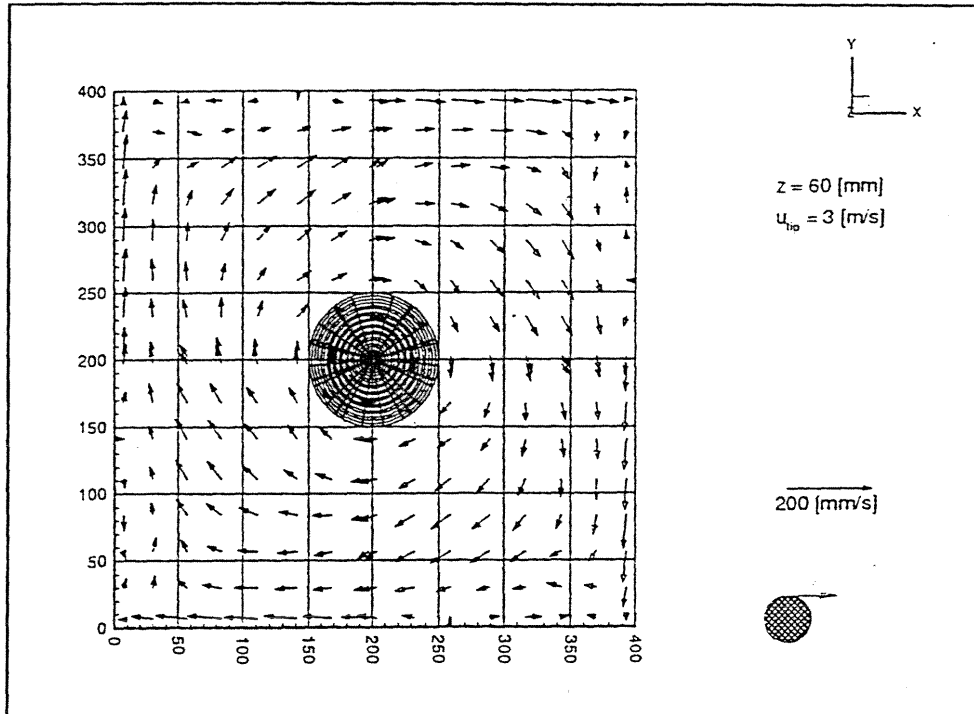


Fig. 4: Vertical flow mapping of one plane

The turbulent flowfield is composed of vortices with a different power density. These fluctuations of the local mean velocity contribute to an effective mixing in a stirred tank. The vortices decay step by step in smaller units and ultimately dissipate. To stir a mixture gently a homogeneous distribution of the dissipated energy is strived for in the whole tank.

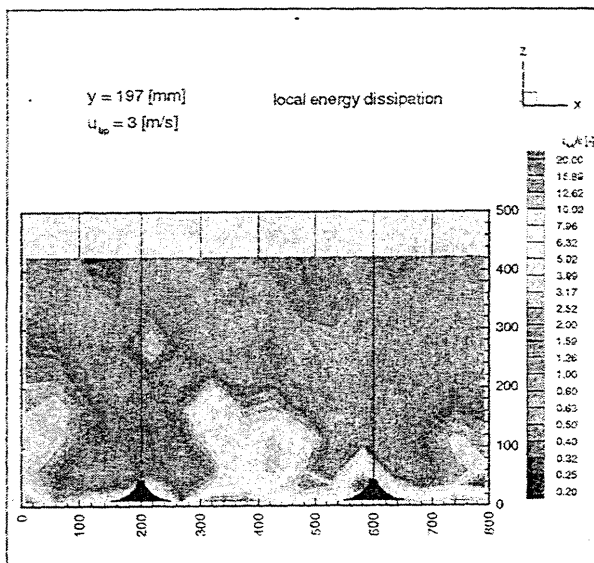


Fig. 5: Turbulence intensity of a horizontal plane

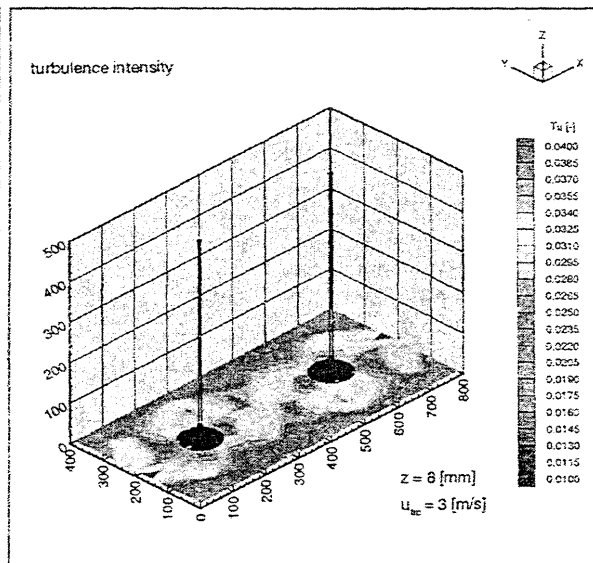


Fig. 6: Local energy dissipation in a vertical plane

Submitted to:
 First International Symposium on Ultrasonic Doppler Methods for Fluid Mechanics and Fluid Engineering, 9-11.
 September 1996, Paul Scherrer Institute, Villigen, Switzerland.

An Overview of Experiments using the Ultrasonic Doppler Method at the Power Reactor and Nuclear Fuel Development Corporation (PNC).

A. Tokuhiko, J. Kobayashi, Y. Ohki, H. Hayashida and H. Kamide
 Oarai Engineering Center, Power Reactor and Nuclear Fuel Development
 Corporation (PNC),
 4002 Narita, Oarai-machi, Ibaraki, Japan, 311-13. T:+81-29-267-4141; F:+81-29-
 266-3867;
 e-mail: tokuhiko@oec.pnc.go.jp

KEY WORDS: *UVP, water, sodium, pipe flow, mixed convective flow, penetrating flow, vertical mixing layer, buoyant jet, stirred vortex flow, flow mapping, two-dimensional velocity field, steady and transient measurement, thermo-acoustic calibration, high-temperature transducers.*

Extended Abstract

The Power Reactor and Nuclear Fuel Development Corporation is engaged in research and development of the Japanese Liquid Metal Fast Breeder Reactor. Within the scope of this program, the Reactor Engineering Section is undertaking various thermal-hydraulic experiments investigating the adequate cooling of the reactor core under normal and transient conditions. One of the major measurement techniques used to study the various convective phenomena is ultrasound Doppler velocimetry. In this extended abstract, we present a brief overview of the experiments in which Metflow's UVP is used as a velocity measurement tool.

1. Investigation of penetrating flow under mixed convection conditions. (COPIES)

The penetration flow of cold coolant into the vertical sub-assembly channels under mixed convection conditions in the conventional design of the LMFBR has been investigated. A simplified schematic is shown in Figure 1. The phenomenon occurs under operating conditions when the natural convection-driven cold flow is such that it penetrates a vertical channel in which there is upward forced-flow of warmer coolant. This situation is subsequently of significance to the natural convection head that determines flow through the reactor core. In the present experiment, we measured the penetration flow into a simulated vertical channel and compared this with temperature measurements taken at several locations. First, since the temperature and velocity signals were qualitatively very similar, temperature measurements were deemed sufficient in order to identify penetration flow. An experimental correlation describing the penetration depth based dimensionless numbers characterizing the operating conditions was derived. Secondly, we are presently investigating the nature of the penetrating flow itself which appears to be determined by a local balance of inertial and buoyant (turbulent) flows. Figure 1 shows the schematic and one typical result.

2. Investigation of jetting flow of one cold jet surrounded by two hot jets. (THERMAL STRIPING)

Thermal striping refers to the phenomenon of thermal stresses induced on reactor components and structures as a result of contact with random streams of poorly mixed cold and hot coolant. One example is the above-core structure from flow of hot/cold streams coming out of the core in a LMFBR. Since the thermal fatigue of such components and their locations are generally known, understanding the thermal mixing (or non-mixing) of buoyant and forced-flow jets is important to the safe design of the reactor. An experiment in water consisting of UVP measurement of a cold planar jet surrounded by two hotter jets is being conducted. An analysis of preliminary data has been done with a traversing thermocouple array and the UVP. Additional 2D and 3D measurements with an ultrasound probe array are underway. One sample result from preliminary measurements and a schematic of the experiment are shown in Figure 2.

3. US-transducer testing in pipe flow in sodium; measurement of transient.

A high-temperature, ultrasound transducer development program for use in sodium is being undertaken at PNC. A simple vertical pipe flow within a sodium loop facility is used as the testbed for various transducer designs. Velocity measurements are being taken with the UVP and indicate that with a sufficient concentration of *tracer* impurities flowing with the sodium, velocity profiles can so far be measured at 300°C. Additional tests at higher temperatures will be performed. Furthermore, we have demonstrated that the UVP can adequately follow a pump-coastdown in our experimental loop. A schematic and one sample result is given in *Figure 3*.

4. Study of vortex dynamics in water.

In a FBR, the entrainment of cover gas situated above the free surface, into the circulation loop is of concern, since the ingested gas may cause operational transients inside the reactor core's flow channels. One recognized entrainment mechanism is by vortices generated in the vicinity of protruding structural components (out of the free surface); that is, sufficiently *energetic* vortices may ingest cover gas and transport this into the circulating flow loop. In a basic experiment investigating the liquid velocity field associated with a vortex generated by stirring or draining a given volume of fluid, the UVP is used as the measurement tool. *Figure 4* shows the experimental apparatus and a sample preliminary result.

5. Convective heat transfer in 4 sub-channel and 37-pin bundle geometries

In convective heat transfer of coolant flow through tube bundles, the existence of flow blockages poses safety questions. Additionally, if the blockage is porous and participates in the heat transfer process, the safety criteria may be different than when the blockage is impermeable. *Figure 5* shows representative schematics of two ongoing convective heat transfer experiments in which there is a flow blockage in the flow path. The 4 sub-channel experiment focuses on the 4 *sub-channels* defined by a triangular flow channel (cross-section) with four (partial) pins and a blockage in the central region. The objective here is to measure the *local* convective heat transfer within these 4 sub-channels. In the second experiment, the *global* flow characteristics of a 37-pin bundle, enclosed in a hexagonal vertical channel (the full-scale geometry of the 4 sub-channel counterpart), is being investigated with the blockage located along one face of the hexagon (see shaded area). Each of the 37-pins additionally has a wire-spacer wound along its length in order to promote *swirling* flow. This flow and that around the blockage are being investigated by both a laser Doppler anemometer (LDA) and a UVP velocimetry. One example UVP velocity profile of flow above the blockage is presented.

6. Inter-wrapper flow (IWF) and heat transfer

In the present design of the FBR, the fuel pins of the reactor are placed inside a hexagonal enclosure conveniently called a *wrapper can*. A large number wrapper cans in turn comprise the reactor core. When thermal energy is transported out of the core by the coolant, it exits into an upper volume called an upper-plenum. Here the hot fluid can be cooled by heat exchangers (DHX, liquid-to-liquid) and may flow back to a lower plenum beneath the core. It has been shown that, under certain thermal-hydraulic conditions, the inter-wrapper convective heat transfer contributes a significant amount to the heat removal capability of the reactor's cooling system. This has been attributed to the inter-wrapper flow (IWF); that is, convective heat transfer amongst the wrapper cans. In order to quantify convective cooling by IWF, a sector model of the relevant geometry is being constructed. A top view and a representative side-view is shown in *Figure 6*. It is our objective in this experiment to use the UVP for: 1) local measurements, 2) cross correlational measurements and 3) regional, 2D and 3D, UVP measurements.

Figure 1a) Schematic of COPIES test section with TCs and UVP-TDX. Cold liquid flows from colling box to vertical channel which has upward, heated flow. b) Example velocity profile of penetrating flow.

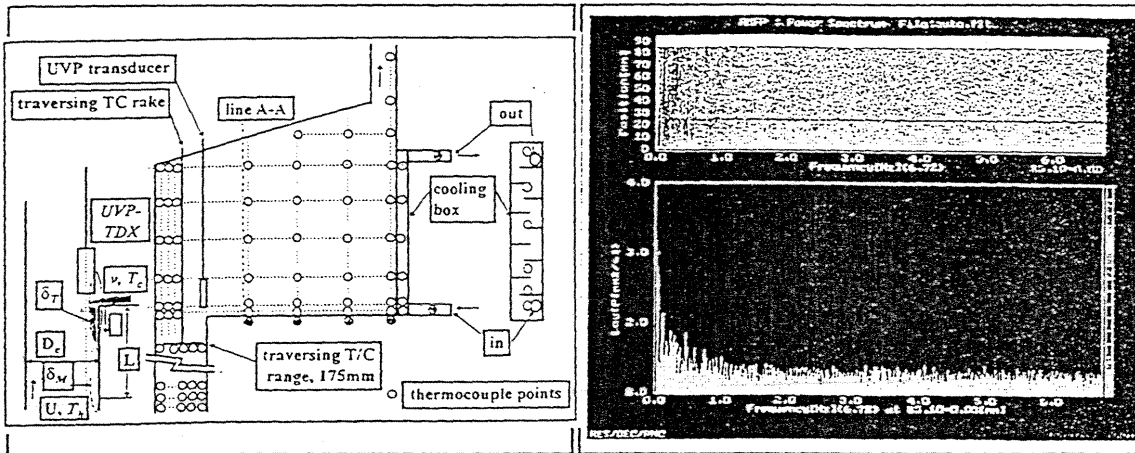


Figure 2a) Schematic of Thermal Striping facility. Three jets flow from central exits; Front window is approximately the measurement region. b) Example average velocity profile with standard deviation.

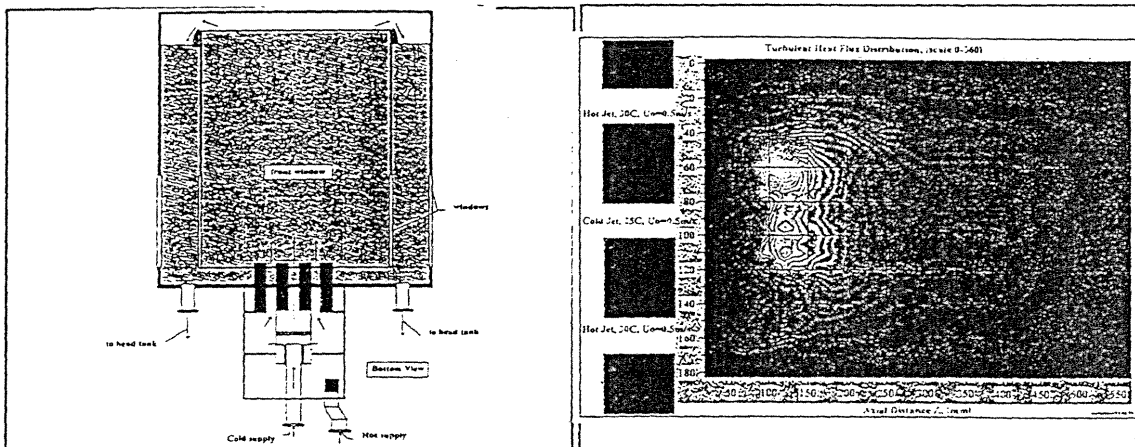


Figure 3a) Schematic of pipe-low in sodium (upward) with high-temperature TDX to be tested. b) Example velocity profiles at three different flowrates and specified sodium and cold-trap temperatures respectively. Solid line is the approximate turbulent 1/7th profile.

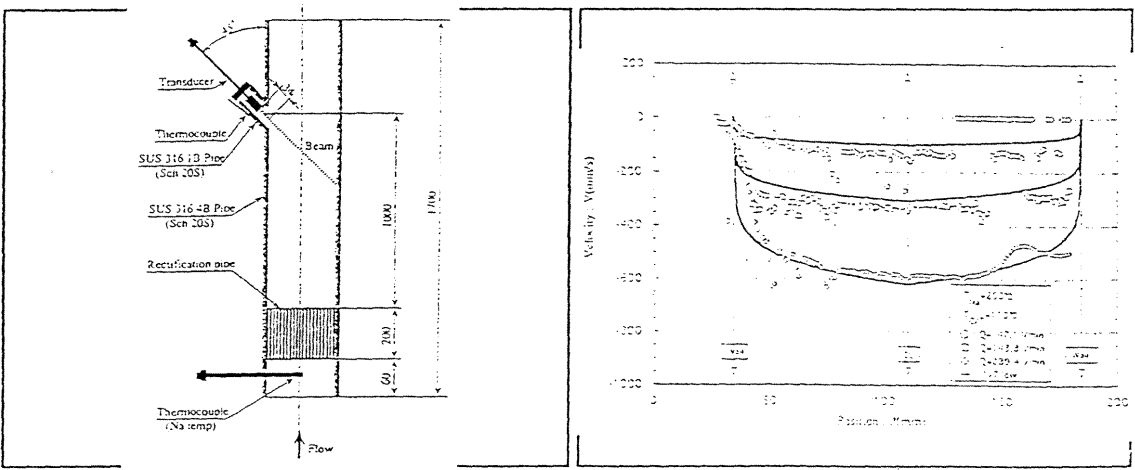


Figure 4a) Schematic of vortex apparatus with multi-probe arrangement. b) Example velocity profile.

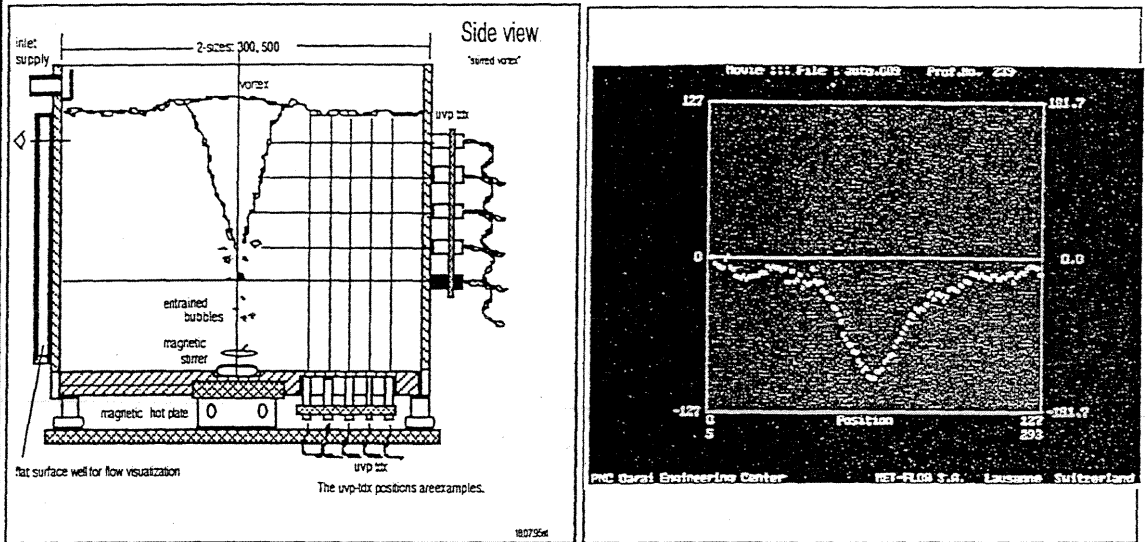


Figure 5a) Isometric view of both the 4-subchannel and a segment of the pin-bundle with wire-spacers, as well as a cross-sectional view of the 37-pins with a blockage. b) Example velocity profile of the wake region above the blockage.

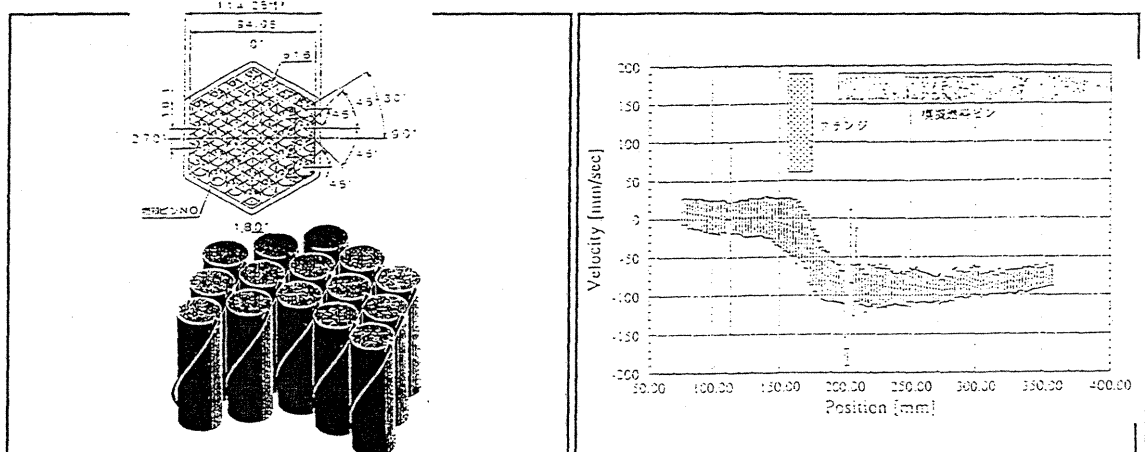
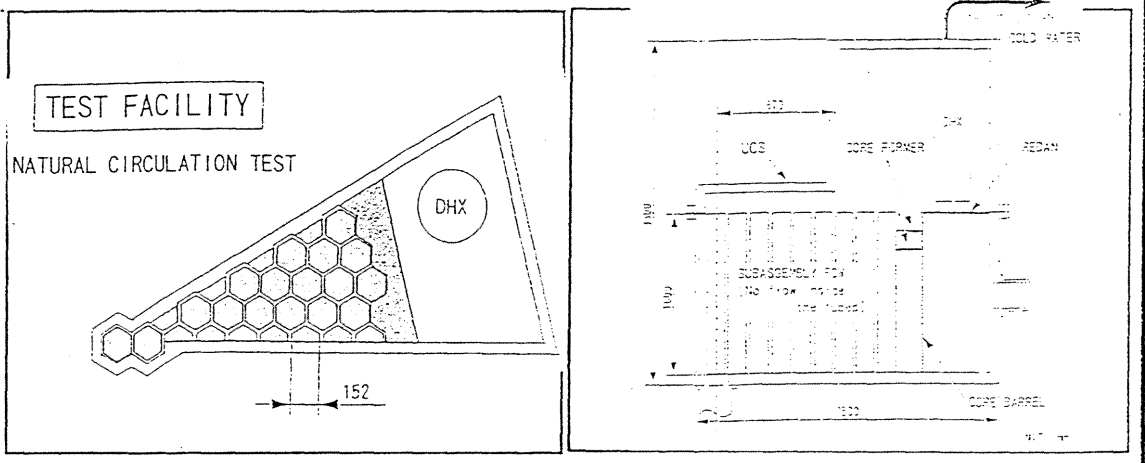


Figure 6 Top-down view of the sector and a schematic view of the IWF test apparatus for natural circulation tests. There is another arrangement for forced circulation. The UVP will be used in various regions



1. ISUD
 1st International Symposium on Ultrasonic Doppler Methods
 for Fluid Mechanics and Fluid engineering
 September 9-11, 1996
 Paul Scherrer Institut, 5232 Villigen PSI, Switzerland

**ACOUSTIC DOPPLER VELOCITY PROFILERS: APPLICATION TO
 TURBULENT FLOW IN HYDRAULIC OPEN CHANNEL AND LAKES**

U. LEMMIN and T. ROLLAND

Laboratoire de recherches hydrauliques
 Ecole Polytechnique Fédérale de Lausanne
 CH-1015 Lausanne, Switzerland

ABSTRACT

Velocity and turbulence are important hydrodynamic parameters. Consequently, many instruments, working on a variety of principles, have been developed for their measurement. Among them the acoustic velocity profiler (ADVP) has a unique combination of advantages:

- it can take instantaneous complete velocity profiles with a resolution of turbulence scales.
- it is non-intrusive
- it can work reliably in the presence of sediment transport.

We have tested its feasibility for hydraulic laboratory research [2,3] based on hardware systems and signal processing algorithms which we have developed and improved since. Promising results were found despite some recent comments by [7] to the contrary.

1. ADVP application in open channel flow

1.1 Monostatic ADVP

In a monostatic mode, one single acoustic transducer is used to emit and receive acoustic waves. In order to verify the validity of the measurements made by a monostatic ADVP, the results obtained are compared either to proven measurement techniques and to the known distribution laws for the flow parameters. Investigating stationary open channel flow over rough and smooth beds good agreement was found for all laws for the distribution of mean velocities and turbulence parameters [8,5]. It has thus been shown that the ADVP is a bona fide research tool capable of resolving turbulence scales in open channel flow. Its application to steep open channel flow is described in [10].

However the determination of turbulence parameters with this system is limited to uniform or very gradually varying flow. It is impossible to apply it to more rapidly accelerating or decelerating flows which are often encountered in rivers and lakes.

1.2 Bistatic ADVP

Recently we have therefore extended the ADVP-technique to a system which is capable to determine instantaneous profiles two or more velocity components with resolution of turbulence scales.

A pulse of sound waves is emitted only from a central transducer (Fig. 1a): As in the monostatic mode this transducer can also work as a receiver of the backscattered sound waves. Additional transducers placed around the emitter will serve as receivers for the backscattered waves coming from same pulse of sound waves. For convenience and ease of signal extraction, these receivers which have to be inclined towards the central emitter are normally placed symmetrically around the emitter. In that case any sound waves which are backscattered from a

certain volume in the central beam will have the same time of flight to all the surrounding receivers. One pair of opposingly inclined receivers is sufficient for the determination of two instantaneous velocity components. An additional pair in a plane perpendicular to the first one will allow to determine all three velocity components instantaneously. For simplicity this system is aligned here with the direction of the mean flow (the along axis flow in an open channel). In this case the two velocity components under consideration are the horizontal velocity u and the vertical velocity v . The emitted sound beam from which the velocity profile is determined is vertical with respect to the channel bottom. This is an advantage over the monostatic system where the profile has to be taken along an inclined sound beam. Details about the signal processing and the determination of the instantaneous velocities are given in [8].

For the evaluation of the possibilities and limits of this system, the measurements made in an open channel with smooth bed with the bistatic ADVP are compared with those obtained simultaneously by a monostatic ADVP and also with available distribution laws for uniform flow conditions. For the two components of the mean velocity, excellent agreement between the two systems is found (Fig. 1b); the profiles correspond to those predicted for open channel flow [5]. For the turbulence parameters, good agreement is found for distribution of the variance of the horizontal and the vertical components as well as for the Reynold's stress profiles (Fig. 1c) over most of the water depth. As with all measuring techniques, surface roughness prevents reliable measurements near the free surface. Near the channel bed the results from the bistatic ADVP tend to diverge from the theoretically predicted profiles. This is mainly due to the large Doppler angle and the unfavourable volume size in this region. Improvements can be expected from beam localization of the emitter beam and a change in transducer geometry.

The above results show that the bistatic ADVP has good potential in turbulent open channel flow investigations. In particular, its capability to take instantaneous simultaneous profiles of two velocity components greatly reduces the measurement time. Furthermore it gives the possibility to obtain insight into flow phenomena which have been difficult to investigate before. As an example we present the flow around a cylinder (Fig. 2). The mean flow pattern has been obtained with nine measurements only. Turbulence profiles have identified zones of accelerated and decelerated flow around the cylinder [1]. The second example shows the distribution of the instantaneous velocity vectors in uniform flow after the mean velocity vectors have been subtracted (Fig. 3). When these vectors are plotted for the highest resolution (profiles taken at 1000 Hz, averaged over 16 consecutive profiles) the temporal and spatial variability but also some structure is visible. This structure becomes more evident when the same data are averaged over 128 consecutive profiles. It is seen that the whole water column is organized in a sequence of alternating upward and downward jets. This may be the result of secondary flow structures [9]. We are further investigating this aspect.

2 ADVP applications in lakes

We have applied the monostatic ADVP to stratified geophysical flow in the Lake of Geneva. In the first study the transducer was gimbals mounted to point vertically upwards and placed on the lateral slope of the lake bottom near the depth of the thermocline [4]. In the presence of critical internal waves a complex profile of the vertical velocity was observed (Fig. 5). The shear which can be calculated from this profile indicates that the instabilities cannot be explained by a thermal structure. Instead, a particle laden turbidity current must be present. The vertical variability of the intensity of the backscattered signal supports this conclusion.

In the second study the instrument was lowered on a cable with constant speed (10 cm s^{-1}), clamped to a high resolution CTD which provided information on the temperature profile and a check on the fall velocity via its pressure sensor. The simultaneous multigate profiling capacity and thus the possibility to establish short time series (of about 10 s duration) at any depth give new insight which cannot be obtained with any other instrument. The vertical velocity fluctuation amplitude is directly linked to the mean stratification in the water column. In layers of strong temperature gradients, even if they are only several cm thick, the amplitude of the vertical velocity fluctuations is strongly reduced. The turbulence intensity is larger and more

homogeneous below the thermocline (the layer 5 to 15 m) in the constant N layer. Turbulence scales have been calculated from the vertical velocity data and the corresponding N-profile (Fig. 4b). In the thermocline of Lake Geneva the vertical turbulence scale is about 0.5 to 1 m. In the other parts of the water column (down to about 45 m depth) the turbulence appears closer to isotropic and the turbulence scale is about 2 m or more. These scales correspond well to the Thorpe scales which have been obtained from instabilities of the temperature profiles.

3. Conclusions and outlook

The Acoustic Doppler Velocity Profiler has been evaluated for its use in boundary layer flow conditions in open channel flows and in the field. From the analysis it is apparent that the ADVP hardware and the software algorithms applied to the extraction of the velocity vector are well suited for the analysis of turbulent flow characteristics. Without the need for a calibration procedure, mean vertical and horizontal water velocities and hydraulic parameters are effectively measured by the ADVP. Measurements can be taken rapidly with a degree of accuracy better than most conventional in situ sensors which at the same time can significantly modify the local flow conditions by intruding into the flow. The ADVP is easier to operate than laser velocimeters and essentially provides instantaneous velocity profiles instead of point measurements. Compared to existing instrumentation, the ADVP profile measurements take only a small fraction of the time for the same resolution. Furthermore, since ADVP profile measurements are taken simultaneously under the same flow conditions, the resultant profiles are found to be smoother than those taken in sequence by existing instruments.

In rivers and lakes, where typical values of sampling frequencies needed for correctly studying turbulence are about 10 Hz, ADVP systems of the type discussed here seem to be the most appropriate instrument. In this context the nature and the effect of the acoustic targets should be further investigated. Indeed, the presence of particles in low to medium concentration in the flow does not influence the acoustic system at all, a great advantage over the LDA. Therefore the pulse-to-pulse coherent technique presented here appears to be a rather promising tool in field studies. In the laboratory the presence of particles, its concentration and the variance may be investigated by exploiting the backscattering intensity information provided by the ADVP at the same time. This information, combined with the instantaneous velocity profile may be used for detailed studies of sediment transport.

In conclusion, the high frequency ADVP is a valuable tool for hydraulic research. More sophisticated techniques for beam focalization, data acquisition and signal processing may have to be further investigated before the optimal configuration and the range of application of a high frequency ADVP designed for hydraulic research can be determined. These developments or beam scanning techniques can extend the capabilities of the acoustic systems to further the understanding of the turbulent water flows.

References

- [1] Julisjanto, B. *Thèse EPFL*, Lausanne. (1996, in preparation)
- [2] Lhermitte, R. and U. Lemmin *Geophys. Res. Letters*, **17** (1990), pp 1549-1552.
- [3] Lhermitte, R. and U. Lemmin *J. of Atmos. and Ocean. Technology*, **11** (1994), pp 1295-1308.
- [4] Lemmin, U. and R. Jiang Proceedings IUTAM symposium on physical limnology, Broome, Australia, (1995) pp. 115-124.
- [5] Lemmin, U. and T. Rolland submitted to *J. Hydr. Eng., ASCE* (1995)
- [6] Nezu, I. and W. Rodi *J. Hydr. Eng., ASCE*, **112** (1986) pp 335-355.
- [7] Nezu, I. and H. Nakagawa *Turbulence in open-channel flows*. (A.A. Balkema, Rotterdam, 1993)
- [8] Rolland, T. *Développement d'une instrumentation Doppler ultrasonore: application aux écoulements turbulents en hydraulique*. (1994) Thèse EPFL N°1281, Lausanne.
- [9] Rolland, T. and U. Lemmin (1996), In preparation.
- [10] Song, T., W.H. Graf and U. Lemmin *J. Hydr. Res.*, **32** (1994), 861-876

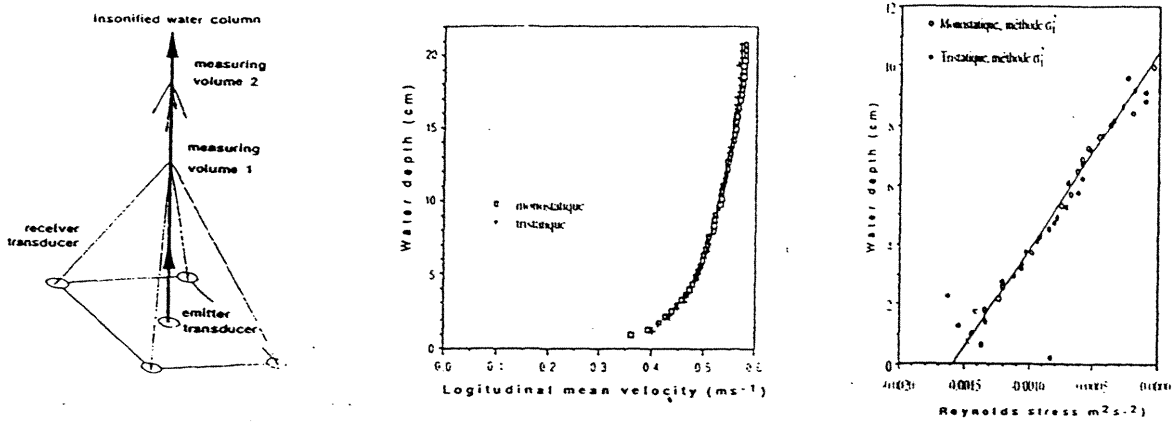


Fig. 1 Bistatic Acoustic velocity profiler: a: Measurement layout; b: Horizontal mean velocity profile; c: Reynold's stress profile.

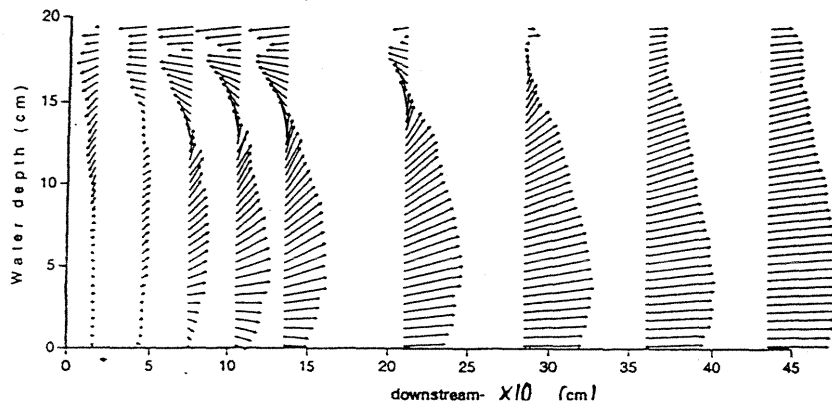


Fig. 2 Mean flow behind a vertical cylinder. Cylinder at $x=0$ cm, diameter $D=15$ cm; $Re=87000$

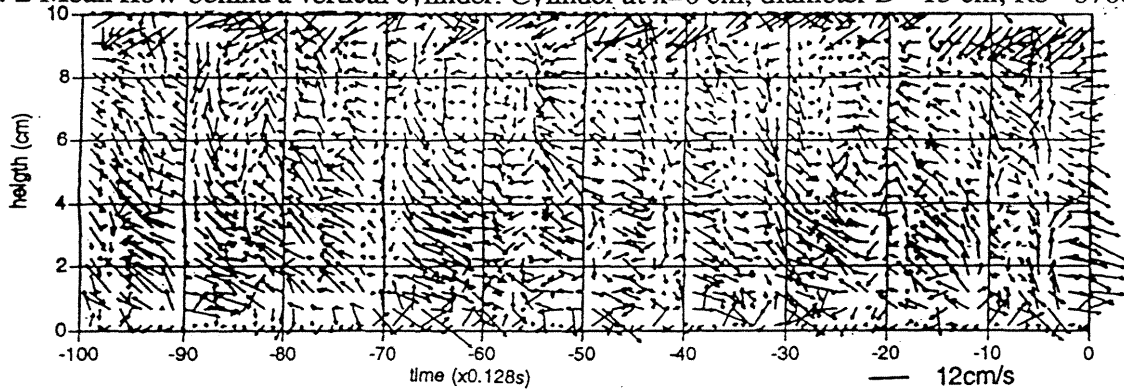


Fig. 3 Time series of 2D velocity fluctuations

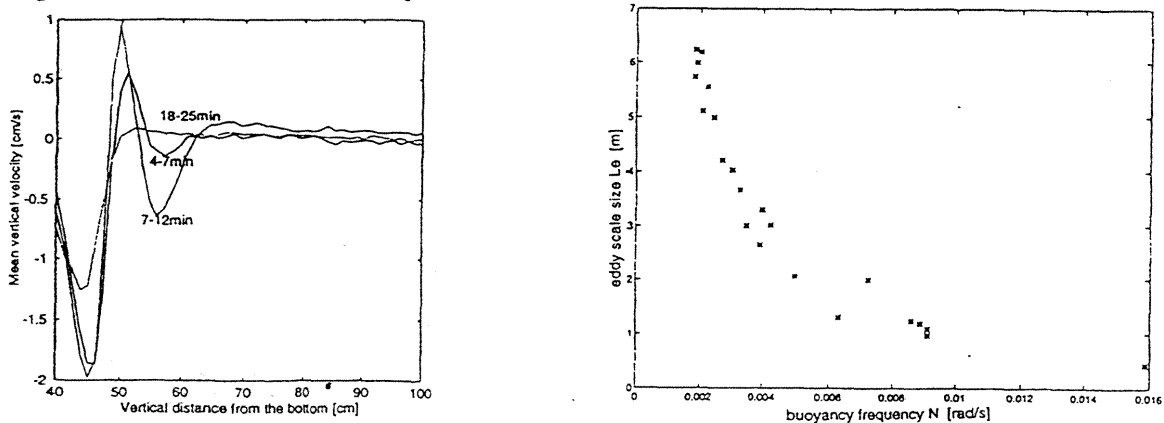


Fig. 4 Results from the stratified Lake of Geneva (taken in July); a: Mean vertical profiles in the bottom boundary layer (depth 29 m) b: Turbulence scales in the open water in the depth range: 2 m to 45 m.

1. ISUD

1st International Symposium on Ultrasonic Doppler Methods
for Fluid Mechanics and Fluid Engineering

September 9-11, 1996

Paul Scherrer Institute, 5232 Villigen PSI, Switzerland

Simultaneous Measurement of Liquid Velocity and Interface Profiles of Horizontal Duct Wavy Flow by Ultrasonic Velocity Profile Meter

Hideo NAKAMURA, Masaya KONDO and Yutaka KUKITA

Japan Atomic Energy Research Institute (JAERI)
2-4 Shirakata Shirane, Tokai, Ibaraki 319-11 JAPAN

ABSTRACT

A simultaneous measurement of the liquid velocity and interface profiles was performed for stratified-smooth and wavy flows in a horizontal duct using a Ultrasonic Velocity Profile Monitor (UVP) Model X-1. Both parameters were successfully measured for the wavy flows with periodical interfacial waves when the influences of multiple reflections of ultrasonic pulses between the gas-liquid interface and the channel bottom was avoided well. Good comparison with the liquid level and velocity profiles measured by other methods was obtained for the smooth-stratified flow. The wavy flow data agreed well with the theoretical prediction of the liquid velocity profile around solitary waves.

1. Introduction

Liquid-phase velocity profile below interfacial waves in horizontally-stratified gas-liquid two-phase flows affects the interfacial exchanges of mass, momentum and heat, and the growth of the interfacial waves. For the cases of practical importance, such as stratified-wavy two-phase flows, it is generally difficult to predict theoretically or measure experimentally the liquid-phase velocity profile that is coupled with the wavy interface profile. The theoretical velocity profile with the wavy interface profile is available only for limited cases like infinitesimal and solitary waves.

The UVP is one of the promising instruments for dynamic measurement of the velocity profile of the liquid flow. However, the use of the UVP in wavy flows has encountered difficulties by the reflection of the ultrasonic pulses at the gas-liquid interface. In JAERI, the UVP measurement not only of the velocity profile, but also of the interfacial wave profile, was successfully performed in the horizontal wavy flow experiments. This paper describes the application method of the UVP on the wavy flows and the obtained results.

2. Experiment

2.1 Test Facility

Figure 1 shows a schematic view of the test facility. The horizontally-leveled test section (a 0.1 m-wide, 0.7 m-high, 28.3 m-long duct) is made primarily of transparent acrylic resin to visually observe the flow. Demineralized-water in a 10-m³ outlet tank (not shown)

is recirculated by pumps to the bottom of inlet tank. Water flow rate is measured by orifice meters. A constant water flow rate of $4.17 \times 10^{-3} \text{ m}^3/\text{s}$ was used for the present experiment. The liquid level in the outlet tank was kept lower than the bottom of the test section to attain free out-flow due to the gravity. The liquid level at the test section exit was thus close to the critical level. A wave generator in the inlet tank was used to generate periodical interfacial waves to compare the data with the theoretical prediction. Stratified-smooth flow with no interfacial waves appeared when the wave generator was stopped. The experiments were performed under atmospheric-pressure, room-temperature conditions.

2.2 Instrumentation

Both the velocity profile and liquid level were measured by the UVP. The UVP sensor was inserted from the bottom of the acryl-made test section facing towards upstream with an angle of 10° from vertical. The top surface of the UVP sensor was placed to be flush with the bottom of liquid stream. The liquid level was measured also by an electrical resistance method, simultaneously with the UVP, using a pair of parallel-wire electrodes (0.09 mm outer diameter, 60 mm apart) made of platinum-coated tungsten. The electrodes were mounted vertically on a plane perpendicular to the flow axis, in which the top of the UVP sensor was located. The liquid level and velocity profile at the same location were measured simultaneously.

Polystyrene beads with a density of 1.01 and diameters of 0.1 to 0.5 mm were used as reflectors of ultrasonic pulses. The polystyrene beads were injected with water through a nozzle at 1.0 m upstream of the UVP sensor as shown in Fig. 1.

The gas-liquid interface totally reflects ultrasonic pulses back towards the test section bottom. Multiple reflections between the interface and the test section bottom as shown in Fig. 1 was observed to occur inherently. Thin (~ 2 mm) butyl rubber sheet^[1] with many tiny dips made by needle tips was placed on the bottom inner wall to absorb the ultrasonic pulses. However, the ultrasonic pulse after one time reflection at the test section bottom was still strong enough to cause an overlap of the echo signal onto that from the next pulse. The intensity of the echo from the remaining pulse after the second reflection was negligibly small for signal processing. Therefore, the "maximum measurement depth" was chosen to become more than twice as large as the liquid level to give a long time interval between two pulses. Bit manipulation of the measured data was necessary to expand the velocity range.

Both the liquid level and velocity profile were measured also by using a flow visualization technique composed of the laser-sheet lighting of polystyrene beads as reflectors for the UVP. Two-dimensional (2D) NTSC video pictures of the flow with beads were taken simultaneously with the above level and velocity profile measurements. The velocity profile for smooth-stratified flow was obtained by the "Current" particle tracking velocimetry (PTV) (KANOMAX Inc.) that employs a four-points particle tracking method.

3. Measured Results and Discussion

Figure 2 compares the UVP velocity profiles with the liquid level data for a smooth-stratified flow. The UVP velocity profile data was found to have a dip at the liquid level of 120 mm. Echoes from a ultrasonic pulse usually propagate isotropically in water. At the gas-liquid interface, however, both the pulse and echoes would reflect together towards a certain direction, causing such a dip in the velocity profile. The direction of the reflected echo and ultrasonic pulse depends on the orientation of the interface. The UVP velocity data appearing above the liquid level in Fig. 2 are based on echoes from the ultrasonic pulse after

one reflection at the gas-liquid interface. These data may be valuable when the path of the reflected pulse can be identified.

Agreement between the UVP data and liquid level data was good when the sound velocity of 1442.5 m/s was used instead of 1479.0 m/s for water at temperature of 17 °C. A large fluctuation appeared in the transient velocity profile data as typically shown in Fig. 2, probably because of a turbulent structure in the flow at the Re number of 3.2×10^4 .

Figure 3 compares the average UVP data for the smooth-stratified flow with the average velocity profile obtained by the "Current" PTV. The horizontal bars in Fig. 3 are the standard deviation σ of the UVP data. A large fluctuation in the UVP data due probably to the turbulence in the flow resulted in a large value of σ . The average PTV data was obtained from 1) piling up several 2D data each of which contains velocity vectors for tracked particles, 2) interpolating these randomly distributing velocity data onto the 2D velocity matrix (31×31) points using continuity equation, and 3) sum-averaging the same-elevation data of the matrix to obtain vertical velocity profile shown in Fig. 3.

The UVP data agreed fairly well with the PTV data except those near the channel bottom where the PTV constructed the 2D velocity distribution using small number of tracked particles. The uncertainty in the PTV increases as the number of particles effective for construction of the velocity distribution decreases.

Figure 4 indicates a typical result of the wavy flow experiments. Theoretically-obtained velocity profiles of the solitary wave^[2] propagating with a certain wave celerity^[3] are compared with the UVP data. The theoretical value is summed with the average velocity distribution obtained from the previous smooth-stratified flow experiment. The agreement of the data with the theoretical prediction is good, while the measured velocity was always larger than the predicted velocity in the wave above the equilibrium liquid level. The interfacial waves generated by the wave generator in this experiment may be steeper than the theoretical solitary wave. In this comparison, fluctuation in the measured velocity profile appeared again, as in the smooth-stratified flow. The dip in the velocity profile that indicates the location of the liquid level was not so clear in this case as shown in Fig. 4, probably because the interface was more ragged than that for the smooth-stratified flow.

In the wavy-flow experiments, it was difficult to use short measurement range that has large velocity range, because of multiple reflection of the ultrasonic pulses as noted before. The wider UVP velocity range is preferable to study characteristics of the large-size waves, since the liquid-phase velocity profile of the wavy flow depends on the wave amplitude, length and liquid depth.

4. Summary

Both the water velocity and gas-liquid interface profiles of smooth-stratified and wavy flows were successfully measured using the UVP Model X-1. Special cares were taken to reduce the significant influence of reflection of the ultrasonic pulses at the gas-liquid interface. These measured UVP parameters agreed well with the velocity profile obtained by the PTV based on the flow visualization and the liquid level measurement. Wider range of the measuring velocity in shorter data processing time is desirable for an advanced application of the UVP onto large-amplitude wavy flows.

5. References

- [1] P. Tamarkin, Tank Wall Lining for Underwater Sound Use, J. A. S. A. 27-4 (1955).

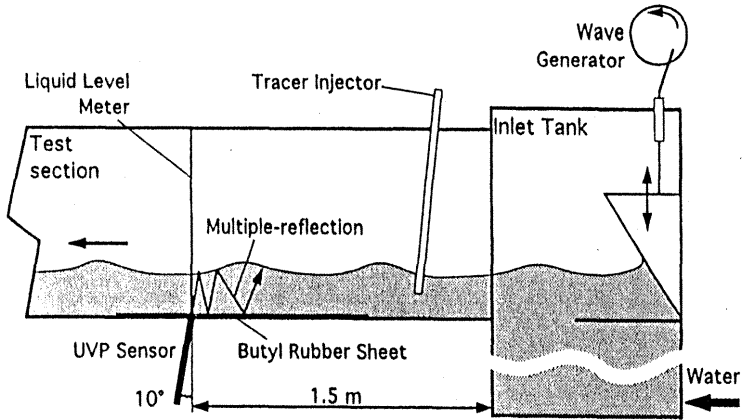


Fig. 1 Schematic of Experimental Setup

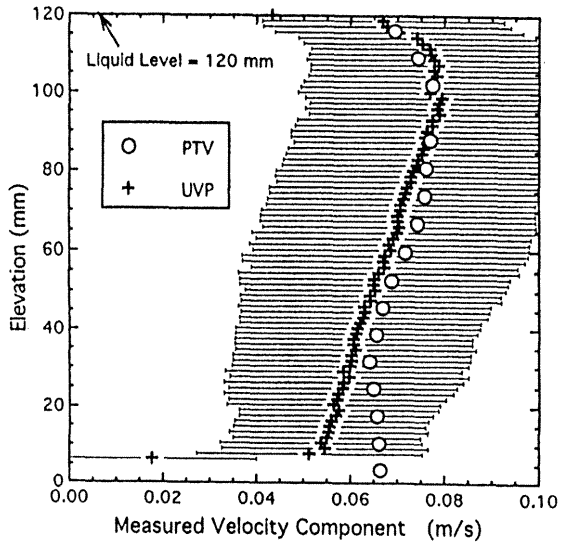


Fig. 3 Comparison of Average Velocity Profiles obtained by UVP and PTV

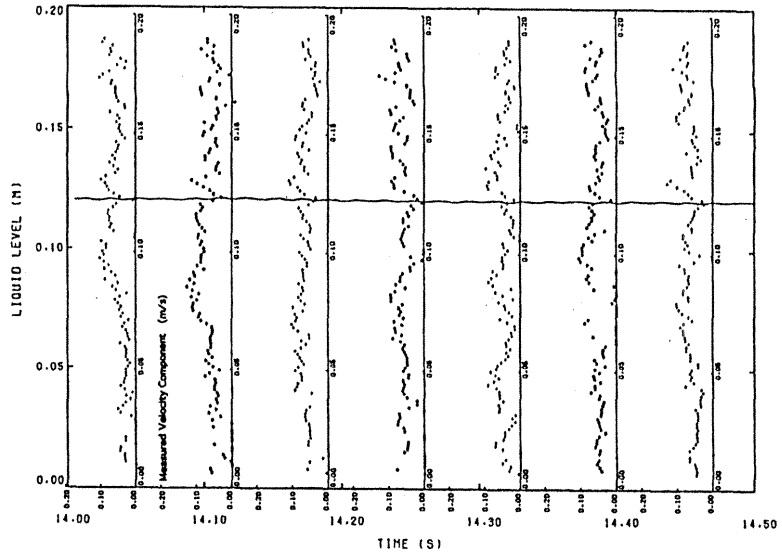


Fig. 2 Comparison of Typical Transient Velocity Profile Data with Liquid Level Data for Smooth-stratified Flow

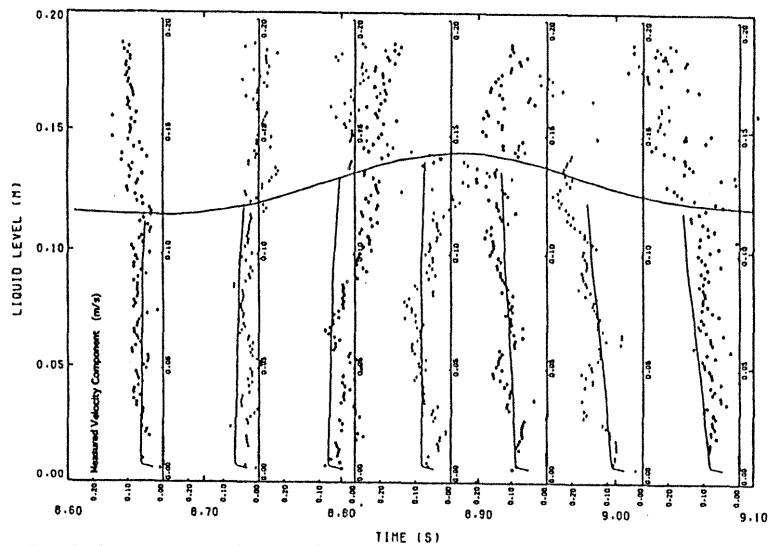


Fig. 4 Comparison of Typical Transient Velocity Profile Data with Liquid Level Data and Theoretical Velocity Profiles for Wavy Flow

- [2] J. McCowan, Phil. Mag., Ser. 5 Vol. 32-7 (1891) 45-48.
 [3] R.L. Wiegand, Oceanographical Engineering, Prentice-Hall, 65-76 (1964).
- Acknowledgment**

The authors are indebted to the experimental team headed by Mr. H. Yamada of Nuclear Engineering Co., Mr. K. Kuni of JAERI for the data analysis using the PTV and Mr. Y. Shimane of ITJ Co. for the UVP data processing.

MEASUREMENT SYSTEM OF TWO-PHASE FLOW USING ULTRASONIC VELOCITY PROFILE MONITOR

Masanori ARITOMI¹, Makoto NAKAJIMA², Shirong ZHOU¹,
Yasushi TAKEDA³, Michitsugu MORI⁴ and Yuzuru YOSHIOKA⁵

1 Tokyo Institute of Technology, 2-12-1 Ohokayama, Meguro-ku, Tokyo, 152 Japan

2 Mitsubishi Heavy Industry Co., 1-1-1 Wadasaki-machi, Hyogo-ku, Kobe, 652 Japan

3 Paul Scherrer Institut, Wurenlingen and Villigen, CH-5232, Villigen, Switzerland

4 Tokyo Electric Power Co., 1-1-3 Uchisaiwai-cho, Chiyoda-ku, Tokyo, 100 Japan

5 Japan Atomic Power Co., 1-6-1 Ohtemachi, Chiyoda-ku, Tokyo, 100 Japan

1. INTRODUCTION

It is one of the most important problem in two-phase flow dynamics to clarify its multi-dimensional flow characteristics. Measurement methods of multi-dimensional characteristics in two-phase flow are classified into two types; contact and non-contact. The contact type sensor such as an electric probe is inserted in a flow and thus disturbs it, so that the measurement accuracy is still not satisfactory. There are measurement methods based on ultrasonic, capacitance, conductance, optics and radiation in non-contact type methods. Laser Doppler Anemometry based on an optical technique is excellent particularly in space and time resolution. This method requires a long time for measuring a spatial distribution of flow characteristics in a channel. Recently, an ultrasonic Doppler method for velocity profile measurement has been developed for liquid flow measurements by Takeda (1995). It has been approved that this method is a powerful tool in flow measurement. It can measure a local velocity instantaneously as a component in the ultrasonic beam direction, so that a velocity field can be measured in space and time domain.

In this work, a measurement system using an Ultrasonic Velocity Profile Monitor (UVP) has been developed, which can measure simultaneously the multi-dimensional flow characteristics of bubbly flow such as velocity profiles of both gas and liquid phases, a void fraction profile and a turbulent intensity profile. The present measurement system is applied to a countercurrent bubbly flow in a vertical rectangular channel to verify its capability.

2. EXPERIMENTAL APPARATUS

The experimental apparatus was composed of a water circulation system, an air supply system, a test section and a measurement system. Air and water were used as working fluids. The test section was a vertical rectangular channel of 10mmx100mmx700mm made of Plexiglas as shown in Fig.1. The measurement system consisted of the UVP and a personal computer to record and treat data. Water was fed into the upper tank and flowed downward in the test section. Micro particles of nylon powder were suspended in water to reflect ultrasonic pulses. The air supply system consisted of a compressor and a pressure regulation valve. Bubbles were injected from five needles located near the bottom of the test section.

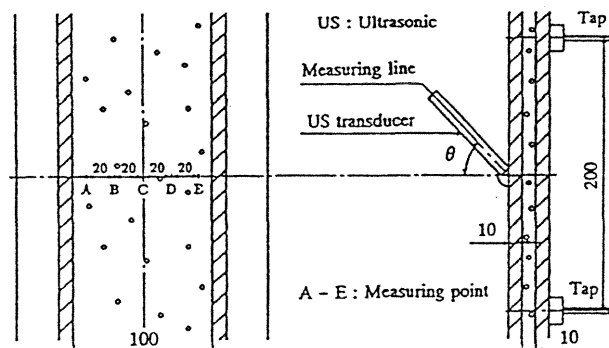


Fig.1 Test section

An ultrasonic transducer was installed on the outside surface of the front wall of the channel with a contact angle, θ , and a gap between the transducer and the wall was filled with a jelly to prevent a reflection of ultrasonic pulses on the wall surface. The hydrostatic head was simultaneously measured as a pressure drop between the pressure taps installed on the side wall using a differential pressure transducer to get an averaged void fraction.

3. MEASUREMENT PRINCIPLE

The working principle of the UVP is to use the echo of ultrasonic pulses reflected by micro particles suspended in the fluid. An ultrasonic transducer takes roles of both emitting ultrasonic pulses and receiving the echoes, that is, the backscattered ultrasound is received for a time interval between two emissions.

The position information, x , is obtained from the time lapse, τ , from the emission to the reception of the echo:

$$x = c\tau / 2 \quad (1)$$

where c is a sound speed in the fluid. An instantaneous local velocity, $u(x)$, as a component in the ultrasonic beam direction, is derived from the instantaneous Doppler shift frequency, f_D , in the echo:

$$u_{UVP} = cf_D / 2f \quad (2)$$

where f is the basic ultrasonic frequency. The UVP specification used in this work is tabulated in Table 1.

Table 1 The specification of the Ultrasonic Velocity Profile Monitor

Basic ultrasonic frequency	4MHz
Maximum measurable depth	758mm(variable)
Minimum spatial resolution	0.74mm
Maximum measurable velocity	0.75m/s(variable)
Velocity resolution	0.75mm/s(variable)
Measurement points	128
The number of profiles	1,024

Since the sound speed of the longitudinal wave is the most fundamental parameter for this method, it is not possible to treat a two-phase medium as a homogeneous single phase medium, because a sound wave experiences multiple reflection among bubbles and its path returning to the transducer cannot be straight.

It is however possible to obtain velocity profiles of liquid phase until the position of the nearest bubble from the transducer. Therefore, the authors attempted to derive information from each individual profiles by analyzing their shapes. 9,216 (1,024x9) velocity profiles per one experimental condition were collected to treat them statistically.

The position and velocity in the ultrasonic beam direction were converted into the horizontal position, y , and axial velocity $u(y)$, respectively by considering the contact angle of the transducer to the wall.

A profile of the probability of data existence, $P_s(y)$ is defined as a ratio of the number of data receiving the echo to the number of total profiles. A probability density function, $P_u(y,u)$, includes the velocity information of both phases. Assuming that each probability density function of both phases can be expressed by a normal distribution,

$$N[\bar{u}, \sigma^2](u) = \frac{1}{\sqrt{2\pi\sigma^2}} \exp\left[-\frac{(u - \bar{u})^2}{2\sigma^2}\right] \quad (3)$$

the probability density function of mixture velocity is given by

$$P_u(y,u) = \varepsilon(y)N[\bar{u}_G(y), \sigma_G^2(y)](u) + (1 - \varepsilon(y))N[\bar{u}_L(y), \sigma_L^2(y)](u) \quad (4)$$

where \bar{u}_G , \bar{u}_L , σ_G and σ_L are average velocities and standard deviations of both phases respectively, $\varepsilon(y)$ is the probability of bubble existence. These five variables are calculated numerically and iteratively by the least squares method.

Since the ultrasonic pulse is reflected at the interface as long as a bubble exists, the bubble velocity can be always detected as an interface velocity. On the other hand, the ultrasonic wave is not reflected in water if a micro particle does not exist therein. As a result, water velocity is not always measured in the profile. Therefore, it is necessary to revise the probability of bubble existence as follows:

$$\kappa(y) = P_s(y) \varepsilon(y) \quad (5)$$

where $\kappa(y)$ is called the probability of bubble data existence in this work.

An example of the probability density function obtained from the UVP data is

representatively shown in Fig.2. It is difficult to derive the genuine information under high void fraction conditions because the multiple reflection of an ultrasonic pulse is induced by bubbles. In addition, very little information on bubble velocities can be obtained at very low void fractions. To solve these problems, several data processing programs were developed in this work in order to eliminate wrong data induced by a multiple reflection under conditions of high void fraction and to select only the profiles including bubble velocities under conditions of very low void fractions. These programs were based on the fact that positive velocity data means bubble upflow velocity and negative velocity data does water downward one because of countercurrent bubbly flows dealt with in this work.

It is clarified that the both \bar{u}_g and \bar{u}_l in the probability density function velocity does not change even if the original data are treated with these program. Therefore, they were used only to get \bar{u}_g and σ_g in the probability density function of bubble velocity. Figure 2 demonstrates a comparison of a typical probability density function of mixture velocities calculated by the above-mentioned procedure with experimental results.

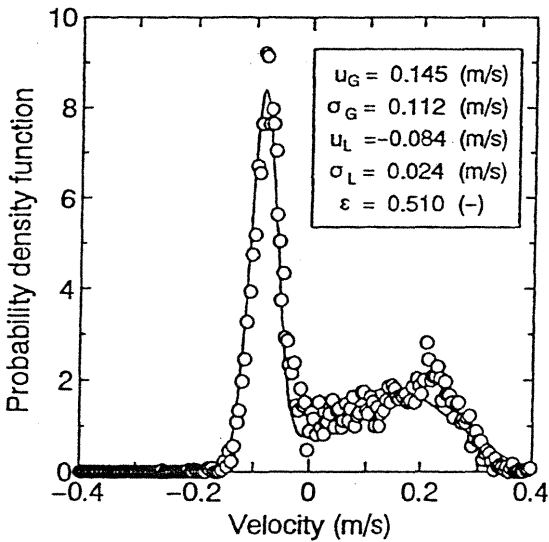
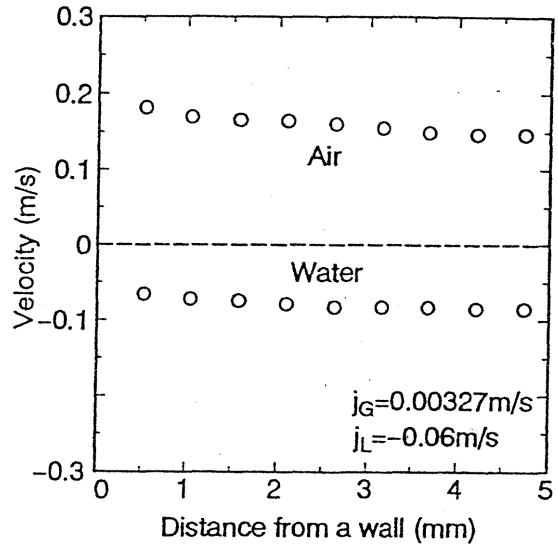


Fig.2 Typical probability density function

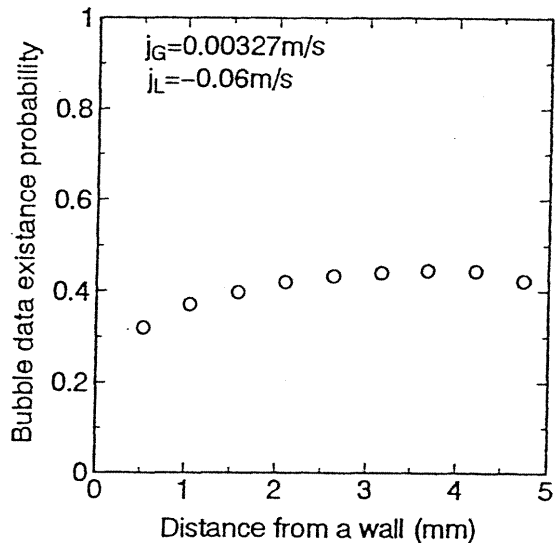
4. MEASURED RESULTS

The developed measurement system was applied to countercurrent bubbly flows channel. Figure 3 (a) and (b) shows measurements of

velocity profiles in both phases and a probability profile of bubble data existence. Velocities of both phases are not zero on the wall because the ultrasonic pulse is emitted at an angle with respect to the channel wall and its diameter of 5mm, which thus induces meaningful error of velocity measurements near the wall. However, this uncertainty is not a feature for two-phase flow measurement but appears for the velocity profiles measured for a single phase flow with the UVP.



(a) Velocity profiles in both phases



(b) Probability profile of bubble data existence
Fig.3 Measured flow characteristics

The probability of bubble data existence means that a bubble exists in an ultrasonic pulse path when the pulse is emitted, and is

closely related to the void fraction. The bubble size, position and configuration cannot be known directly from UVP measurements. It is supposed that the bubble size and configuration are at random and that they are statistically uniform at the whole points in the channel. Assuming that the local void fraction is proportional to the local probability of bubble data existence and that the proportional constant (the conversion factor), k , is uniform in the channel since it is dependent on bubble size and configuration, the average void fraction is expressed by

$$\langle \alpha \rangle = k \int_A \kappa dA / A = k \langle \kappa \rangle . \quad (6)$$

Since the average void fraction was obtained by measuring the hydrostatic head, the conversion factor, k , was calculated by substituting measured average void fraction, $\langle \alpha \rangle$, and average probability of bubble existence, $\langle \kappa \rangle$ into Eq.(6). Then, local void fraction, $\alpha(y)$, is given by

$$\alpha(y) = k \kappa(y). \quad (7)$$

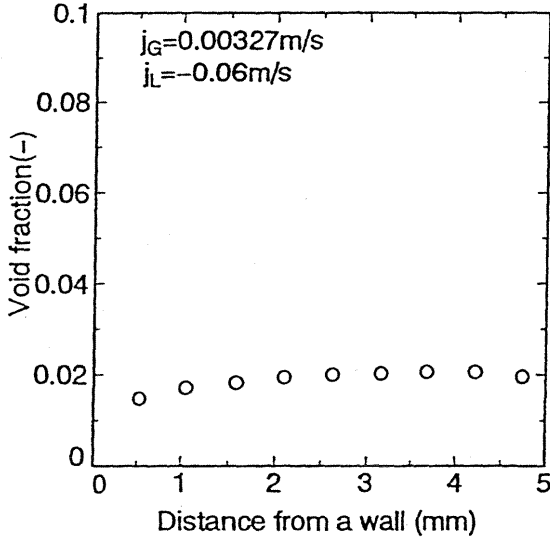


Fig.4 A typical void fraction profile

Figure 4 shows a typical void fraction profile obtained by this method. Furthermore, the average volumetric flux of bubble, $\langle j_G \rangle$, is

$$\langle j_G \rangle = \frac{\int_A \alpha u_G dA}{A} = \frac{k \int_A \kappa u_G dA}{A}. \quad (8)$$

The conversion factor can also be calculated by substituting $\kappa(y)$ and $u_G(y)$ obtained by experiments and $\langle j_G \rangle$ given from the experimental condition into Eq.(8). The accuracy of the average void fraction evaluated by this procedure is within 20% error.

In this work, turbulent intensity is defined as a standard deviation of water velocity fluctuation which is a continuous phase, σ_L . The standard deviation profile in the channel can be calculated from Eq.(2). Typical results of a water single flow and a countercurrent bubbly flow are shown in Fig.5. Local velocities were however measured not at a point but on the area because of an ultrasonic beam diameter of 5mm, so that the absolute value of the standard deviation in a water phase is not significant. Hence, the standard deviation ratio of a countercurrent bubbly flow to a water single phase flow is selected as two-phase multiplier of turbulent intensity, $\sigma_{LTPF} / \sigma_{LSPF}$ in this work. The results are also shown in Fig.5. In general, turbulent intensity in a bubbly flow is larger than that in liquid single phase flow because bubbles agitate the flow. It can be seen from the figure that $\sigma_{LTPF} / \sigma_{LSPF}$ is larger than unit and that the two-phase multiplier becomes larger with going toward the center of the channel.

REFERENCE

Takeda, Y., Velocity Profile Measurement by Ultrasonic Doppler Method, *Experimental Thermal and Fluid Sci.*, **10** (1995) 444-453.

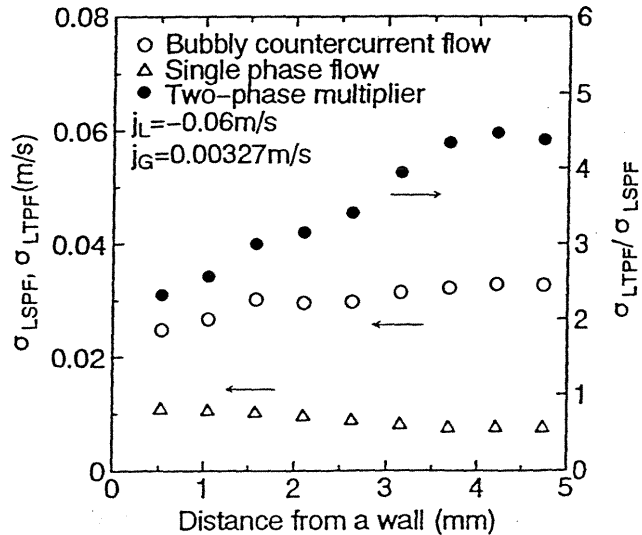


Fig.5 Turbulence intensity

MULTI-DIMENSIONAL FLOW CHARACTERISTICS OF COUNTERCURRENT BUBBLY FLOW, (II) EFFECTS OF AIR AND WATER FLOW RATES

Shirong ZHOU¹, Masanori ARITOMI¹, Junji MIZOGUCHI²,
Yasushi TAKEDA³, Michitsugu MORI⁴ and Yuzuru YOSHIOKA⁵

1 Tokyo Institute of Technology, 2-12-1 Ohokayama, Meguro-ku, Tokyo, 152 Japan

2 Shibaura Institute of Technology, 307 Tameihara, Fukasaku, Omiya, 330 Japan

3 Paul Scherrer Institut, Wurenlingen and Villigen, CH-5232, Villigen, Switzerland

4 Tokyo Electric Power Co., 1-1-3 Uchisaiwai-cho, Chiyoda-ku, Tokyo, 100 Japan

5 Japan Atomic Power Co., 1-6-1 Ohtemachi, Chiyoda-ku, Tokyo, 100 Japan

1. INTRODUCTION

It is one of the most important subjects in the research of two-phase flow dynamics to clarify its multi-dimensional flow characteristics. Therefore, the authors have developed a new measurement system which is composed of an Ultrasonic Velocity Profile Monitor (UVP) (Aritomi et al., 1996) in order to clarify the multi-dimensional flow characteristics in countercurrent bubbly flows and to offer a data base to validate numerical codes for multi-dimensional two-phase flow. The ultrasonic Doppler method for velocity profile measurement has been developed for liquid flows by Takeda (1995). It has been approved that this method is a powerful tool in flow measurement in the following ways: It can measure a velocity profile instantaneously so that velocity field can be measured in space and time domain.

In this paper, the proposed measurement system was applied to fully developed countercurrent bubbly flows in a vertical rectangular channel in order to verify its capability. At first, both bubble and water velocity profiles and void fraction profiles in the channel were investigated statistically under various conditions of both gas and liquid phase flow rates. Next, a two-phase multiplier profile of turbulent intensity in the channel was discussed as a ratio of the standard deviation of velocity fluctuation in a countercurrent bubbly flow to that in a water single phase flow. Finally, concerning the drift flux model, the distribution parameter and the drift flux are calculated directly from these profiles.

2. EXPERIMENTAL APPARATUS

Figure 1 shows a schematic diagram of an experimental apparatus. Air and water were used as working fluids. The experimental apparatus was composed of a water circulation system, an air supply system, a test section and a measurement system. The test section was a vertical rectangular channel of 10mmx100mm x700mm made of Plexiglas. The measurement system consisted of the UVP and a personal computer to record and treat data.

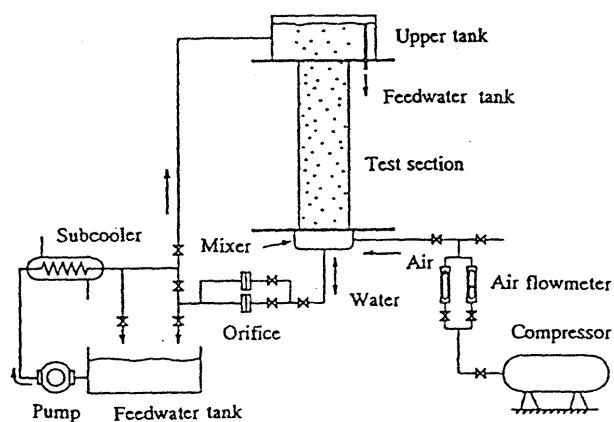


Fig.1 A schematic diagram of experimental apparatus

An ultrasonic transducer was installed on the outside surface of the front wall of the channel with a contact angle of 45° and a gap between the transducer and the wall was filled with a

jelly to prevent a reflection of ultrasonic pulses on the wall surface. After both air and water flow rates were set up at the desired values, 9,216 (1,024x9) velocity profiles along a measured line were measured under one experimental condition to treat them statistically. The hydrostatic head was simultaneously measured as a pressure drop between the pressure taps installed on the side wall using a differential pressure transducer to get an averaged void fraction. The experimental conditions are tabulated in Table.1.

Table 1 Experimental conditions

System pressure	Atmospheric pressure
Water specific velocity	-0.06, -0.12m/s
Air specific velocity	0.00195 - 0.00418m/s

The working principle of the UVP is to use the echo of ultrasonic pulses reflected by micro particles suspended in the fluid. An ultrasonic transducer takes roles of both emitting ultrasonic pulses and receiving the echoes. The position information is obtained from the time lapse from the emission to the reception of the echo and a sound speed in the fluid. An instantaneous local velocity as a component in the ultrasonic beam direction is derived from the instantaneous Doppler shift frequency in the echo. Horizontal position and axial velocity can be obtained by considering the contact angle of the transducer to the wall.

A probability density function includes the velocity information of both phases. Assuming that each probability density function of both phases can be expressed by a normal distribution,

$$N[\bar{u}, \sigma^2](u) = \frac{1}{\sqrt{2\pi\sigma^2}} \exp\left[-\frac{(u - \bar{u})^2}{2\sigma^2}\right], \quad (1)$$

the probability density function of mixture velocity is given by

$$P_u(y, u) = \varepsilon(y)N[\bar{u}_G(y), \sigma_G^2(y)](u) + (1 - \varepsilon(y))N[\bar{u}_L(y), \sigma_L^2(y)](u). \quad (2)$$

where \bar{u}_G and \bar{u}_L are average velocities of gas and liquid phases respectively, σ_G and σ_L are standard deviations of both phases

respectively and ε is the probability of bubble existence. These five variables, \bar{u}_G , \bar{u}_L , σ_G , σ_L and ε , are calculated numerically and iteratively by the least squares method.

As long as a bubble exists, the ultrasonic pulse is reflected at its surface. Therefore, the bubble velocity can be always detected as the interfacial velocity. On the other hand, the ultrasonic wave is not reflected in water where a micro particle does not exist. As a result, water velocity is not always measured in the profile. Therefore, it is necessary to revise the probability of bubble existence as follows:

$$\kappa(y) = P_s(y) \varepsilon(y) \quad (3)$$

where $P_s(y)$ is the probability of data existence. $\kappa(y)$ is called the probability of bubble data existence in this work.

The average void fraction was obtained by measuring the hydrostatic head. Assuming that the local void fraction is proportional to the local probability of bubble data existence and that the proportional constant, k , is uniform in the channel since it is dependent on bubble size and configuration, the average void fraction is expressed by

$$\langle \alpha \rangle = k \int_A \kappa dA / A = k \langle \kappa \rangle. \quad (4)$$

The proportional constant, k , was calculated from measured average void fraction, $\langle \alpha \rangle$, and measured average probability of bubble existence, $\langle \kappa \rangle$. Then, local void fraction, $\alpha(y)$, is given by

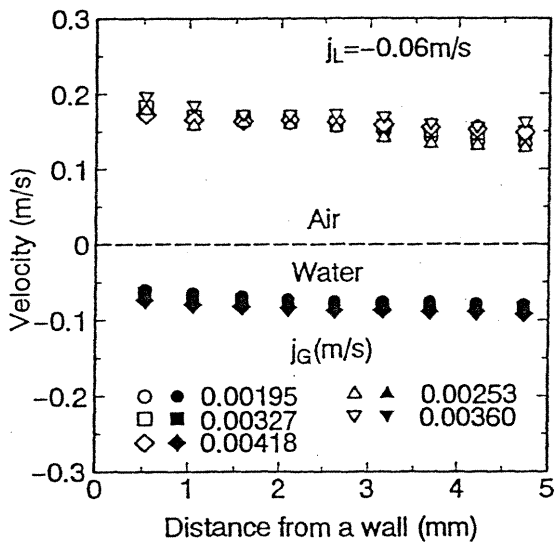
$$\alpha(y) = k \kappa(y). \quad (5)$$

3. RESULTS AND DISCUSSION

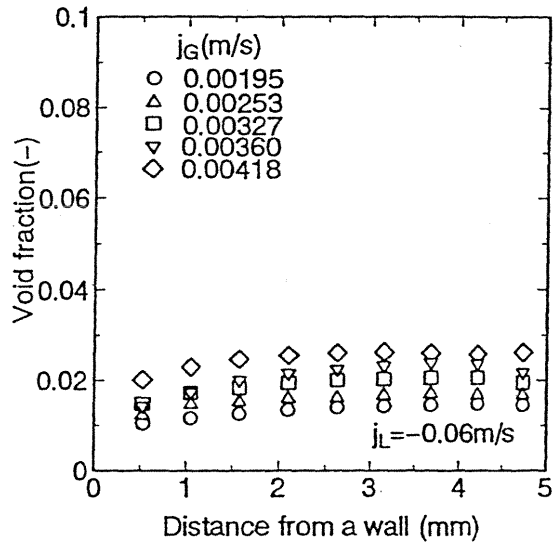
Velocity profiles of both phases in the channel were measured with the UVP. The typical experimental results, which were measured under the condition of a constant water flow rate and various air flow rates, are shown in Fig.2 (a). Since it is very difficult to measure the velocities near the wall with significant accuracy due to an ultrasonic beam diameter of 5mm, they are omitted in the figure. Water velocities becomes higher toward the center of the channel from the wall in the same tendency as water single phase flow. In contrast with this, bubble velocities are higher

near the wall than those in the core. The flow characteristics of a countercurrent bubbly flow is strongly dependent on the water velocity which is a continuous phase and a bubble rising velocity is induced by the difference between the buoyancy and interfacial drag force. Since air flow rates are much lower than water ones under the present conditions, the velocity profiles of both phases are scarcely varied even if an air flow rate increases. Figure 2 (b) shows the experimental results of velocity profiles of both phases at a constant air flow rate and in reference to water flow rates. It can be seen from the figure that water velocities becomes higher but their profiles are scarcely influenced with a change in a water flow rate.

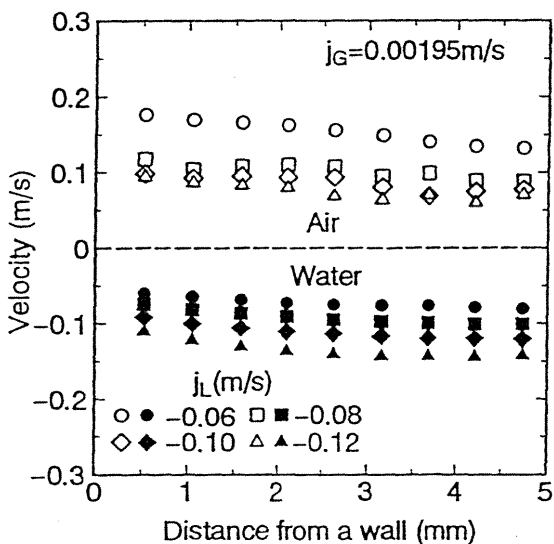
Figure 3 (a) and (b) show the typical experimental results of void fraction profile in reference to air flow rates and water flow rates, respectively. It can be seen from these figures that void fraction profiles are almost flat in countercurrent bubbly flows. Since air flow rates are much lower than water ones under the present experimental conditions, water velocity profiles are scarcely varied even with a change in air flow rates and bubble velocity is dependent on the water velocity profiles. The void fraction, therefore, increases with an increase in air flow rates as shown in Fig.3 (a). Moreover, as the water flow rate increases, the bubble rising velocity is decreased, so that void fraction becomes larger as shown in Fig.3(b).



(a) Effect of air flow rates

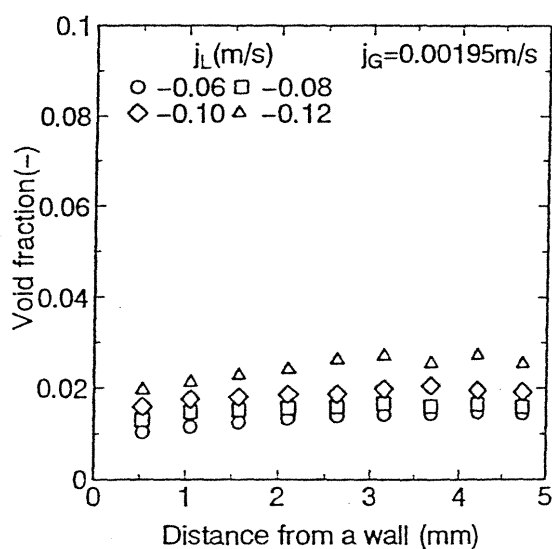


(a) Effect of air flow rates



(b) Effect of water flow rates

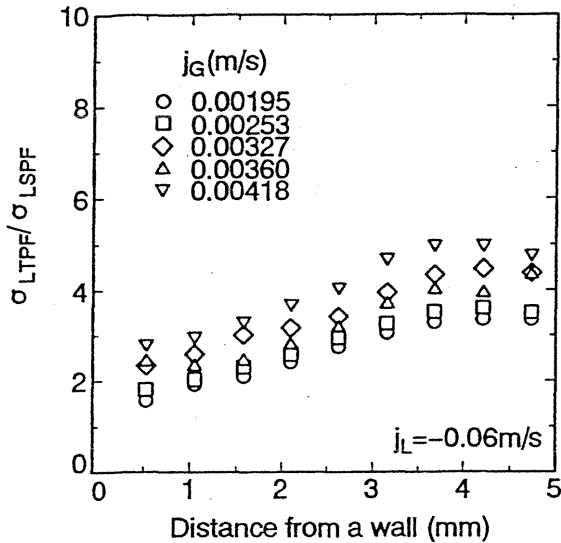
Fig.2 Typical velocity profiles of both phases



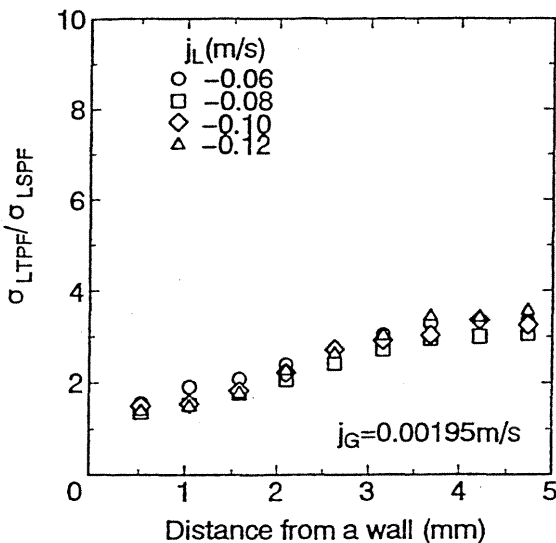
(b) Effect of water flow rates

Fig.3 Void fraction profiles

As a general rule, turbulent intensity in a bubbly flow is larger than that in liquid single phase flow because bubbles agitate the flow. In this work, turbulent intensity is defined as a standard deviation of water velocity fluctuation which is a continuous phase, σ_L . The standard deviation profile in the channel can be calculated from Eq.(2).



(a) Effect of air flow rates



(b) Effect of water flow rates

Fig.4 Turbulent intensity profiles in countercurrent bubbly flow

Since local velocities were measured not at a point but on the area because of an ultrasonic beam diameter of 5mm, the absolute value of the standard deviation in a water phase is not significant. Hence, the standard deviation ratio

of a countercurrent bubbly flow to water single phase flow is selected as two-phase multiplier of turbulent intensity, $\sigma_{LTPF}/\sigma_{LSPF}$. Figures 4 (a) and (b) show the typical experimental results of the two-phase multiplier of turbulent intensity in reference to air flow rates and water flow rates, respectively. The two-phase multiplier of turbulent intensity becomes larger with going toward the center of the channel. It can be seen from the figures that $\sigma_{LTPF}/\sigma_{LSPF}$ is enhanced with increases in air or water flow rates.

The drift flux model proposed by Zuber and Findley (1965) is applied widely to two-phase analysis codes. The drift flux, V_{gj} , and the distribution parameter, C_0 , in the drift flux model can be calculated by

$$V_{gj} = \int_A (u_G - j) dA/A \quad (6)$$

and

$$C_0 = \frac{\int_A \alpha j dA/A}{\int_A \alpha dA/A \cdot \int_A j dA/A} \quad (7)$$

where j is volumetric flux. In this work, the drift flux and the distribution parameters were calculated by substituting the measured velocity profiles of both phases and void fraction profiles in to Eqs.(6) and (7), respectively. It can be seen from Fig.3 (a) and (b) that a void fraction profiles are almost flat. Consequently, the distribution parameter is almost 1.0. Substituting properties of air and water into the correlation proposed by Zuber and Findley (1965), $V_{gj} = 0.231 m/s$. The experimental results are identical to this value.

REFERENCE

Aritomi, M., Nakajima, M., Zhou, S., Takeda, Y., Mori, M. and Yoshioka, Y., Measurement System of Two-Phase Flow Using Ultrasonic Velocity Profile Monitor, *Proc. 1st Int. Symp. Ultrasonic Doppler Methods for Fluid Mechanics and Fluid Engineering*, Villigen (1996.9) to be published.

Takeda, Y., Velocity Profile Measurement by Ultrasonic Doppler Method, *Experimental Thermal and Fluid Sci.*, **10** (1995) 444-453.

Zuber, N. and Findley, A., Average Volumetric Concentration in Two-Phase Flow System, *Trans. ASME, J. Heat Transfer*, **87** (1965) 453-468.

1. ISUD
 1st International Symposium on Ultrasonic Doppler Methods
 for Fluid Mechanics and Fluid Engineering
 September 9-11, 1996
 Paul Scherrer Institut, 5232 Villigen PSI, Switzerland

ON THE STRUCTURE OF THE CYLINDER WAKE

I. Peschard^①, P. Le Gal^① and Y. Takeda^②

^①Institut de Recherche sur les Phénomènes Hors Equilibre
 UM 138, CNRS - Universités d'Aix-Marseille I & II
 12, Avenue Général Leclerc, 13003 Marseille, France

^②Laboratory for Spallation Neutron Source
 Paul Scherrer Institut
 CH-5232 Villigen PSI, Switzerland

ABSTRACT

The wake of a single and short aspect ratio cylinder placed in a uniform flow is experimentally investigated. Using an ultrasound anemometry technique, the critical behavior of the spatial shape of the transversal velocity of the Bénard-Von Kàrmàn streets is studied. It is shown that the envelop of the velocity fluctuations which is called the global mode of the wake, follows universal scaling laws given by the theory of phase transitions. In a second set of experiments, the behavior of the longitudinal velocity fluctuations is also investigated. The presence several diameter behind the cylinder of a special point playing the role of a wave maker, is discovered.

1. Experimental arrangement

Our experimental facility consists of a water loop and is fully described in [1]. A single cylinder having a diameter d equal to 4 mm, is positionned on one of the horizontal walls of the channel. Its length being 20 mm, it is in close contact with the other horizontal wall. The shape of the Bénard-Von Kàrmàn wake of this confined flow is studied by ultrasound anemometry whose operation principle is also presented in [1].

We proceeded to two sets of experiments. In the first, the ultrasound probe is placed in a groove machined in the middle plane of the side-wall of the channel. The complete transversal velocity profile can be measured along lines crossing the main flow in the y direction. The transversal velocity profiles are recorded every 69.8 ms, in 128 space positions separated by 0.74 mm. 1024 instantaneous profiles are then digitized and recorded for several Reynolds numbers R . In the second set of experiments, the ultrasound probe is

positioned inside the water flow, 10 cm downstream of the cylinder and 2 mm on its side ($y/d= 0.5$). In this manner, longitudinal velocity profiles are obtained with the same configuration of the acquisition channel.

2. Results and discussion

Modelling the Bénard-Von Kármán instability in terms of global modes, needs to represent the velocity wake fluctuations by the product of two independent functions linked to the temporal and spatial evolutions of the velocity field. It has then been proved that the temporal behavior of the vortex shedding can be modelled by a Landau equation [2] which represents the growth and the non linear saturation of a periodic disturbance which has the same frequency every where in space. On the contrary, the spatial behavior of this periodic disturbance is much more difficult to study because traditional anemometry techniques (hot wire or laser anemometry) need heavy mappings of the flow. The ultrasound profile monitor presents in this context a new and interesting alternative.

2.1 Transversal velocity profiles

The first experimental studies of the envelop of the fluctuations in a wake [3] have shown that these fluctuations possess a maximum whose position is clearly defined and varies with the Reynolds number. More recently, experimental [4] and numerical [5] studies have shown that the wakes of triangular bodies present a critical behavior at small Reynolds numbers. In particular, it is shown that the amplitude and the position of the maxima of the transversal velocity oscillations obey power laws of the Reynolds number.

As explained in the introduction, we measure the complete profiles of the transversal velocity in 8 different positions downstream the cylinder and for several Reynolds numbers. Figure 1 presents such a space time diagram, where we recognize the periodic oscillation of the transversal velocity due to the vortex shedding.

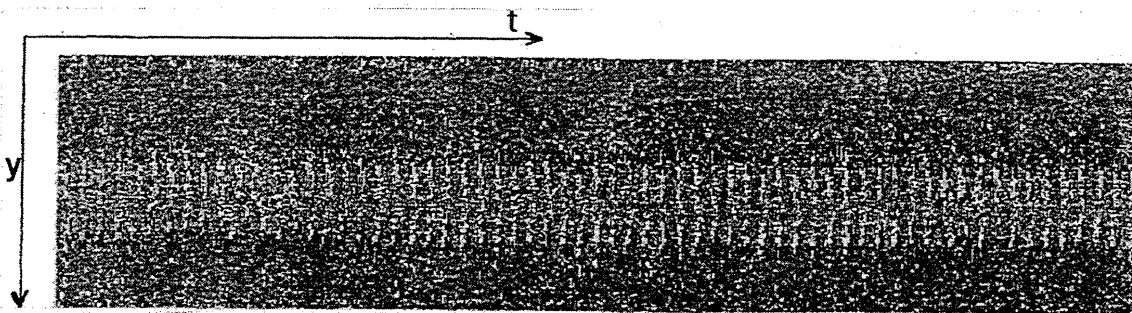


Figure 1: Space time diagram of the transversal velocity fluctuations ($x/d= 7$, $R=142$)

Then, taking the temporal Fast Fourier Transform in each of the 128 space points, it is possible to compute the profiles of the squared amplitude of the fundamental mode. These profiles are then gathered on the same diagram and give a three-dimensionnal view of the global mode of the circular cylinder wake.

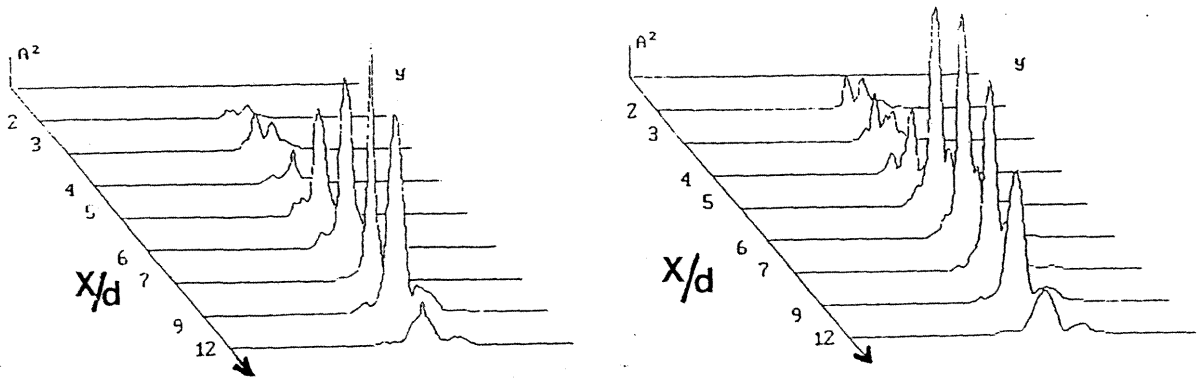


Figure 2: Three-dimensionnal representation of the energy of the transversal velocity oscillations ($R=170$ and $R=185$).

Plotting the amplitudes taken by these profiles along the x axis, in the direction of the fluid flow, we can observe the deformation of the global mode with the Reynolds number. On Figure 3, we observe a rapid increase of the amplitude of oscillation up to a maximum whose position varies between 5 and 9, when decreasing the Reynolds number. Then, the decrease of these envelopes far away from the cylinder can be interpreted as a viscous relaxation of the far wake.

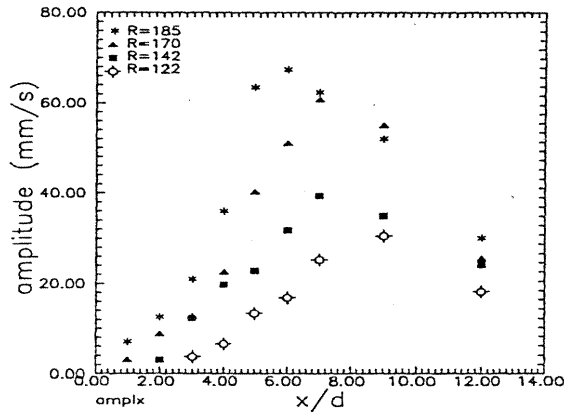


Figure 3: Amplitude of the transversal velocity oscillations downward the cylinder ($y/d=0$).

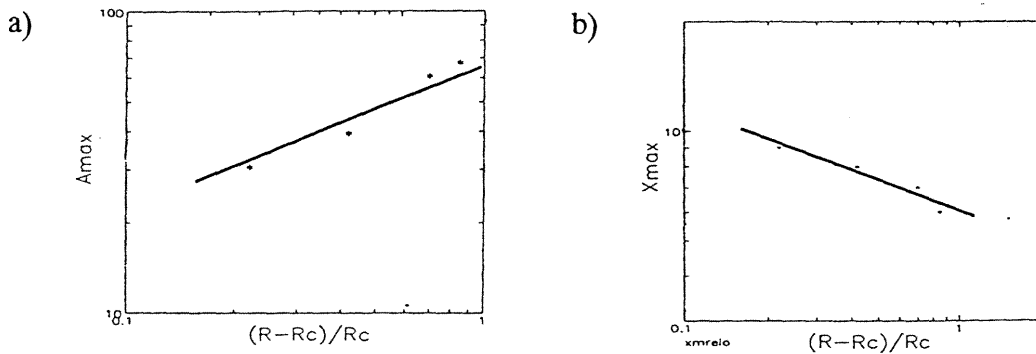


Figure 4: Amplitude (a) and position (b) of the maximum of the transversal velocity oscillations as a function of the Reynolds number.

It is then easy to compute the evolution of the position and level of the maximum of the mode as a function of the Reynolds number. The logarithmic representations of figure 4 show the critical behavior of the envelopes as already observed in [4] and [5]. Moreover, we confirm the exponent of the power laws (1/2 and -1/2) observed in [5] contrary to what was measured in [4].

2.2 Longitudinal velocity profiles

In the second set of experiments, the probe is placed inside the water channel, aligned with the x axis in order to measure the longitudinal velocity fluctuations. Because this mode is odd, its amplitude is null along the x axis, and we placed the probe at the transversal position $y = 0.5d$. Figure 5 gives a space time diagram obtained by the ultrasound monitor. As it can be observed, waves representing the alternate vortex shedding are generated from a point positioned at $x/d=6$ downstream of the cylinder. Thus some waves propagate in the downstream direction, but also others in the upstream direction. This experimental observation confirms the existence in the cylinder wake of a region of the flow where the instability is of "absolute type"[6].

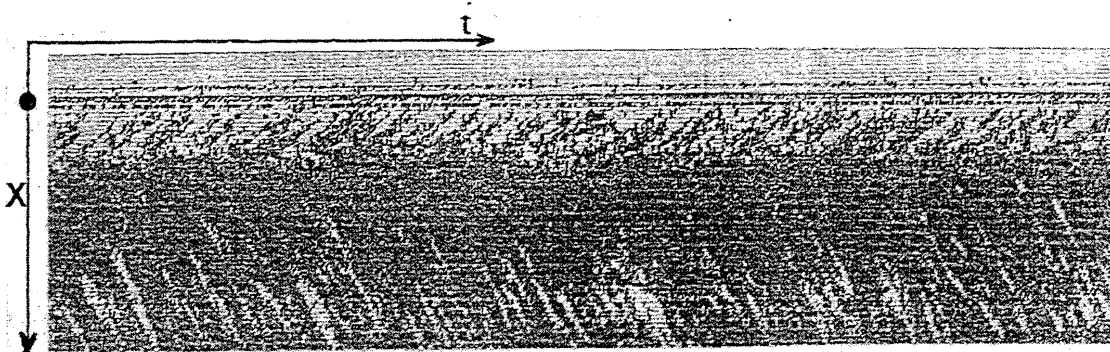


Figure 5: Space time diagram of the longitudinal velocity component ($R=142$, $y/d=0.5$)

3. References

- [1] I. Peschard, J.F. Ravoux, P. Le Gal, Y. Takeda and M.P. Chauve, Collective behavior of wakes shed by a row of cylinders, 1st International Symposium on Ultrasonic Doppler Methods, these proceedings, (1996).
- [2] M. Provansal, C. Mathis and L. Boyer, Bénard-Von Kàrmàn instability: transient and forced regimes, *J. Fluid Mech.* **182**, 1 (1987).
- [3] J. Dusek, P. Le Gal and Ph. Fraumíé, A numerical and theoretical study of the first Hopf bifurcation in a cylinder wake, *J. Fluid Mech.* **264**, 59 (1994).
- [4] C. Mathis, Propriétés des composantes transverses dans l'écoulement de Bénard-Von Kàrmàn aux faibles nombres de Reynolds, Thèse, Univ. de Provence, France (1983).
- [5] S. Goujon-Durand, J.E. Wesfreid and P. Jenffer, Downstream evolution of the Bénard-Von Kàrmàn instability, *Phys. Rev. E* **50**, 308 (1994).
- [6] B.J.A. Zielinska and J.E. Wesfreid, On the spatial structure of global modes in wake flow, *Phys. Fluids* **7**, 6 (1995).
- [6] P. Huerre and P. Monkewitz, Local and global instabilities in spatially developing flows, *Annu. Rev. Fluid Mech.* **22**, 473 (1990).

1. ISUD

1st International Symposium on Ultrasonic Doppler Methods
for Fluid Mechanics and Fluid Engineering
September 9-11, 1996
Paul Scherrer Institut, 5232 Villigen PSI, Switzerland

**COLLECTIVE BEHAVIOR OF WAKES
SHED BY A ROW OF CYLINDERS**

I. Peschard^①, J.F. Ravoux^①, P. Le Gal^①, Y. Takeda^② and M.P. Chauve^①

^①Institut de Recherche sur les Phénomènes Hors Equilibre
UM 138, CNRS - Universités d'Aix-Marseille I & II
12, Avenue Général Leclerc, 13003 Marseille, France

^②Laboratory for Spallation Neutron Source
Paul Scherrer Institut
CH-5232 Villigen PSI, Switzerland

ABSTRACT

This experimental study is devoted to visualization and ultrasonic velocity measurement of the wakes formed behind a row of parallel cylinders placed side by side, perpendicular to an incoming flow at low Reynolds numbers. When the distance separating the cylinders is small compared to their diameter, two instability mechanisms, associated with different patterns and dynamics compete. A first spatial symmetry breaking appears when the stationary wakes behind each cylinder are deviated towards one side or the other and form large clusters containing from 2 to sometimes more than 10 wakes. These clusters are separated by intense recirculating zones. When the Reynolds number is increased, the wakes belonging to the widest clusters experience a secondary temporal oscillatory bifurcation. Classical Bénard-Von Kàrmàn vortex streets are thus shed in phase by these cylinders (acoustic mode), by contrast with the wakes outside these cells which stay stationary. Finally, the flow around far apart cylinders is also investigated. The primary instability does not occur in this case and a perfect optical mode of vortex shedding, with neighbours in phase opposition, takes place in the flow.

1. Experimental arrangement

Our experimental facility consists of a water loop with two reservoirs: the first one is set at 3 meters from the floor in order to generate the hydrostatic pressure that creates the flow which is stabilized by a classical 1 meter long settling chamber. Then, a home-made convergent creates a uniform velocity profile at the entry of a horizontal rectangular test channel 20 mm high and 128 mm wide. The length of this channel is 700 mm and a 50 mm

diameter circular pipe leads to the second reservoir which lies on the floor. A water pump equipped with a by-pass, permits to adjust the flux of water through the loop. 21 cylinders having a 4mm diameter, are glued on one of the horizontal walls of the channel. Their length being 20 mm, they are in close contact with the other horizontal wall. The rather small aspect ratio of these cylinders was chosen to freeze the three-dimensional phase dynamics of the cylinder wakes. The row of the 21 cylinders is set 15 cm downstream the convergent and fill entirely the channel, from one side to the other, with only half a pitch between the end cylinders and the sidewalls of the channel.

The electro-chemical technique used to visualize the flow is based on the oxydation of a tin wire which is stretched across the experimental channel at mid-height and upstream of the cylinders row. When a 0.1 Ampere electric current flows between this 0.5 mm diameter wire and a carbon electrode, a white smoke of tin hydroxyde is emitted by the wire. When enlightened from the side, this smoke allows a perfect visualization of the entire flow. The video images are recorded by a frame grabber driven by a micro-computer. The Reynolds number of the flow is calculated on the diameter of each cylinder and on the flux of water passing through the row of cylinders. The ultrasonic transducer is set in a groove, machined in the mid-plane of the vertical wall of the channel. The diameter of the beam is 5 mm and the probe is positionned perpendicular to the channel at a distance of 20 mm from the cylinders axes. The operation principle is echography. An ultrasonic burst signal is emitted through the excitation of a piezoelectric transducer. The beam propagates through the fluid seeded with 100 micron size bubbles. These hydrogen bubbles are generated upstream by a platinum wire inducing an electrolysis of water and we have checked that their small size allows them to behave as a passive scalar. The sound waves reflect on these bubbles moving with the flow and are received by the same piezoelectric transducer. Thus the position of the reflecting bubble can be calculated from the time delay between the burst emission and the reception of the echoe. We can also obtain the velocity of the bubble by an analysis of the Doppler shift of the sound frequency. Therefore, the complete transversal velocity profile can be measured along the line crossing the flow. The velocity profiles are recorded every 135 ms, in 128 space positions separated by 1.48 mm. The width of the test channel being 128 mm, only the 85 first data points are used to cover the entire flow width. 1024 instantanneous profiles are then digitized and recorded.

2. Results and discussion

Each wake is coupled to its neighbours and as expected, global behavior of the one dimensionnal array of oscillators are observed. Different dynamical regimes are obtained when controlling the Reynolds number of the flow and the distance separating the cylinders. Two typical situations have been extensively studied: a strong and a weak coupling situation.

In the first one, the distance separating two successive cylinder axes is 1.5 times the cylinder diameter. At a Reynolds number equal to about 100, a first spatial symetry breaking

arises. Due to the Coanda effect, each wake can be deviated towards one side or the other [1]. Thus several groups of merged wakes (or jets) are created. These regions are separated by recirculation zones. An analogy with magnetic domains separated by Bloch walls can be made. When increasing the Reynolds number to a value close to 110, some of the wakes exhibit an oscillatory instability. The oscillating wakes are confined in some regions of the flow and are locked in phase. This mode of vortex shedding is analog to the acoustic mode of phonons propagation. We present in figure 1 such flow patterns with one or two cells of oscillating wakes. Note that these different flows are obtained just by changing the initial conditions.

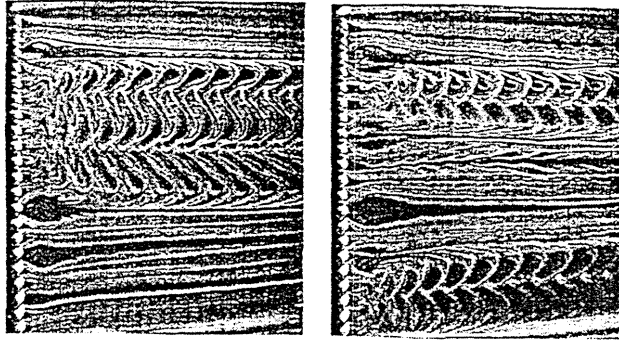


Figure 1: Two visualizations obtained at a Reynolds number of 115.

Figure 2 shows an example of space-time diagrams acquired by the ultra-sound anemometer for $R=140$. The color coding used on the picture allows the observation of two oscillating zones separated by a strong recirculation. Inside each zone we observe in phase oscillations made visible by the succession of black and white strips: all the wakes inside these groups are thus entirely correlated in a collective oscillation. Moreover, we notice also that the global oscillation of the wakes in one of these regions is in phase opposition with the global oscillation of the wakes in the other region. So, the recirculating zone between the two oscillating clusters is pulsating in a kind of varicose mode.

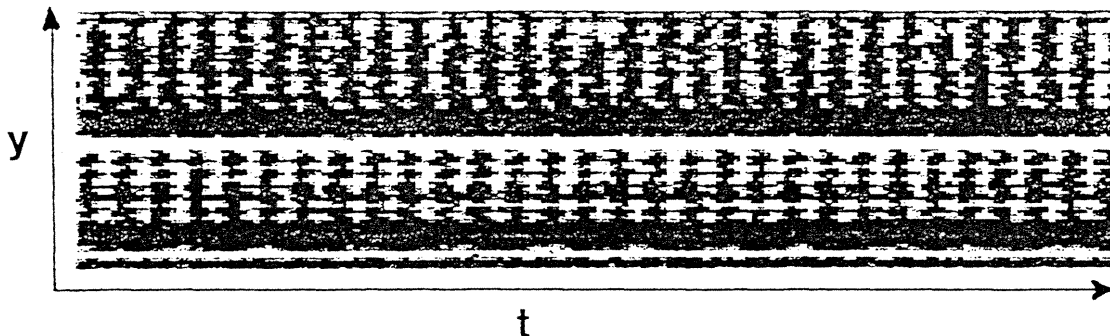


Figure 2: Two cells of in phase vortex shedding (acoustic mode) at strong coupling.

In the second set of experiment, the distance separating two successive cylinder axes is 3 times their diameter. In this case, no stationary spatial bifurcation occurs and at a Reynolds number about 110, Bénard-Von Karman streets are shed with first neighbours in

phase opposition. Figure 3 presents a space time diagram of this mode which is called the optical mode of phonons propagation.

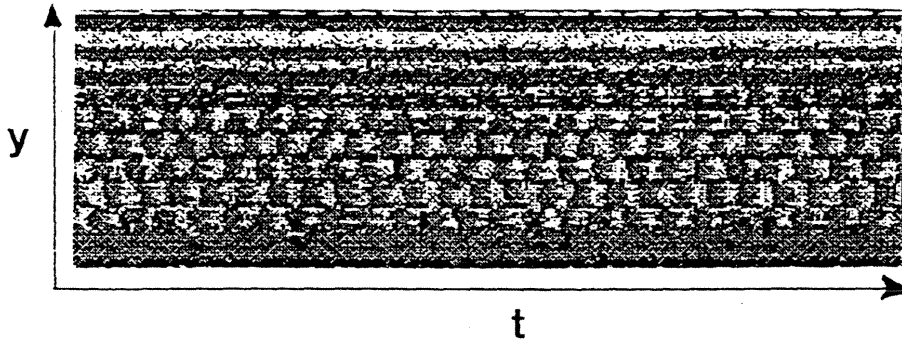


Figure 3: The optical mode of vortex shedding at small coupling.

The space-time diagrams are then analysed using the Bi-Orthogonal Decomposition which permits to separate the different components of the dynamics. We present in figure 4 the two first modes which represent respectively the main spatial and temporal structures of the flow.

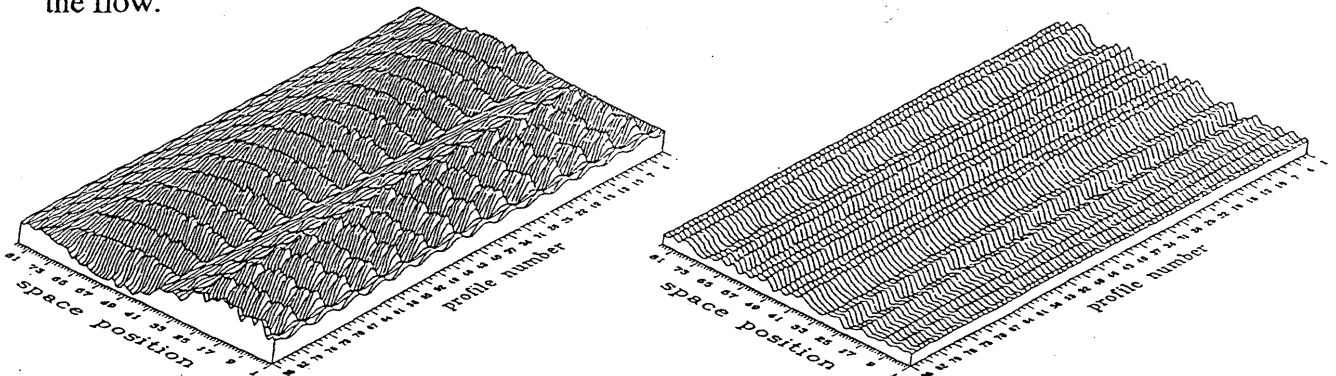


Figure 4: The two first modes of the BOD analysis of the flow.

3. Conclusion

Besides these experimental investigations, analytical and numerical studies of a coupled oscillators model have been realized. The model which is based on the diffusive coupling of Hopf bifurcations leads to a discrete form of the Ginzburg-Landau equation [2]. Stable states and transition to chaos in this model present strong similarity with the experimental observations.

4. References

- [1]- Ishigai S. and Nishikawa E., Experimental study of structure of gas flow in tube banks with tube axes normal to flow, Bulletin of the JSME., 18, 528, (1975).
- Auger J.L. et Coutanceau J., Ecoulement transversal de l'air à travers une grille de tubes, Entropie, 86,13, Edt Bartheye, (1979).
- [2] - Chauve M.P. and Le Gal P., Complex bi-orthogonal decomposition of a chain of coupled wakes, Physica D, 58, 407 (1992).

1. ISUD
 1st International Symposium on Ultrasonic Doppler Methods
 for Fluid Mechanics and Fluid Engineering
 September 9-11, 1996
 Paul Scherrer Institut, 5232 Villigen PSI, Switzerland

AN EXPERIMENTAL STUDY ON A WAKE OF A TORUS USING UVP MONITOR

Yoshihiro INOUE*, Shintaro YAMASHITA† and Masaya KUMADA†

* Department of Mechanical Engineering, Suzuka College of Technology, Suzuka, Japan

† Department of Mechanical Engineering, Gifu University, Gifu, Japan

ABSTRACT

Measurements by using the ultrasonic velocity profile monitor (UVP) are presented for the spatiotemporal flow structure behind a torus. The flow around the torus has a complicated three-dimensional structure, and it is very difficult in this flow to measure the multi-components of velocities by means of other usual methods. In this study the instantaneous velocities along the measuring line are successively measured, and the spatial distribution of power-spectra and two-point correlation are analyzed in case that the torus is set at zero incidence.

1. Introduction

The flow around a torus body is a basic flow applicable to many problems including bio-fluid mechanics for DNA polymer, flows with micelles, those around helical heating tubes, and so on. This flow has a three-dimensional complicated structure, and so far little studies have been made but for analytical one for low Reynolds numbers (Johnson & Wu [1] and Goren & O'Neill [2]) and flow visualization experiments focused on vortex arrangement or its stability in the wake behind the torus (Amarakoon et al. [3], Monson [4] and Leweke & Provansal [5]). The details of the three-dimensional spatial structure on this flow is remained to be clarified.

The objective of this study is to make clear the flow structure around the torus. The present authors have so far made some experiments in which, for the torus set aslant with the mean flow direction, the flow around the torus is visualized, and the drag and lift of the torus are measured. In this experiment, the instantaneous velocity distribution behind the torus set at zero incidence against the main flow is measured by using a ultrasonic velocity profile monitor explained in detail in reference [6], and then the spatiotemporal flow structure is examined.

2. Experimental apparatus and procedure

Flow field and coordinate system are shown in Fig. 1. The cross-sectional diameter and center-line diameter of a torus are defined as d and D , respectively. A ratio D/d is a geometrical parameter of the torus, and in this study the case of $D/d = 3$ and 5 with $d = 30$ mm are investigated. The torus is set at zero incidence against the main flow, so that its axis of symmetry is coincided with the x -axis, i.e., the main flow direction. The origin of coordinate system is at the center of the symmetrical plane of torus, and the y -axis is normal to the x -axis, that is, parallel to

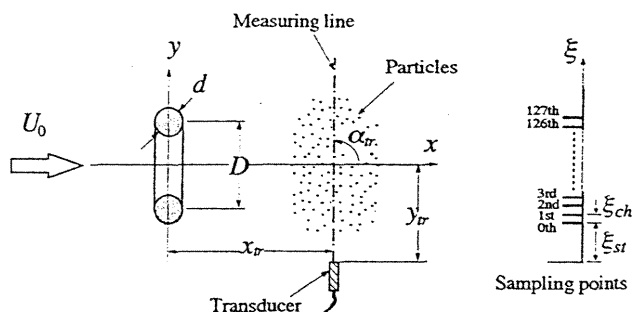


Fig. 1 Flow field and coordinate system.

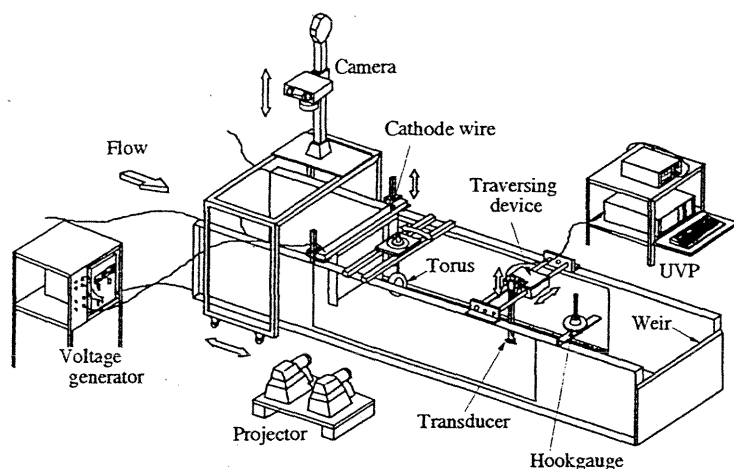


Fig. 2 Sketch of the test section.

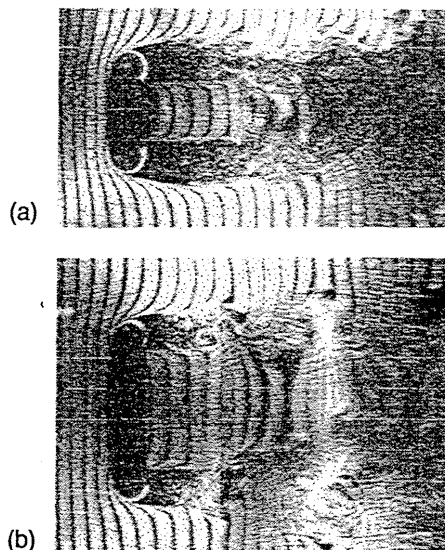
supported at the 1 m downstream position from the entry by an 8 mm diameter brass-rod, and can be rotated normal to a uniform flow. An ultrasonic transducer is inserted parallel to the x - y plane at the positions shown in Table 1 using a traversing device. The uniform flow velocity U_0 is kept constant 50 mm/s and then the Reynolds number based on the cross-sectional diameter is about 1500.

The UVP monitor used in this study is a model X3-PS (Met-Flow). A basic frequency of the ultrasonic transducer is 4 MHz and the other measuring parameters are shown in Table 1. Hydrogen bubbles electrolytically generated from a 30 μ m diameter Pt-wire are utilized for the ultrasonic reflection and also for the flow visualization. The UVP data are processed on the personal computer PC-9801BA3 (NEC).

3. Results and discussion

3.1 Spatiotemporal velocity field

For the sake of taking the general view of the flow field around the torus, the flow visualized by means of a hydrogen-bubble method is shown in Fig. 3. Mean flow fields for $D/d = 3$ and 5 are axi-symmetric, but the vortical structures for these flows are different from each other. For $D/d = 5$, in the near wake region, say within $1 D$ downstream of the torus, the separated shear layers from the inner and outer surface of the torus roll up alternately, and vortex rings are shed in the downstream, whereas in case of $D/d = 3$ any vortex ring is

Fig. 3 Flow visualization.
(a) $D/d = 3$, (b) $D/d = 5$.

the horizontal plane in a test section.

The experiment has been made using a water channel with a test section of 3 m length, 0.7 m width and about 0.6 m depth, as shown in Fig. 2. The torus is

Table 1 Specifications of measurement

	x - direction	y - direction
ξ_{st} (mm)	15.29	5.00
ξ_{ch} (mm)	4.41	3.68
f_{prf} (Hz)	978	1050
x_{tr} (mm)	600	-200, -190, ..., 200
y_{tr} (mm)	100, 150, ..., 700	-254
α_{tr} ($^\circ$)	180	90

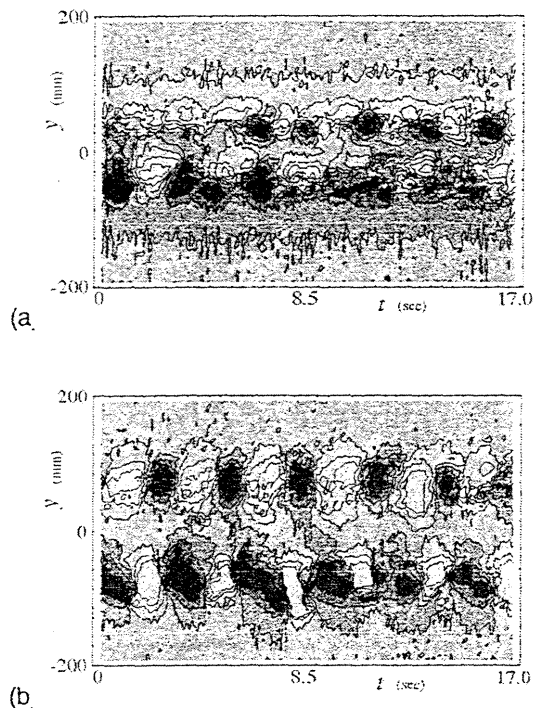


Fig. 4 Contours of velocity component in the y -direction at $x = 150$ mm. (a) $D/d = 3$, (b) $D/d = 5$.

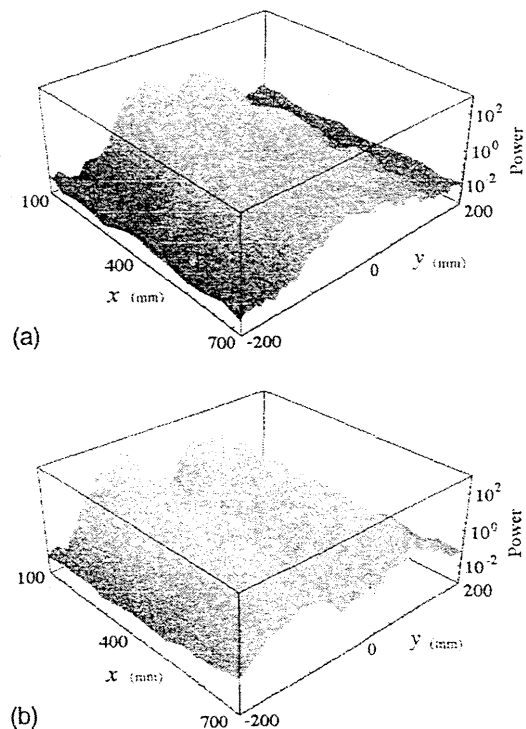


Fig. 5 Power of fluctuating velocity in the x - y plane. (a) $D/d = 3$, $f = 0.31$ Hz, (b) $D/d = 5$, $f = 0.34$ Hz.

not discernible in this visualization picture.

Figure 4 shows the contours of the instantaneous velocity component in the y -direction \bar{v} measured by UVP along the line parallel to y -axis at $x = 150$ mm. The abscissa is time, but the figure shows nearly the flow pattern in space in which the flow direction is right to left. Although the flows for $D/d = 3$ and 5 are both periodic, the latter is more regular and the periodical structure of this flow is also axi-symmetric.

3.2 Power spectra of fluctuating velocity

As mentioned in the preceding section, the vortices are shed in the wake of the torus. In case of $D/d = 5$, in particular, the regular street of vortex ring is formed. The regularity of the periodic motion will appear in power spectral distribution of fluctuating velocities. In this study, 512 points time-series data are Fourier transformed, although one data set of velocity profile consists of the data of 128 points in space and 1024 points in time domain. Then the two power spectra obtained from one data set are averaged.

Figure 5 shows the power spectral density of v -fluctuating velocity with dominant frequency of vortex shedding f_s . Two mountain ranges of this power spectral density are clearly discernible in case of $D/d = 5$ compared with $D/d = 3$, showing the regularity of the former flow is higher.

3.3 Flow structure

The space correlation of fluctuating velocities at two point separated in the main flow direction is difficult to measure by the method of hot-wire, because the upstream probe disturbs the flow seriously. The UVP can measure such quantities without error due to the probe-induced disturbance, and the two-point correlation coefficients of u -component R_{11} so measured is presented at the reference position $x = 150$ mm in Fig. 6, where r_x denotes the streamwise spacing. The correlation shows the periodical structure of this flow.

Figure 7 shows the conditionally averaged profiles of the velocity component in the y -direction for $D/d = 5$ at $x = 150$ mm. The reference signal is a signal at $y = 60$ mm of the same data set, and each of maxima of the reference signal is used as a trigger. The upper figure is the condi-

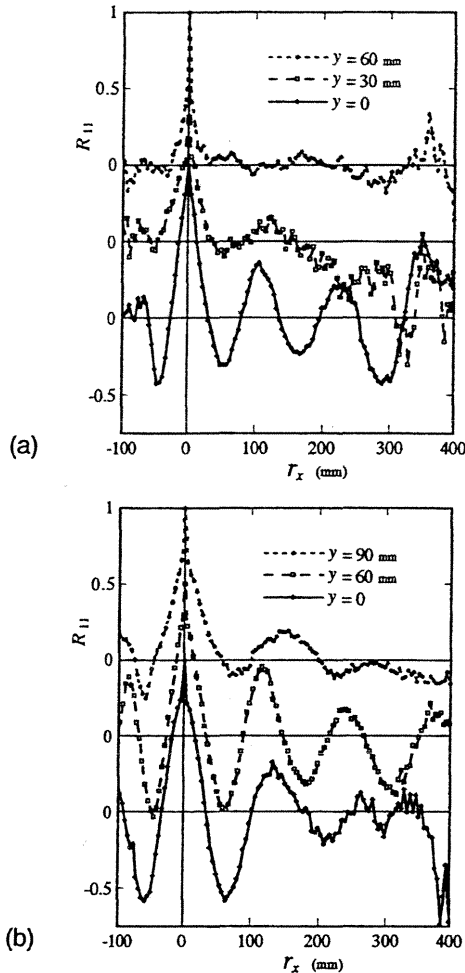


Fig. 6 Two-point correlation in the x -direction (reference position; $x = 150$ mm).
(a) $D/d = 3$, (b) $D/d = 5$.

4. Concluding remarks

The spatiotemporal flow structure behind a torus was investigated by using the UVP monitor. Instantaneous flow pattern and various statistical quantities including the streamwise two-point correlation, power spectral density of fluctuating velocity and conditionally averaged velocity profiles were analyzed. These quantities made clear the structural properties of the wake of the torus. Experiments and their analysis utilizing the UVP system are relatively speedy and easy in comparison with the traditional measuring system such as hot-wire anemometer, and it is expected that the flow structure around a torus set at attack angle will be clarified with the UVP system.

Acknowledgement

The authors wish to express their appreciation to Dr. Ing. Yasushi Takeda of Paul Scherrer Institut for his advice on UVP system.

References

- [1] R. E. Johnson and T. Y. Wu, *J. Fluid Mech.*, **95** (1979), 263.
- [2] S. L. Goren and M. E. O'Neill, *J. Fluid Mech.*, **101** (1980), 97.
- [3] A. M. D. Amarakoon, R. G. Hussey, B. J. Good and E. G. Grimsal, *Phs. Fluids*, **25** (1982), 1495.
- [4] D. R. Monson, *Trans. ASME J. Fluids Eng.*, **105** (1983), 308.
- [5] T. Leweke and M. Provansal, *J. Fluid Mech.*, **288** (1995), 265.
- [6] Y. Takeda, *Experimental Thermal and Fluid Science* (Elsevier Sci. Inc., New York, 1995), 444.

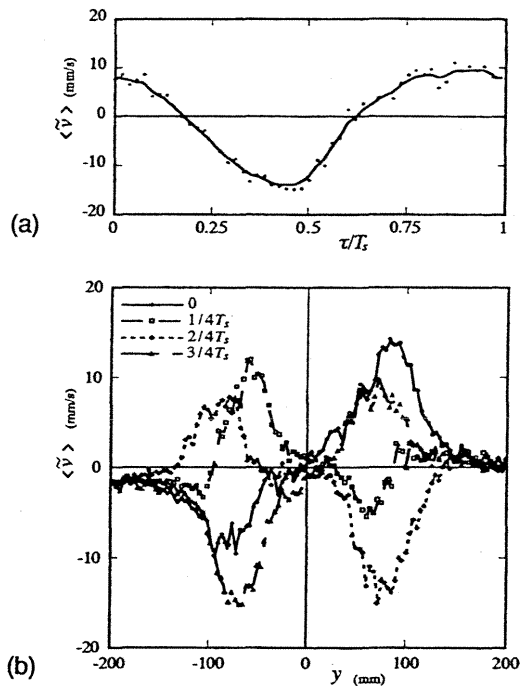


Fig. 7 Conditionally averaged profile of the v -component. (a) Reference signal, (b) averaged profiles corresponding to each phase.

tionally averaged reference signal. The number of averaging times is 18 and the mean periodic time T_s is 2.96 sec. This kind of conditional average elucidates the flow structure quantitatively, and these profiles clearly show that, although the flow is unsteady, it has an axi-symmetrical nature.

BENARD VON KARMAN VORTEX STREET DEVELOPMENT BEHIND A HEATED CYLINDER

N. MICHAUX-LEBLOND*, M. BELORGEY*, J.C. ATTIACH**

* Laboratoire de Mécanique des Fluides et Génie Civil

Université du Havre, Quai Frissard, BP 265, 76055 Le Havre Cedex, FRANCE.

** Signal Processing, 25 avenue Galliéni, 93800 Epinay sur Seine, FRANCE.

ABSTRACT

The alteration of the bi-dimensional wake behind a heated circular cylinder was previously investigated when buoyancy effects were added to the viscous ones. Velocimetry and thermocouples pointed out the configurations of forced and natural convection with respect to a critical heat input, and how they rule the wake when it is dominated on the one hand by the viscosity and on the other hand by the gravity (Michaux-Leblond 1994 [1]). The experimental results reported in this paper concern the three dimensional effects created by the ends of the cylinder (walls of the test section), how they spread all over the cylinder and how they affect the flow in a median plan when the vortex street is completely developed ($Re = 199$) behind a small length to diameter ratio cylinder ($L/d = 6.84$).

The temporal and spatial resolutions were respectively privileged by the use of an Ultrasonic Doppler Velocimeter (V.D.U.) and a Laser Doppler Velocimeter (V.D.L.).

I - INTRODUCTION

The present paper deals with the control of the vortex formation and shedding behind a circular cylinder. We particularly want to exhibit in which way the walls of the test section alter the characteristics of the wake.

What we know at this time is that the critical Reynolds number increases as far as the length to diameter ratio decreases (Shair *and al.* [2] and Nishioka *and al.* [3]). The length of the recirculating region follows a linear and growing variation with the Reynolds number (Taneda [4]). The recent studies of Le Masson [5] and Michaux-Leblond [1] put in clearness the presence of a threshold beyond which the position of the wake stagnation point decreases. Like the evolution of the Reynolds number, the point location is strongly dependant on the length to diameter ratio. If we consider that the cylinder is bounded at its ends by the walls of the test section, the closeness of the walls stabilises the wake. The cylinder end boundaries, whatever they may be, end plates or simple free ends, alter the vortex shedding mechanism near these boundaries and introduce three dimensional structures in the core of the flow, inherent in boundary layers created by the plates. In the past, this effect has usually been neglected. Studies were then accomplished with cylinder which length to diameter ratio sufficiently large to neglect the end-boundaries influence.

II - WORKING PRINCIPLE

The working principle of the Ultrasonic Doppler Velocimeter is to detect and process the echoes of ultrasonic pulses reflected by the microparticles contained in a flowing liquid. A single transducer emits the ultrasonic pulses and receives the echoes. All moving particles contained in the measured liquid introduce a frequency shift in the echo due to the Doppler effect. The velocity information is extracted by measuring these frequency shifts. The

measurement of time lapse between the emission and reception of the pulse gives the position of the scattering volume. By measuring the Doppler frequency shift at different times after the emission of the pulse, it is possible to obtain a velocity profile after a number of ultrasonic emissions. The axis resolution is a function of emitted pulse. If the time between two pulses decreases, the spatial resolution may improve but the echoes energy decreases.

III - EXPERIMENTAL CONFIGURATION

When the waves cross the walls of the test section, several reflections and diffractions appear, that are characterised by fixed echoes. These ones depend especially on the Doppler angle, the composition and the thickness of the wall and the transducer power supplied and will influence the velocity information quality near the walls but they can be easily filtered by a adapted treatment. Besides, this technical requires the use of particles with a minimum diameter so that the flow was sowed by corn starch particles. The ultrasonic pulsed wave used for this experimental configuration was governed by the flow regime previously investigated [1], [6].

In the same way, the U velocity field measurements were made by using an one component Laser Doppler Velocimeter operating in the forward scattering. The light supply comes from a 15 mW Helium-Neon Laser.

Measurements were made in an open loop water tunnel which test section is $80 \times 300 \text{ mm}^2$ in cross section and 1000 mm long. This apparatus presents two main features such as a vertical test section and an ascensional flow : the preoccupation is here to hold in position a symmetrical vortex shedding despite of the cylinder heating, and viscosity and buoyancy actions in a single direction. A detailed description of the apparatus working as well as its kinematics and geometrical characteristics are found in the reference [1].

The schematic diagrams of the transducer disposition and the reference system are presented respectively in figure 1 and 2.

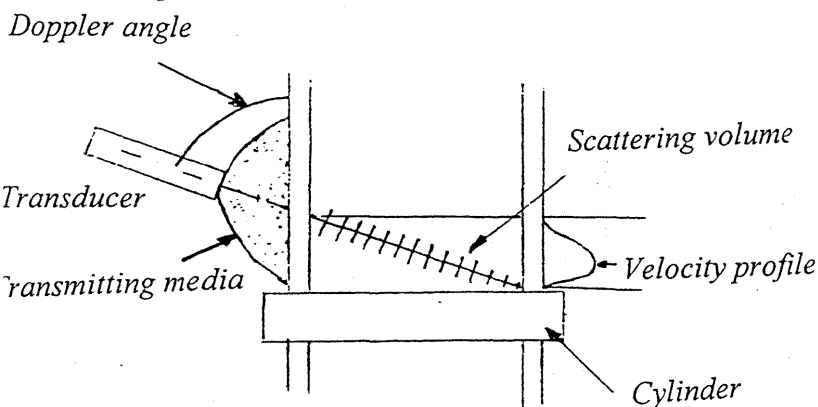


Figure 1 : *Experimental apparatus*

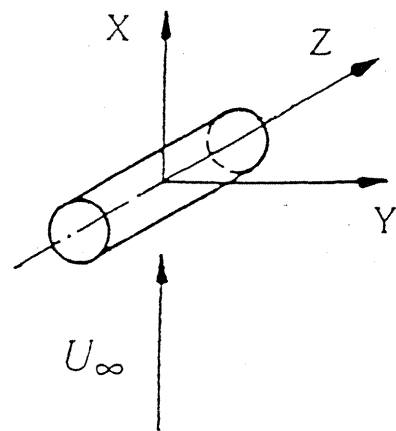


Figure 2 : *Reference system*

The origin of the coordinate system is situated on the revolution axis of the cylinder at half way of the walls of the test section.

IV - RESULTS

IV- 1. Isothermal wake

The first results concern the 3D isothermal wake for $x/d = 1.35$ when the vortex street is completely developed ($Re = 199$). The data represented in figures 3, 4 and 5 were respectively obtained by V.D.U. (figure 3 and 4) and V.D.L (figure 5).

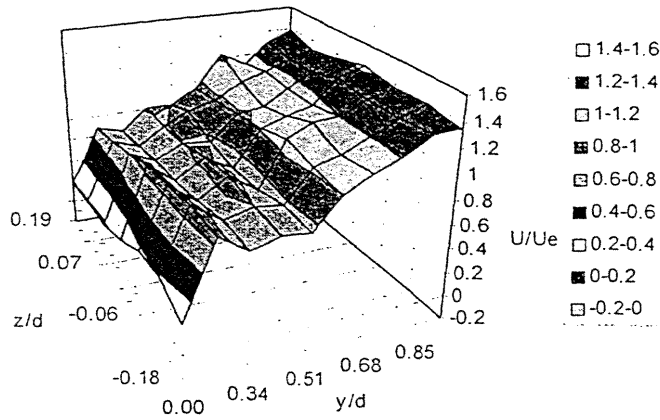


Figure 3 : *Velocity profiles - V.D.U.*
 $Re = 199 - x/d = 1.35 - 0.19 < z/d < 0.19$

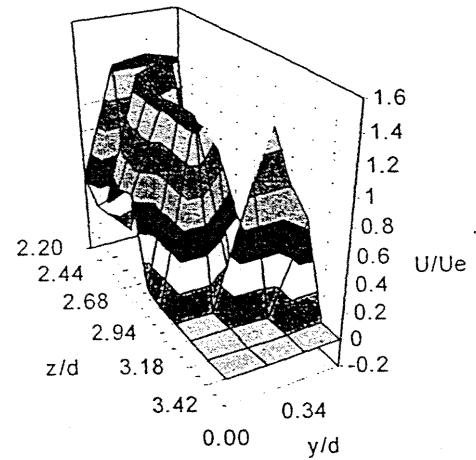


Figure 4 : *Velocity profiles - V.D.U.*
 $Re = 199 - x/d = 1.35 - 0 < z/d < 2.2$

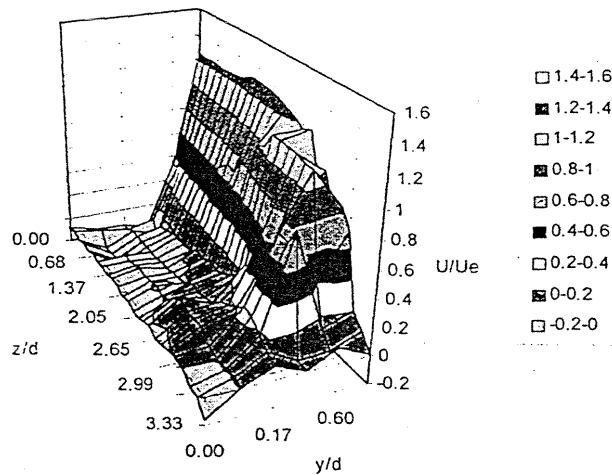


Figure 5 : *Velocity profiles - V.D.L* - $Re = 199 - x/d = 1.35 - 0 < z/d < 3.33$

Near the walls of the test section, a wide peak appear, strongly marked by the V.D.U. technical whereas, in the median part of the cylinder, the spatial resolution difference that characterises the two investigation methods does no more persist.

The further informations given by V.D.U. pointed out a temporal evolution of the spatial structures created by the walls of the test section.

IV- 2. Non isothermal wake

The figures 6, 7 and 8 represent the velocity field obtained by V.D.U. for $Re = 199$ and $x/d = 1.35$ when the cylinder is progressively heated.

For $P/L = 0$ W/m, the velocity field is relatively uniform. The heating of the cylinder creates fluctuations that spread over the cylinder axis and increase with the heat. However, these transverse structures are reduced in the cylinder recirculation area.

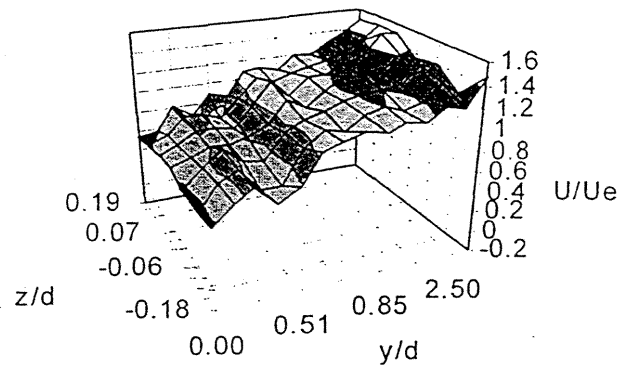
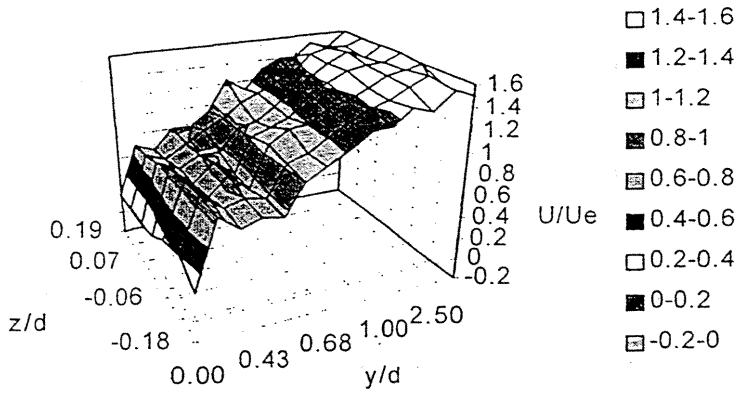


Figure 6 : *Velocity profiles - V.D.U.*
 $Re = 199 - x/d = 1.35 - P/L = 0 \text{ W/m}$

Figure 7 : *Velocity profiles - V.D.U.*
 $Re = 199 - x/d = 1.35 - P/L = 25 \text{ W/m}$

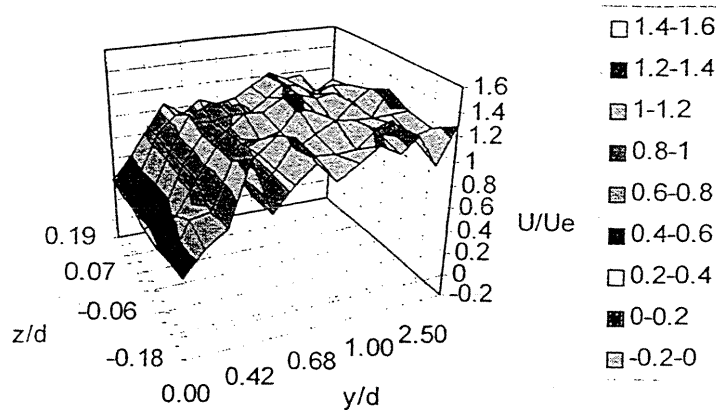


Figure 8 : *Velocity profiles - V.D.U.* - $Re = 199 - x/d = 1.35 - P/L = 93.75 \text{ W/m}$

V - CONCLUSION

The results obtained respectively by V.D.U. and V.D.L. pointed out the parts of the wake dominated by 3D structures.

The cylinder heating creates perturbations outside the recirculation area that are amplified as far as the heat input increases.

VI - REFERENCES

- [1] Michaux - Leblond N. : « Etude du comportement dynamique du sillage à l'aval d'un cylindre chauffé en régime mixte », Ph. D. Thesis, University of Le Havre, 1994.
- [2] Shair F. H., Grove A. S., Petersen E.E., Acrivos A. : « The effect of confining walls on the stability of the steady wake behind a circular cylinder », J.F.M. vol.35, part 2, pp.546-550, 1963.
- [3] Nishioka M., Sato H. : « Measurements of velocity distributions in the wake of a circular cylinder at low Reynolds numbers », J.F.M., vol 65, part 1, pp 97-112, 1974.
- [4] Taneda S. : « Experimental investigation of the wakes behind cylinders and plates at low Reynolds numbers », J. Phys. Soc. of Japan, vol 11, n°13, pp 302-304, 1972.
- [5] Le Masson S.: « Contrôle de l'instabilité de Benard Von-Karman en aval d'un obstacle chauffé à faible nombre de Reynolds », Ph. D. Thesis, University of Rouen, 1991.
- [6] Teufel M., Trimis D., Lohmüller A., Takeda Y, Durst F. : « Determination of velocity profiles in oscillating pipe-flows by using Laser Doppler Velocimetry and ultrasonic measuring devices », Flow Meas. Instrm., vol 3, n°2, 1992.

Submitted to:
 First International Symposium on Ultrasonic Doppler Methods for Fluid Mechanics and Fluid Engineering, 9.-11.
 September 1996, Paul Scherrer Institute, Villigen, Switzerland.

Investigation of free and forced flows of relevance to fast reactor thermohydraulics using the ultrasonic Doppler method.

A. Tokuhiro

*PNC International Fellow, Reactor Engineering Section, Safety Engineering Division, Oarai Engineering Center, Power Reactor and Nuclear Fuel Development Corporation (PNC), 4002 Narita, Oarai-machi, Ibaraki, Japan, 311-13.

KEY WORDS: *UVP, water, mixed convective flow, penetrating flow, vertical mixing layer, buoyant jet, stirred vortex flow, flow mapping, two-dimensional velocity field, steady- and transient measurement, spectral analysis.*

1. March 1996, a.tokuhiro

Extended Abstract

This extended abstract describes two experimental investigations of general interest to the convective heat transfer community, but of particular interest to those engaged in the design of liquid metal-cooled, energy intensive facilities such as the liquid metal fast breeder reactor.

1. Thermal Striping

Thermal striping refers to the phenomenon of fluid-structure interactions in nuclear reactors (specifically liquid-metal cooled reactors), the result of which reactor structures and components incur undesirable thermal stresses. The thermal-hydraulics aspects of this problem concern the random streams of poorly mixed hot and cold coolant. One critical area is the above-core structure of a LMFBR, which due to flow of hot/cold jets out of the core, may experience thermal striping. Since the thermal fatigue behavior of above-core components and their locations are generally known, understanding the convective mixing (or non-mixing) of buoyant and forced-flow is important to the safe design of the reactor. In the present case a basic experiment using a water test facility and consisting of LDA, UVP and recently PIV velocity measurement techniques, as well as temperature measurement has been initiated. The flow geometry is a central cold jet surrounded by two hotter jets, each exiting out of a rectangular nozzle.

In **Figure 1** we show a schematic of the test section and a magnified view of the probe orientation with respect to the jet nozzles. The UVP transducer was set at a 10° incline with respect to the horizontal and measurements were taken from both the left and right sides. Unless noted the vertical transverse increments were 5 mm. In the cases shown here, the central jet was set at 30°C while the two adjacent jets were at 35°C. All three jets had equal flowrates out of the nozzle and an exit average velocity of 0.5 m/s.

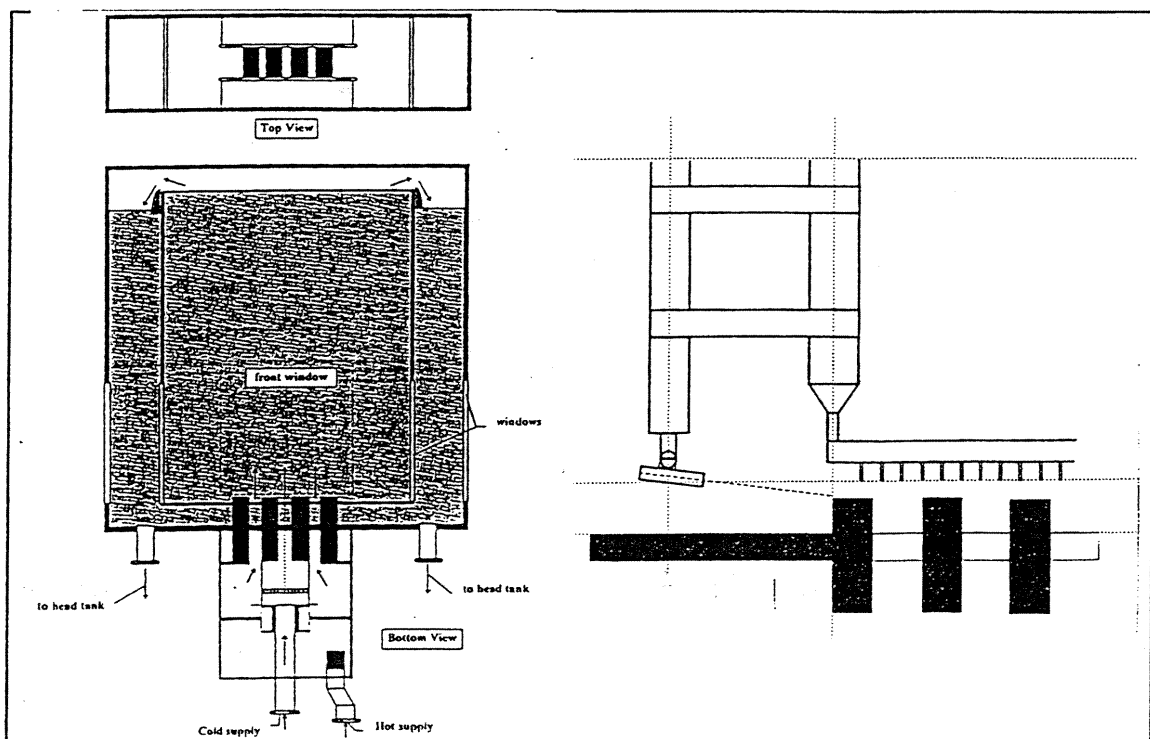
Figure 2, 3, 4 and 5 show some typical results and these are summarized as follows. They are:

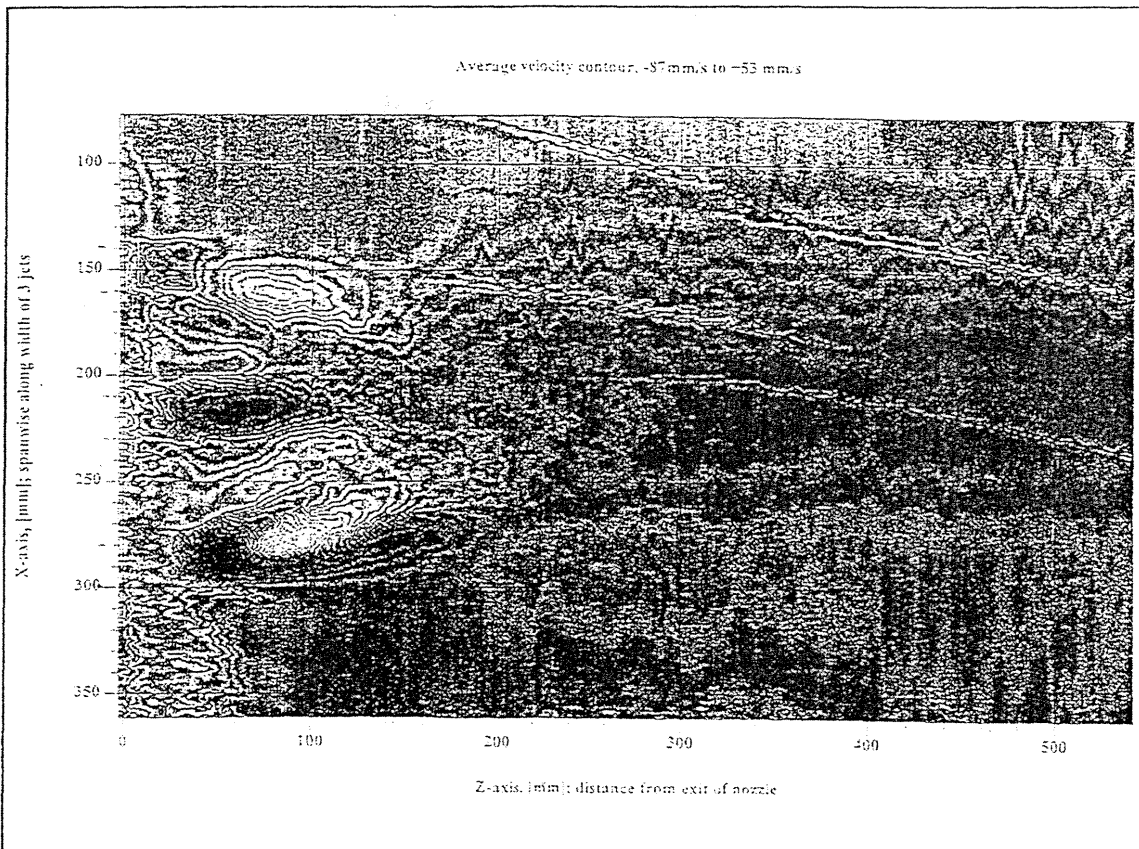
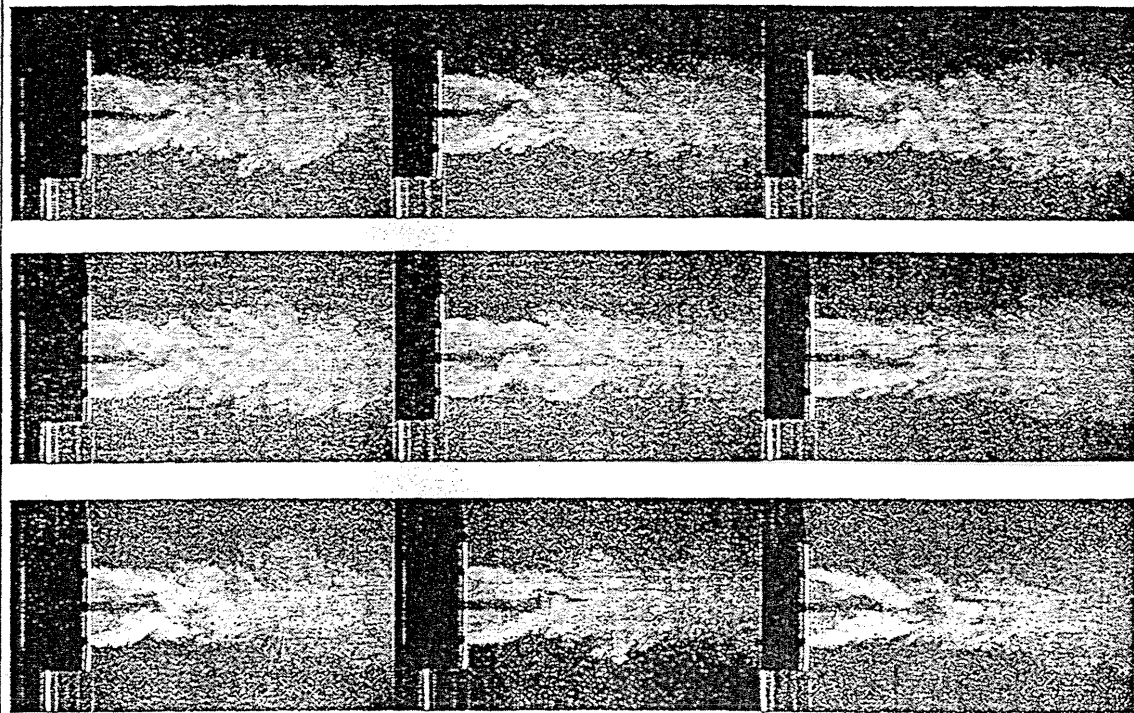
Figure 2. A sequence of four consecutive images as digitized from video pictures during an experimental run. A laser sheet was introduced from the right of the image in order to enhance visualization of the flow.

Figure 3. A grayscale image of the temperature fluctuation distribution as taken with a spanwise array of 35 thermocouples positioned on a traversing mechanism. Two spanwise profiles at $z \sim 45$ and 200 mm from the exit are inset. The vertical and horizontal axes are respectively, the spanwise width covering the exit of the three jets and the axial distance along which temperature measurements were made.

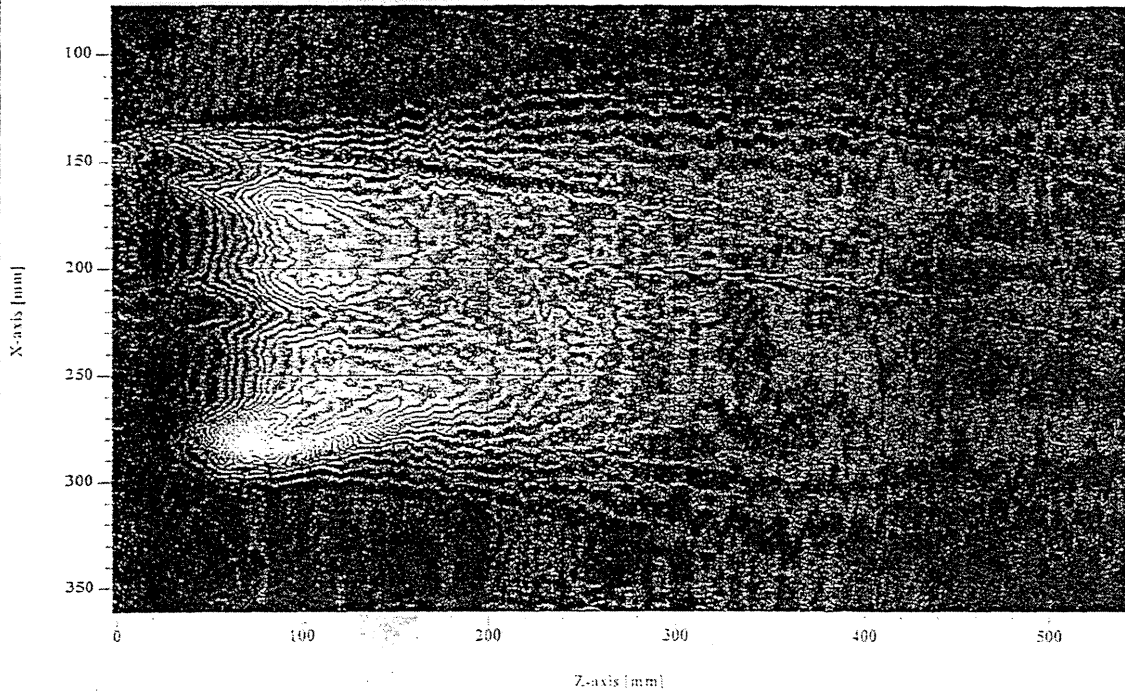
Figure 4. A grayscale image of the velocity fluctuation distribution that nearly corresponds to w' . The vertical and horizontal axes are respectively, the spanwise width covering the exit of the three jets and the axial distance along which UVP measurements were made.

Figure 5. The *constructed* turbulent heat flux distribution, $w't' = f(x,z)$, where w' and t' are respectively, the fluctuating component of velocity, as measured using the UVP, and that of the temperature, as measured using a thermocouple array. The distribution shows that under these conditions, most of the thermal mixing takes place within the first $z \sim 200$ mm from the exit of the jets and that spanwise, the regions with the highest calculated fluxes are approximately those in between the cold and hot jets.

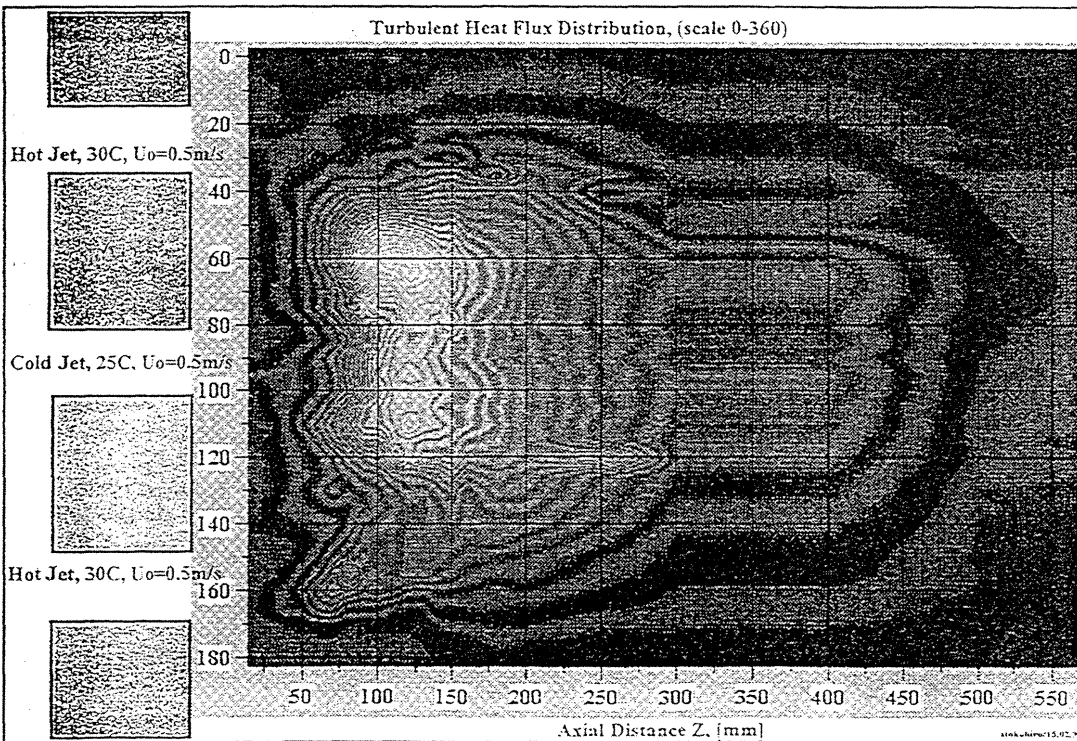




Std. Dev. Contour of Triple-Jet



Turbulent Heat Flux Distribution, (scale 0-360)



1. ISUD

1st International Symposium on Ultrasonic Doppler Methods
for Fluid Mechanics and Fluid Engineering

September 9-11, 1996

Paul Scherrer Institute, 5232 Villigen PSI, Switzerland

Visualization Techniques for Fluid Flow Fields

Prof. Dr. Thomas Ertl

Universität Erlangen-Nürnberg

Institut für Mathematische Maschinen und Datenverarbeitung

Lehrstuhl für Informatik 9 (Graphische Datenverarbeitung)

1.ISUD
 1st International Symposium on Ultrasonic Doppler Methods
 for Fluid Mechanics and Fluid Engineering
 September 9-11, 1996
 Paul Scherrer Institut, 5232 Villigen PSI, Switzerland

Influences of fixed and moving interfaces in the measurement of velocity profiles

Dr. J.-Cl. Willemetz

Signal Processing S.A., 21 av. de la Gare, 1003 Lausanne, Suisse

ABSTRACT

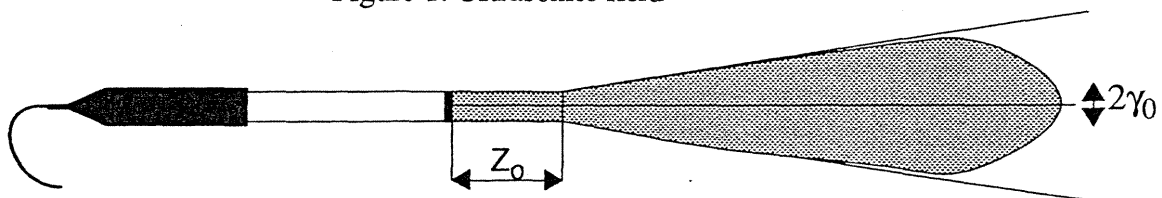
The knowledge of the size and positions of the measuring volumes of a multigate Doppler velocimeter are often difficult. These difficulties arise from many factors. The precise knowledge of the ultrasonic field is seldom known. Moving or fixed interfaces affect the shape of the ultrasonic field.

In order to profit from the main advantage of pulsed ultrasonic Doppler velocimeters, which is a depth resolution, it is of utmost importance to have a good understanding of acoustical phenomena which generate the echoes.

1. Acoustical field

In Doppler echography, the object is not to make use of a plane longitudinal wave, but rather an ultrasonic beam that is as thin as possible throughout the measurement depth. The geometry of the acoustic field generated by the ultrasonic wave determines the lateral resolution. The characteristics of the acoustic field depend on the size and shape of the piezoelectric element for a single element transducer, and on the combination of the individual emissions in the case of a multi-element transducer. Using Huygen's principle, one may theoretically predict the geometry of the acoustic field. In this approach, the transducer is modeled as a combination of several adjacent point sources, each generating a spherical wave. For a circular transducer operating in a piston-like manner, the acoustic field possesses two characteristic regions, the near field and the far field.

Figure 1: Ultrasonics field



The geometry of the acoustic field in the near field is basically contained in a cylinder having the same diameter as the transducer and a length equal to:

$$Z_0 = \frac{r^2}{\lambda}$$

where r is the radius of the transducer and λ the wave length. The zone lying beyond z_0 is called the far field. In the far field, the intensity of the acoustic field varies approximately as the inverse of the square of the distance from the transducer. In the far field, the acoustic field may possess intensity lobes as one moves away from the axis of the transducer. The angle of divergence of the main lobe γ is given by:

$$\gamma_0 = \sin^{-1} \left(\frac{0.61\lambda}{r} \right)$$

The acoustic energy contained in the secondary lobes is always much smaller than that contained in the main lobe. For a circular transducer, the acoustic energy contained in the secondary lobe is 18 dB less than in the main lobe.

2. Influences of interfaces

The above simplified approach shows that it is possible to have an approximate knowledge of the acoustic field generated by circular ultrasonic transducers when no interfaces are present. Or this situation rarely appears. The interfaces reflect and modify the acoustic field. The intensity of the acoustic field received in a point, which depends on the material, the shape and the number of these interfaces, is very difficult to evaluate. This lack of knowledge does not allow a precise determination of the size of the measuring volume.

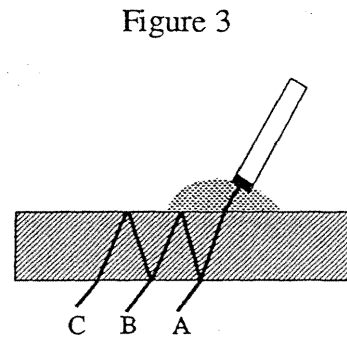
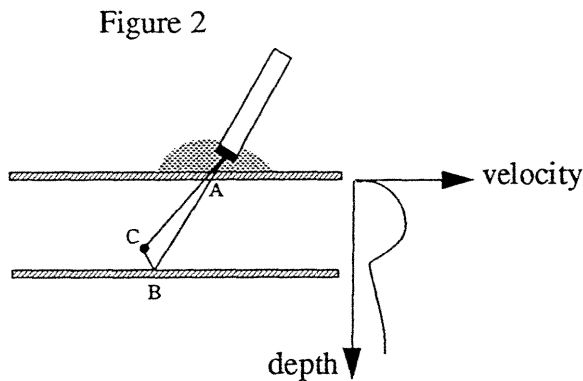
These interfaces may generate, in certain situations, artifacts and induce modifications in the velocity profiles as presented in the figures 2 and 3.

The ultrasonic beam BC reflected by the far interface of the figure 2 transforms this interface in a transmitter. The same particles contained in the liquid will backscatter a second time energy in the direction to the transducer. The depth associated to the path ABC is located outside the flowing liquid. Imaginary velocity components are added to the real velocity profile. The measurement of velocities near the far interface is affected by this phenomenon. The size of the ultrasonic beam determines mainly the level of this artifact.

The figure 3 displays another situation often founded. The reflected ultrasonic waves inside a wall enlarge the ultrasonic beam inside the liquid and modify its shape. These reflections disturb the determination of the size and the shape of the measuring volume. The thickness, the acoustical impedance and the attenuation coefficient of the interface determines the level of this phenomenon.

The interfaces often give strong reflections. Despite of the many reflections which are necessary to reach the transducer, the energy reflected by these interfaces is often stronger than the energy coming from the particles flowing with the liquid. Most of the algorithms used to compute the Doppler frequency shift do not allow stationary components. The elimination of these stationary components by high-pass filtering implies an increase in the dynamic of the analyzed echoes

and a reduction in the sensitivity in the measurement of low velocities.

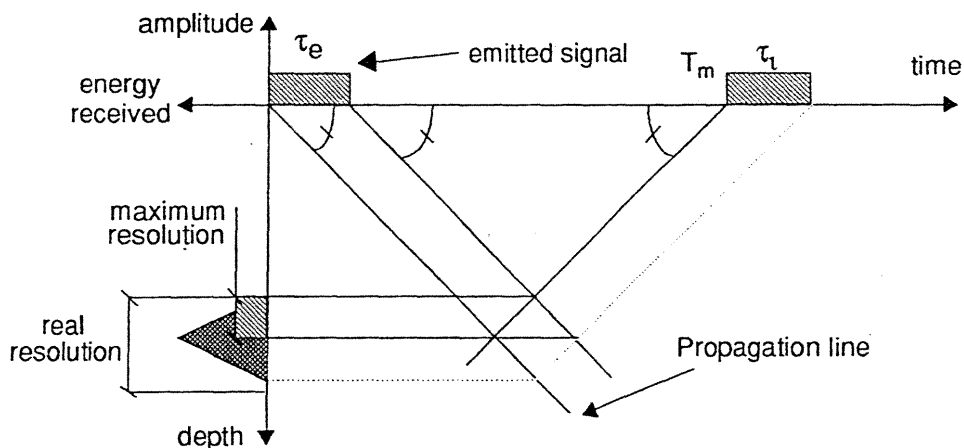


When some interfaces are in movement the correct estimation of all the velocity field is very difficult. The echoes generated by such interfaces may affect the velocity profile in many places due to the combination of many reflections. The Doppler frequency shift induced by these movable interfaces can not be removed if their values have the same values as the flowing particles.

3. Spatial resolution

For an unlimited bandwidth receiver and if no interfaces are present, the duration of the impulse determines the depth resolution by determining the longitudinal size of the sample volume. The other dimensions are determined by the beam pattern of the transducer.

Figure 4: Longitudinal resolution



Consider an impulse of duration τ_e as illustrated in the figure 4. The impulse propagates in time along a straight slanted line, with the slope being the speed of sound. Consider a measurement time T_m on the time axis. By drawing a straight line which is perpendicular to the propagation line and which passes through T_m , the depth resolution may be determined by the projection of the intersection of these two lines on the depth axis. The corresponding resolution is the maximum attainable resolution for this type of emission.

The demodulated Doppler signals must be filtered in order to eliminate unwanted frequencies generated by the demodulation process. This filter acts as an integrator and reduces the depth resolution, as shown in the figure by the broken line. There is an optimum value for the product of the bandwidth and the impulse duration which will give the maximum SNR, provided the

frequency and temporal characteristics of the noise are known. This value also depends on the characteristics of the filter and the signal to be filtered.

4. Conclusion

In order to be able to correctly use the results of an ultrasonic pulsed Doppler velocimeter it is of utmost importance to have a good understanding of the generation process of the echoes. This understanding is much easier when the velocimeter can:

- adapt the emitting frequency to the analyzed medium,
- adapt the acoustical level emitted,
- adapt the amplification level of the echo in relation to the depth,
- visualize the modulus of the echo versus depth,
- visualize the Doppler energy versus depth,
- have a powerful Doppler frequency shift estimator, which gives the first moment order of the power spectrum density,
- adapt the number of ultrasonic bursts emitted used to compute the Doppler frequency shift.

5. References

- [1] Willemetz J.C.
Etude Quantitative de l'Hémodynamique de Vaisseaux Profonds par Echographie Doppler Ultrasonore
Thèse No 893, EPFL Lausanne, Switzerland, 1990
- [2] Willemetz J.C., Nowicki A., Meister J.J.
Bias and Variance in the Estimate of the Doppler frequency Induced by a Wall Motion Filter.
Ultrasonic Imaging, No 11, 1989
- [3] Newhouse V.L.
The Dependence of Ultrasound Doppler Bandwidth on Beam Geometry
IEEE Trans. on Sonics and Ultrasonics, Vol 27, 1980
- [4] Y. Takeda, W.E. Fisher, J. Sakakibara
Measurement of Energy Spectral Density of a Flow in a Rotating Couette System
Physical Review Letters, Volume 70, Number 23, 1993
- [5] M. Teufel, D. Trimis, A. Lohmüller, Y. Takeda, F. Durst
Determination of velocity profiles in oscillating pipe-flows by using laser Doppler velocimetry and ultrasonic measuring devices
Flow Meas. Instrum., Vol. 3, No 2, 1992
- [6] Gordon S. Kino
Acoustic waves
Prentice-Hall, Signal Processing series, ISBN 0-13-003047-3 025 (1987)

1. ISUD
 1st International Symposium on Ultrasonic Doppler Methods
 for Fluid Mechanics and Fluid Engineering
 September 9-11, 1996
 Paul Scherrer Institut, 5232 Villigen PSI, Switzerland

UVP MEASUREMENT ON MAGNETIC FLUID SLOSHING

T. Sawada¹⁾, H. Kikura²⁾, Y. Takeda³⁾, and T. Tanahashi¹⁾

1) Department of Mechanical Engineering, Keio University
 3-14-1 Hiyoshi, Kohoku-ku, Yokohama 223, Japan

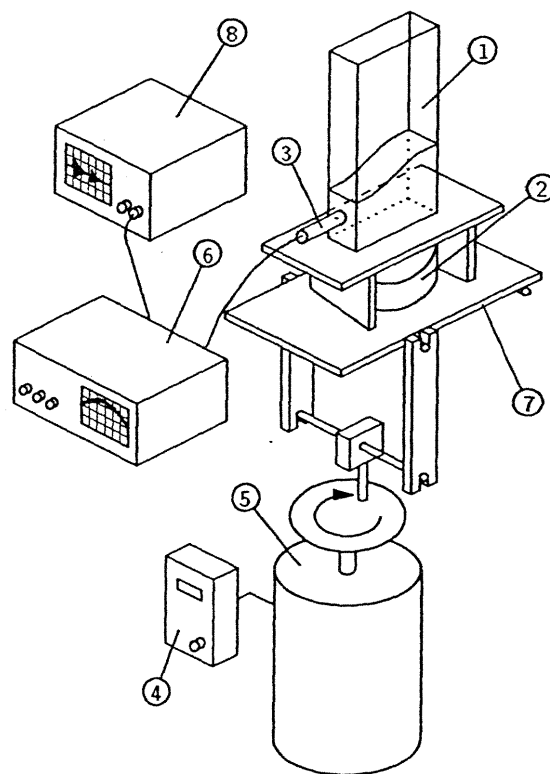
2) Lehrstuhl für Strömungsmechanik, Universität Erlangen-Nürnberg
 Cauerstraße 4, 91058 Erlangen, Germany

3) Paul Scherrer Institut, 5232 Villigen PSI, Switzerland

1. Introduction

A magnetic fluid is a stable suspension of solid magnetic particles (5~15nm). These particles are coated with a layer of surfactant which inhibits their coalescence. As a result, the magnetic fluid is a stable colloidal dispersion of rather small surfactant-coated magnetic particles in a liquid carrier. When a magnetic field is applied to a sample of magnetic fluid, the magnetic particles in the fluid tend to remain rigidly aligned with the direction of the orienting field. Then, several interesting behaviors have been observed[1].

Recently, interfacial instability of a magnetic fluid in an applied magnetic field has attracted the attention. Zelazo and Melcher[2] studied dynamic behavior of a magnetic fluid in an oscillated container. Dodge and Garza[3] demonstrated a simulation of liquid sloshing in low-gravity by using a magnetic fluid. Sawada, et al.[4] investigated two-layer liquid sloshing of a magnetic fluid and a silicon oil in a rectangular container, and clarified effects of magnetic field on



1.Container	2.Magnet	3.US Transducer
4.Controller	5.Motor	6.UVP Monitor
7.Shaking table	8.Oscilloscope	

Figure 1: Experimental Apparatus

the resonant frequency. Ohaba and Sudo[5] examined surface responses of a magnetic fluid in a vertically vibrated container subjected to a normal magnetic field.

The sloshing problem does not seem easy from a mathematical point of view. Obvious nonlinearities are occurring especially in the vicinity of the resonant frequency. In order to understand and explain this complex problem, a nonlinear approach and detailed measurement of internal velocity profiles are necessary. However, any optical method like laser Doppler anemometry or flow visualization technique have not been applicable because a magnetic fluid is opaque. An ultrasonic velocity profile(UVP) measurement is a method for measuring a velocity profile on a line with respect to the velocity component along this line[6,7]. The aim in the present paper is to examine the applicability of UVP measurement to a magnetic fluid sloshing which has periodic velocity field. We attempt also to obtain nonlinear sloshing responses up to the third order perturbation. These experimental and theoretical results are compared.

2. Experiment

Figure 1 shows a schematic diagram of the experimental apparatus. The rectangular container measures $80\text{mm} \times 20\text{mm} \times 150\text{mm}$, and is made of transparent acrylic resin. The adjustable crank is mounted on the output shaft of the motor. The frequency of the motor is controlled continuously by the inverter. The shaking table is oscillated sinusoidally and its range of oscillation is $1.17\text{Hz} \leq f \leq 4.33\text{Hz}$. The amplitude of the oscillation is $X_0=1.5\text{mm}$ for all experiments. Magnetic field is applied by a cylindrical permanent magnet whose diameter is 110 mm. We use a water-based magnetic fluid. Its kinematic viscosity, density and sound velocity are $\nu=4.2 \times 10^{-6} \text{ m}^2/\text{s}$, $\rho=1.24 \times 10^3 \text{ kg/m}^3$ and $c=1410\text{m/s}$ at 25°C , respectively. The fluid depth is $h=40\text{mm}$ in the present experiment. Since magnetic particles in the magnetic fluid are too small as reflecting particles for the ultrasonic wave, we use porous SiO_2 powder with a mean diameter of $0.9\mu\text{m}$ (MSF-10M, Liquidgas Co., Ltd.). The ultrasonic(US) transducer is fixed on the side wall of the container in order to measure the horizontal velocity profile V_x . Its nominal diameter is 5mm, and the measuring volume has a thin-disc shape, $\phi 5\text{mm} \times 0.71\text{mm}$. The UVP monitor is X-1 PS manufactured by Met-Flow AG. The basic frequency is 4MHz and the pulse repetition frequency is 3096Hz.

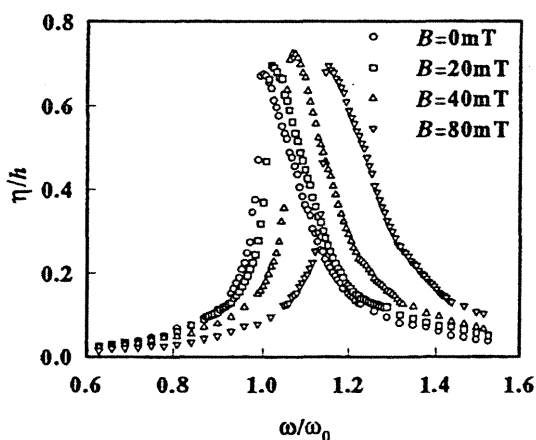


Fig.2 Frequency responses of the free surface of a magnetic fluid

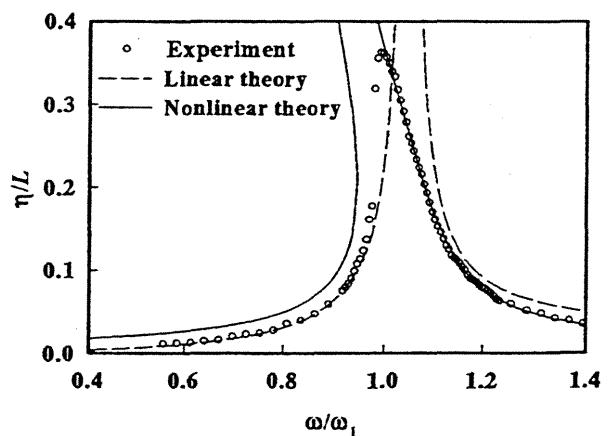


Fig.3 Comparison with theoretical and experimental results of frequency response for $B=40\text{mT}$

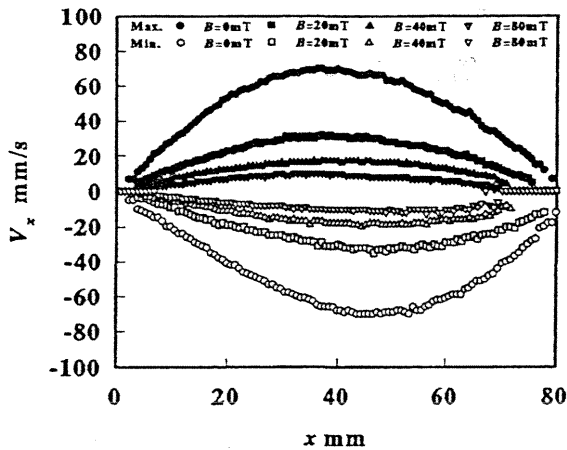


Fig.4 Maximum velocity profiles for $f=2.75\text{Hz}$ at $h_z=10\text{mm}$

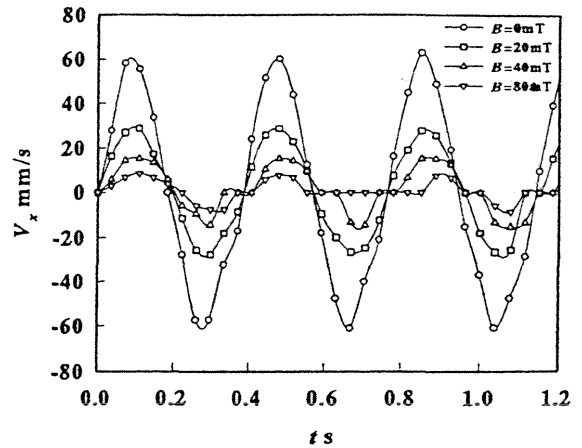


Fig.5 Time dependent velocity profiles for $f=2.75\text{Hz}$ at $x=39.96\text{mm}$ and $h_z=10\text{mm}$

3. Results and Discussions

Frequency responses of the free surface of a magnetic fluid are shown in Fig.2. Here B is the surface magnetic field induction at the center of the permanent magnet, η is the maximum free surface elevation at the side wall and ω_0 is the first resonant angular frequency for $B=0$. As the forcing frequency increases, the surface elevation also increases

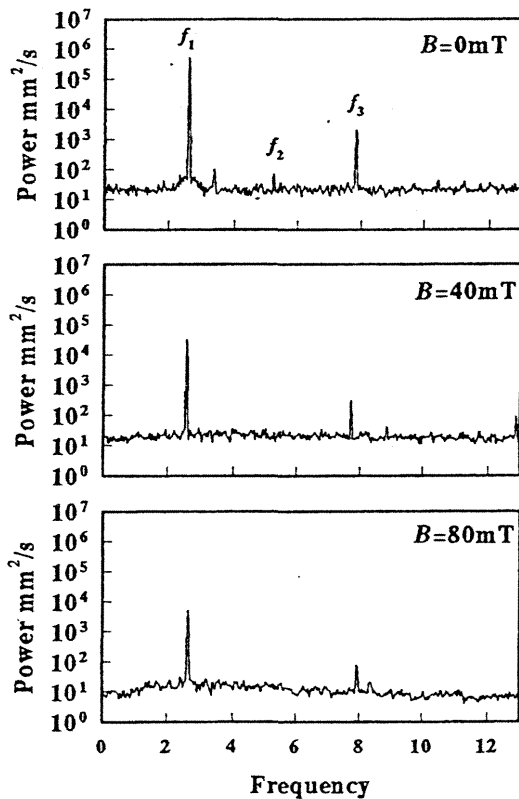


Fig.6 Averaged power spectra for $f=2.75\text{Hz}$ over $30.34\text{mm} \leq x \leq 50.32\text{mm}$ at $h_z=10\text{mm}$

and the free surface is intensively shaken near the resonant frequency. When the frequency goes over the resonant frequency, the surface disturbance is repressed. The first resonant frequency is shifted to the high frequency region as the magnetic field intensity becomes large. Assuming a potential flow and using a perturbation method, we have obtained nonlinear sloshing responses up to the third order perturbation $O(\varepsilon^3)$, where ε is $(X_0/L)^{1/3}$ and L is the length of the container. In Fig.3 experimental results are compared with the linear and nonlinear theoretical results for $B=40\text{mT}$. Here ω_1 is the first resonant angular frequency obtained by the linearized wave theory. In the low frequency range, the nonlinear solution is larger than experimental values because calculated amplitude does not become zero with a decrease of the frequency[8]. Experimental and nonlinear theoretical results have a good agreement in a high frequency region.

UVP measurements were mainly carried out at near-resonant frequencies.

Figure 4 shows maximum velocity profiles for several applied magnetic fields. There are 1024 measurement points along the measurement axis and each datum point represents the maximum velocity value over a 39ms period. Time dependent velocity profiles at the middle point are illustrated in Fig.5. Here x is the distance from the side wall where US transducer is fixed, and h_z is the position of the US transducer from the bottom wall. $f=2.75\text{Hz}$ is the resonant frequency for $B=0$. Positive velocity means the flow direction away from the US transducer. When the magnetic field increases, the velocity decreases because of the magnetic force. The spatial velocity profiles are not symmetric with respect to the center axis ($x=40\text{mm}$) as shown in Fig.4. It is caused by nonlinearity of the fluid motion.

From measured velocity data, we calculated 128 power spectra by using a fast Fourier transform in time domain. Figure 6 shows the power averaged over a center region ($30.34\text{mm} \leq x \leq 50.32\text{mm}$, $h_z=10\text{mm}$). The most dominant peak is f_1 , which corresponds to the forcing frequency. f_2 and f_3 represent the twice and three times the forcing frequency, respectively. Every height of peaks decreases with increasing B because the disturbance of the fluid is suppressed by the magnetic field.

Figure 7 illustrates time averaged spatial distributions of the power spectra for f_1 , f_2 and f_3 at a resonant state ($f=2.93\text{Hz}$) for $B=40\text{mT}$. Nonlinear theoretical spatial spectra for f_1 , f_2 and f_3 are drawn by broken line, chain line with two dots and full line, respectively. Distributions of the frequency component f_1 are in agreement with theoretical results. But other power spectra deviate from theoretical lines, especially near the side wall away from the US transducer. The clustering and chaining of the magnetic particles of a magnetic fluid are formed under an applied magnetic field. Consequently, it is supposed that the US echo signal diminishes.

References

- [1] see e.g., R.E.Rosensweig, *Ferrohydrodynamics* (Cambridge University Press, New York, 1985), p.177.
- [2] R.E.Zelazo and J.R.Melcher, *J.Fluid Mech.* **39** (1969) 1.
- [3] F.T.Dodge and L.R.Garza, *Tech.Rep.* No.9, Contract No. NAS8-20290 (1970)
- [4] T.Sawada, et al., *J.Magn.Magn.Mater.* **122** (1993) 424.
- [5] M.Ohaba and S.Sudo, *J.Magn.Magn.Mater.* **149** (1995) 38.
- [6] Y.Takeda, *J.Heat Fluid Flow* **7** (1986) 313.
- [7] Y.Takeda, *Nucl.Technol.* **79** (1987) 120.
- [8] S.Hayama, K.Aruga and T.Watanabe, *Bull.JSME* **26** (1983) 1641.

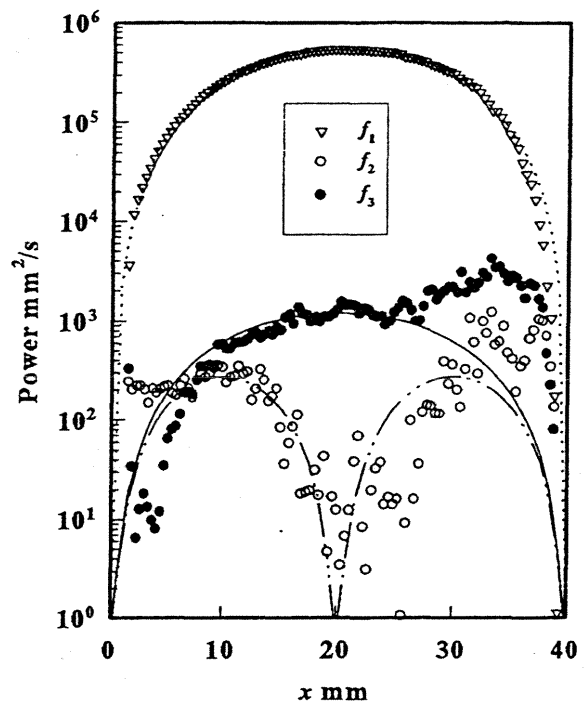


Fig.7 Spatial distributions of the power spectra for $f=2.93\text{Hz}$ and $B=40\text{mT}$

1.ISUD

1st International Symposium on Ultrasonic Doppler Methods
for Fluid Mechanics and Fluid Engineering

September 9-11, 1996

Paul Serrer Institut, 5232 Villigen PSI, Switzerland

TAYLOR VORTEX FLOW OF A MAGNETIC FLUID

H.Kikura¹⁾, Y.Takeda²⁾ and F.Durst¹⁾

1) Lehrstuhl für Strömungsmechanik, Universität Erlangen-Nürnberg
Cauerstrasse 4, 91058 Erlangen, Germany

2) Paul Scherrer Institute, 5232 Villigen PSI, Switzerland

ABSTRACT

Flows of magnetic fluids are increasing importance in a number of fields of engineering and this has increased the interest in studying flows of this kind. For such flow investigations conventional methods, such as hot wire anemometry, cannot be applied because of the special properties of magnetic fluids. In addition, the dark coloured liquid does not permit laser-Doppler-techniques to be used to locally study the flow fields. In order to investigate fluid flow fields of liquids with optically non-transparent media, the Ultrasound Velocity Profile Method (UVP-method) has been developed. Recently velocity information obtained in liquid metal flows has become available, i.e. measurements in mercury[1] and measurements in sodium[2]. Hence, a method has become available that can be applied to also investigate flow fields of magnetic fluids.

The UVP-method employs the instantaneously measured frequency of pulsed ultrasound wave, backscattered from small tracer particles suspended in a flowing fluid which is transparent to ultrasound, although it might not be transparent to light. In spite of the fact, that magnetic fluids are composed of solid, magnetic, single domain particles coated with the molecular layer of a dispersant, the diameter of these particles lying in the size range of 5 to 15 nm is too small to yield good ultrasound signals. To yield such signals, tracer particles have been added (Micro Sphericalfeather: MSF) made of a SiO₂-shell yielding a spherical, uniform diameter particle (0.9 μm) of low effective, specific gravity. Although these particles are much smaller than the wavelength of the ultrasound, the reflected power is efficient for good signal-to-noise ratio of the detected ultrasound wave. This will be explained in the presentation.

The present investigations are based on the propagation of ultrasound waves in magnetic fluids which possess a large absorption of ultrasound. Thus the measuring length in the magnetic fluid was only 100 mm in the present case. The propagation of ultrasound in magnetic fluids was investigated by Gogosov et al.[3]. They showed that the sound velocity in a magnetic fluid was smaller than in the solvent, and also that the sound velocity changed when a magnetic field was applied. They also found that the sound velocity did not depend on the frequency of ultrasound and did not change monotonically with the temperature of the magnetic fluid.

To consider the differences in sound velocity in different magnetic fluids, it is also investigated the velocity of ultrasound in the present magnetic fluid. Test liquid is a magnetic fluid with 40% weight concentration of fine magnetite(Fe_3O_4) particles in a water carrier. The sound velocity 1410m/s at 22°C is measured. Since the intensity of the magnetic field is small, no difference in sound velocity under the magnetic field is obtained.

The UVP method is applied to time-dependent Taylor vortex flows obtained between two concentric rotating cylinders to measure time-dependent dynamics of the flow of a magnetic fluid. Some experimental investigations by mean of torque characteristics for cylindrical and spherical Couette flow on magnetic fluids were studied[4],[5]. Niklas[6] solved the ferrohydrodynamic equation for Taylor vortex flow and obtained the changes in the critical Taylor number T_c and wave number k_c which characterize the instability of the flow.

Taylor vortex flow is typically studied for flow transition from laminar to turbulent flow[7]. The aim of the present paper is to measure the internal flow of a magnetic fluid on Taylor vortex flow. Two concentric cylinders were made of transparent acrylic (Fig.1). The length of the cylinders are 160mm, the outside radius of the inner cylinder $R_i=15\text{mm}$ and the inside radius of the outer cylinder $R_o=23\text{mm}$. They were placed vertically and the UVP transducer was located in order to measure the axial velocity distributions. In a system with the outer cylinder fixed, the fluid in the annular gap moves in a plane perpendicular to the cylinder axis for small Reynolds number ($Re = \Omega R_i (R_o - R_i) / \nu$). The nonuniform magnetic field was applied horizontally using a 70mm \times 70mm \times 15mm magnet from outside of cylinders. Three different intensity of magnetic fields at the surface of outer cylinder are 36mT, 57mT and 79mT which are measured by changing the distance between the cylinders and the magnet. The UVP monitor is X-1 PS in 4MHz.

Steady-state velocity distributions at $Re/Re_c = 1.72$ are given in figure 2. This shows the time-averaged velocity profiles of the axial component at the inner wall position. Since the data set consists of 128 times series of 1024 data points, the temporal characteristics of the flow were studied using a Fourier transform in the space domain[8]. This is an energy spectral density in wavenumber with sufficient data points and resolution. Figure 3 shows the time-averaged energy spectral density(ESD). The wavelength of the roll structure can be readily obtained for the profile and was estimated for steady state data as an average of 6 rolls(3 vortex pairs) which are influenced with the magnetic field. A decreasing tendency is seen on maximum ESD and wavelength along with a decline in the intensity of the magnetic field(Figure 4). From approaching to zero value of multiply by the maximum velocity($A^2 = Vx_{MAX}^2$), it is possible to determine the critical Reynolds number as shown in figure 5. The critical Reynolds number under the non magnetic field is $Re_c=75$ which is in good agreement with the analytical value of the radial ratio $\eta=0.65$ [9]. This suggests that the magnetic fluid shows relatively good Newtonian fluid behavior on present flow without the magnetic field. However the data with the magnetic field show different trend. Increasing the intensity of magnetic field, the line shift toward a higher value and the critical Reynolds number also shift up. This shows that the apparent viscosity of magnetic fluid under the magnetic field is increased.

Reference

- [1] Takeda, Y., *Nuclear Technology*, **79** (1987), 120.
- [2] Kamoshida, H., *et al.*, (1995), E57.
- [3] Gogosov, V.V. *et al.*, *J. Mag. Mag. Mat.*, **122** (1993), 70.
- [4] Kamiyama, S., Appl. Eng. Publication Ltd., Tokyo(1989).
- [5] Yamaguchi, H. and Koori, I., *J. Mag. Mag. Mat.* **122** (1993), 221.

- [6] Niklas, M., *Zeitschrift für Physik B* (1987), 493.
 [7] Takeda, Y. *et al.*, *Science* **263** (1994), 502.
 [8] Takeda, Y., *Int. J. Heat Mass Flow* **7** (1986), 313.
 [9] Di Prima, R.C. and Swinney, H.L., *Topics in Applied Physics* **45** (1985), p.139.

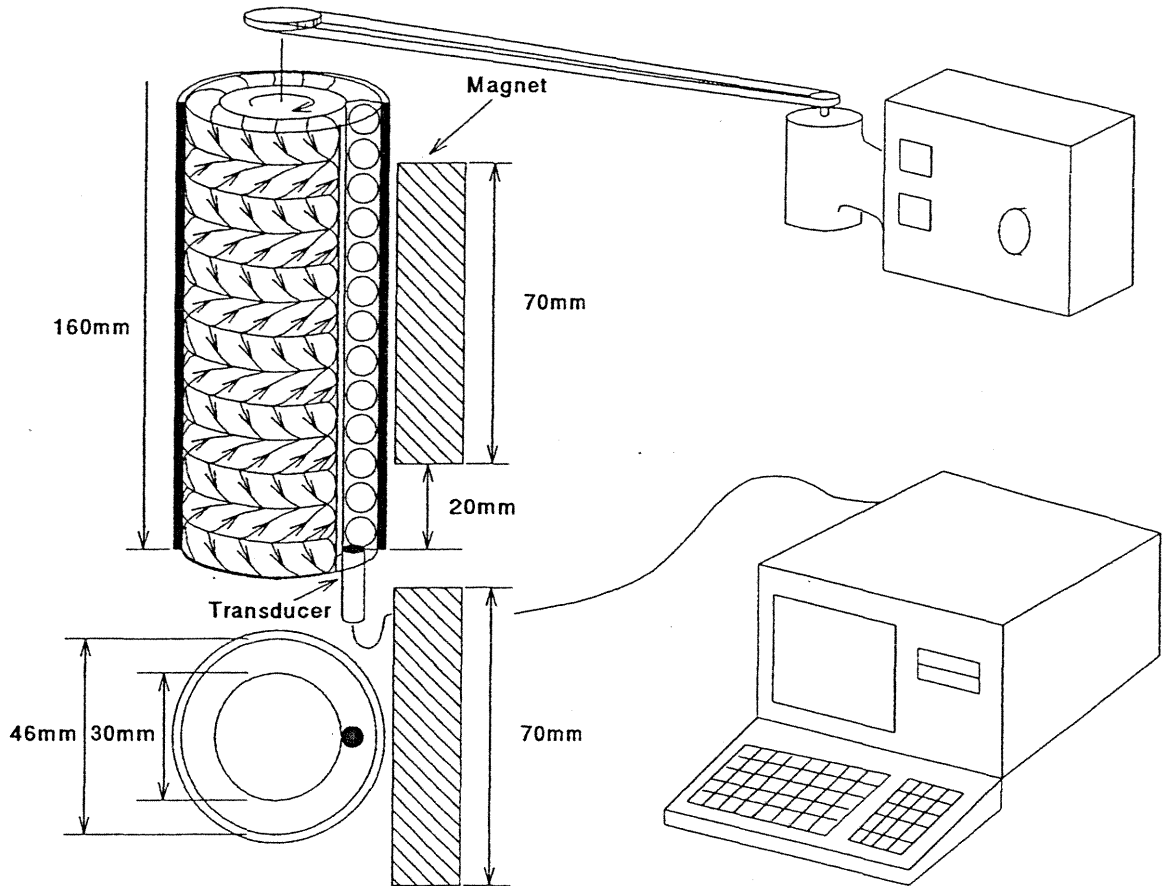


Fig.1 Experimental Apparatus

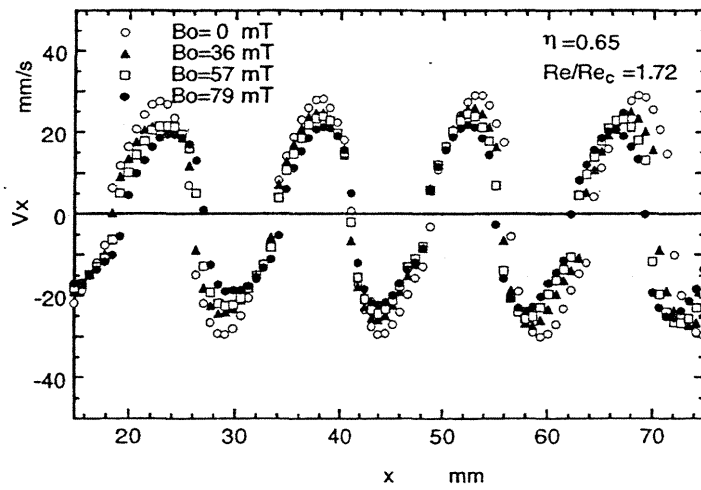


Fig.2 Mean Velocity Profiles

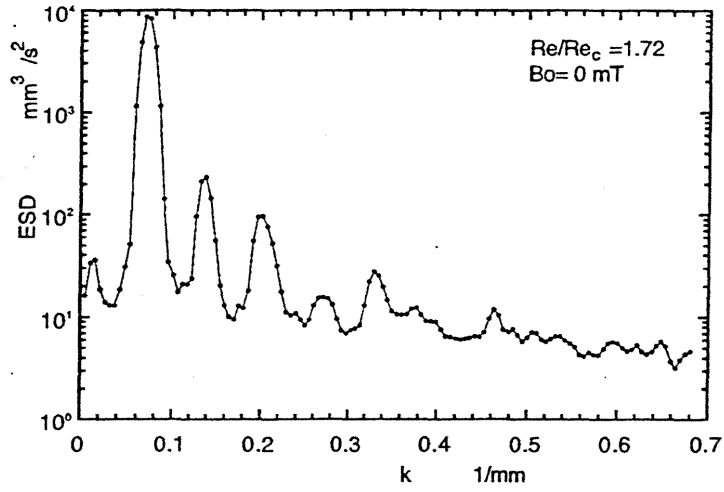


Fig.3 Time-Averaged Energy Spectral Density

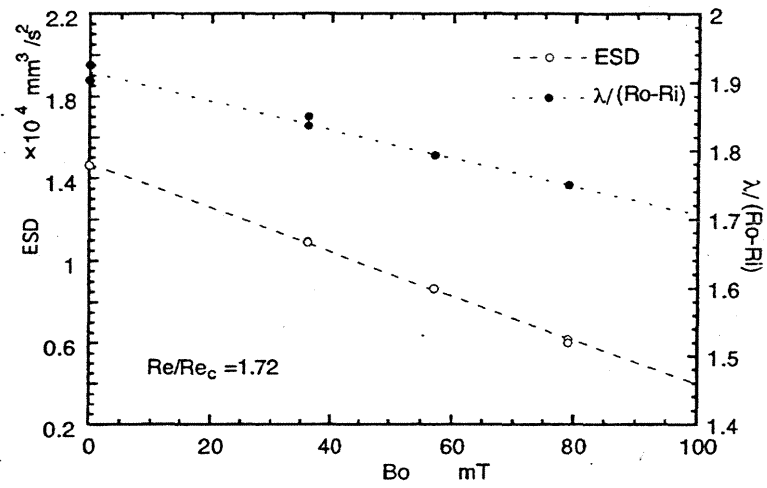


Fig.4 Maximum ESD and Wave Length

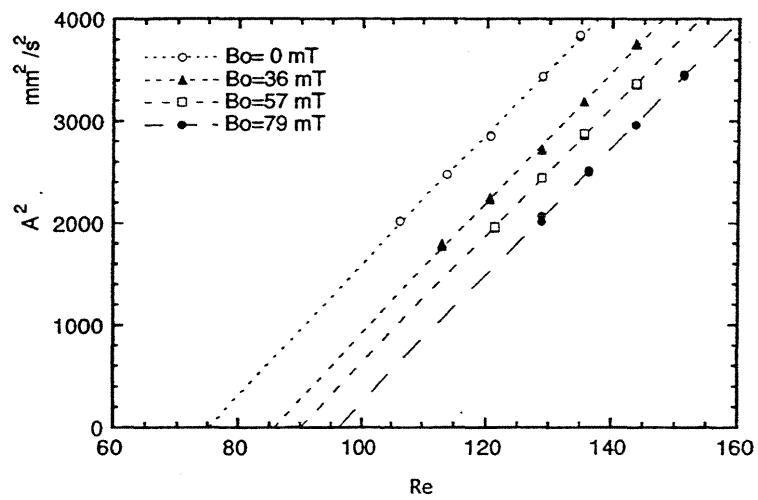


Fig.5 Critical Reynolds Number

1.ISUD

1st International Symposium on Ultrasonic Doppler Methods
for Fluid Mechanics and Fluid Engineering

September 9-11, 1996

Paul Scherrer Institut, 5232 Villigen PSI, Switzerland

Velocity measurements in a vortex of liquid Gallium

Ph. CARDIN*, H.C. NATAF*, B. PASCAL* and J.C. ATTIACH†.

*Géophysique, École Normale Supérieure, 24 rue Lhomond, 75231 Paris Cedex 05, France.

† LOT Oriel, Z.A. de Courtaboeuf, 9 av. de Laponie, 91951 Les Ulis Cedex, France.

We present experimental measurements of the fluid velocity in a vortex of fluid Gallium. Liquid Gallium is an opaque metallic liquid, which melts at 29 °C and has a dynamic viscosity similar to that of water. The liquid Gallium is contained in a nylon 6,6 tank (cf figure 1). Nylon was chosen because its sound velocity is close to the sound velocity of liquid Gallium. The external boundaries are a parallelepiped 230 mm (height) × 94 mm × 94 mm. The internal boundary is a cylinder 80mm (diameter) × 230 mm (height). A single vortex, with vertical axis, is produced by spinning a crenellated 40 mm diameter disk. The disk is driven by a tachimetric brushless motor, which maintains the rotation velocity constant within 10^{-3} . The maximum rotation velocity is 8000rev/min. The tank is symmetrically placed between the 160mm diameter poles of an electromagnet, which can produce a horizontal magnetic field up to 0.1 T. This experiment was designed to study the interaction between the magnetic field and the fluid motion and to model electromagnetic induction in the Earth's core which is responsible for the generation of the Earth magnetic field. In this presentation, we will focus on the velocity measurements we have done. We have five different methods of measurement:

1. Ultrasonic Doppler measurements with a DOP 1000 multigate, built by Signal Processing. The ultrasonic probe is orthogonal to the vertical boundary of the tank. We introduce small balls (5 μm) of Borure of Zirconium inside the fluid Gallium. The balls are the scatterers required by the Doppler technique. Different profiles were done for different velocity disk, different ultrasonic beam lines and different magnetic fields (cf figure 2).
2. Direct measurements using a particle tracking method. These experiments were done in water.
3. Dynamical pressure profiles at the top of the cylinder obtained by measuring height of Gallium in a set of Venturi tubes.
4. Differences of electrical potential on the side and on the bottom of the cylinder.
5. Induced magnetic field measured by a gaussmeter or magnetic fluxmeter on the side or below the cylinder.

We will discuss the precision, the validity and stability of the Doppler measurements in comparison with the other methods, and the results of numerical models built to reproduce the flow. This Doppler results are a breakthrough for velocity measurements in liquid metals and this technique could be applied in a more general environment.

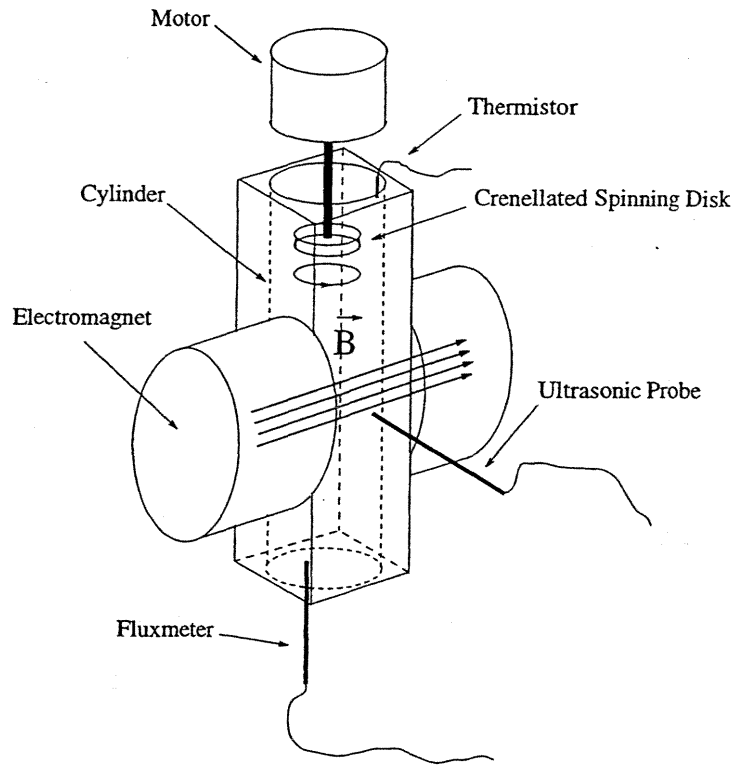


FIG. 1 - sketch of the experimental set-up

Ultrasonic Doppler velocity in a vortex of Gallium

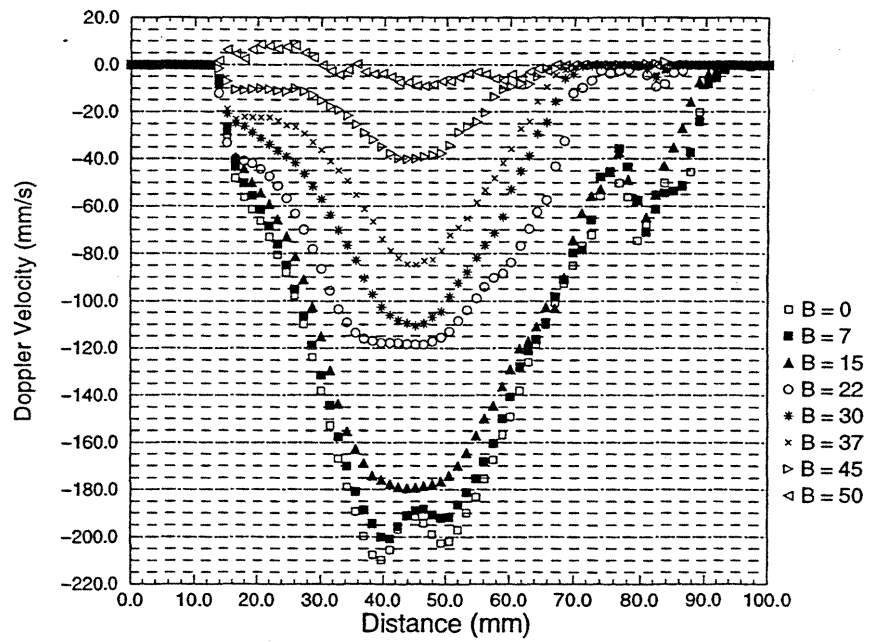
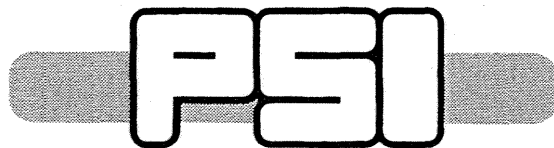


FIG. 2 - Direct measurements of velocity using the DOP 1000 multigate in a vortex of liquid Gallium for different magnetic fields (values in mT)

PAUL SCHERRER INSTITUT



Paul Scherrer Institut
CH-5232 Villigen PSI
<http://www.psi.ch>

Phone 056 310 21 11
Fax 056 310 21 99